12-2007

# INVESTIGATION OF STRUCTURE AND PROPERTIES OF NOVEL MULTI-LAYER CLAY NANOCOMPOSITE FILMS PRODUCED CONTROLLABLY BY CONTINUOUS CHAOTIC ADVECTION BLENDING

Chaitra Mahesha
*Clemson University*, chaitra.m@gmail.com

# INVESTIGATION OF STRUCTURE AND PROPERTIES OF NOVEL MULTI-LAYER CLAY NANOCOMPOSITE FILMS PRODUCED CONTROLLABLY BY CONTINUOUS CHAOTIC ADVECTION BLENDING

---

A Dissertation
Presented to
the Graduate School of
Clemson University

---

In Partial Fulfillment
of the Requirements for the Degree
Doctor of Philosophy
Materials Science and Engineering

---

by
Chaitra Mahesha
December 2007

---

Accepted by:
Dr. David A. Zumbrunnen, Committee Chair
Dr. Michael Ellison
Dr. Igor Luzinov
Dr. Jian Luo

# ABSTRACT

Polymer nanoclay composites have been studied extensively in the past decade due to the excellent combination of properties they can offer at low loadings of clay. Despite robust research, the potential enhancements that nanoclays are theoretically predicted to offer have not been achieved. Such potential improvements in mechanical and gas barrier properties are realized only when the internal structure of the nanocomposite is optimized in terms of arrangement and orientation of nanoclay within the matrix. The mixing-based approach and the accompanying complex flow fields of conventional processing techniques widely used to produce nanoclay composites are unable to control the internal structure. This has also impeded the documentation and verification of the effect of orientation and arrangement of clay platelets on the matrix and the nanocomposite properties. Hence, a unique processing technique based on chaotic advection developed at Clemson University and shown to controllably produce structured materials in the past was employed to produce structured nanocomposites with a high degree of clay orientation as well as localization of platelets within layers of nanoscale thicknesses.

Continuous lengths of nanocomposites with different clay contents were extruded in the form of films by feeding separately melts of virgin polyamide-6 polymer and polyamide 6-clay masterbatch into a continuous chaotic advection blender. A variety of composite structures were producible at fixed clay compositions. The internal structure was characterized by transmission electron microscopy (TEM), x-ray diffraction (XRD) and differential scanning calorimetry (DSC). Nanocomposites with novel in-situ multi-layered structures and a high degree of platelet orientation were formed by the recursive stretching

and folding of the melt domains due to chaotic advection. Clay platelets were localized within discrete regions to form alternating virgin and platelet-rich layers leading to a hierarchical structure with multiple nano-scales. The thicknesses of the layers reduced with prolonged chaotic advection, eventually leading to nanocomposites in which the multi-layering was no longer discernible. The oriented platelets appeared to be homogenously dispersed through the bulk of the nanocomposite.

Investigation of the morphology of the matrix by XRD showed that the homogeneity of the crystalline phase and the orientation of polymer chains parallel to the film surface increased with increased chaotic advection. Also, as the layer thickness reduced, the number of polymer chains restricted by clay platelets increased causing the γ-crystalline fraction to increase. While XRD results suggested a change in total crystallinity with chaotic advection and clay content but without a specific trend, no change in crystallinity was measured by DSC. Such contradictions are consistent with results of other investigators.

Concentrating and orienting the clay platelets within layers increases the path length of the diffusing molecule and hence may improve barrier properties. The effect of multi-layering and platelet orientation on the gas permeability of the nanocomposite films was investigated both experimentally and theoretically. Experimental measurements of 2% clay films showed that a multi-layered structure with oriented clay platelets gives a 40% greater reduction in oxygen permeability compared to a structure with a homogenous dispersion of oriented clay platelets. Also, the nanocomposite films with homogenous dispersion of platelets produced by chaotic advection due to their high degree of platelet alignment exhibited improved barrier properties than nanocomposites produced by mixing. The combination of high degree of orientation and multi-layering conferred to the 2 wt% clay

film produced with the chaotic advection blender a relative permeability lower than a 6 wt% clay film produced with a single screw extruder.

A theoretical model was formulated to explore the barrier properties of nanocomposites comprising a wide range of clay contents and platelet aspect ratio. The model showed the importance of orientation and layered structure. Permeabilities close to the intrinsic platelet permeability (i.e., near zero) can be realized by localizing and orienting a relatively low volume fraction (4%) of very high aspect ratio platelets (≥350) in the matrix or high volume fractions (20%) of platelets with aspect ratios around 100 (typical of the montmorillonite (MMT) clay). The chaotic advection blender was unable, however, to process such masterbatches due to limitations of available screw extruders intended for polyolefins. Experiments considered low volume fractions of MMT clay less than 4%.

Other physical properties of the films important for packaging applications were also evaluated. The presence of die lines, particulate contaminations and variations in thicknesses of the films led to data scatter of measured properties. However, even with film quality substantially less than obtained in industry, the nanocomposites of this study showed a slight increase in tensile strength with clay content without sacrificing impact toughness and resistance to tear. In addition, due to the high degree of orientation parallel to the film surface, the clay platelets were able to reinforce the material in both machine and transverse directions. The nanocomposites also retained the optical clarity of the pure polymer matrix.

Experimental and modeling results suggest that high barrier properties may be attainable if improvements to the chaotic advection blending system are made such that higher quality films can be produced with only slightly higher clay content or higher aspect ratio clay platelets than considered in this study.

# DEDICATION

This work is dedicated to my parents who germinated the seed of knowledge in me and all those who nurtured it.

# ACKNOWLEDGEMENTS

I sincerely thank Dr. David A. Zumbrunnen for his support and guidance for the entire period of my doctoral program.

I gratefully acknowledge Randy Martenson, Appleton Performance Packaging, Rhinelander, WI for providing the testing facilities and Mr. Kyle LaDean for conducting the physical property testing of the nanocomposite films. I also thank Dr. Ajji Abdellah, IMI-NRC, Canada for his assistance. I appreciate Mr. Dilru Ratnaweera and Dr. Dvora Perahia, Department of Chemistry, Clemson University for contributing to the research with x-ray diffraction measurements. A special thanks to Amar Kumbhar, Donald Mulwee and Dr. JoAn Hudson, Electron Microscope Facility, Clemson University, and Kim Ivey, School of Materials Science and Engineering, Clemson University for their assistance. I also acknowledge the assistance of members of our research group, especially Dr. Jin, Trevor and Leigh.

Support for this work by the U.S. Army Soldier Center of Natick, Massachusetts and interactions with Ms. Jeanne Lucciarini are appreciated. I thank Mr. Mark Kampf, Appleton Inc., WI for serving as the primary contact for the project and ensuring its smooth sailing. I also thank the members of my dissertation committee – Dr. Igor Luzinov, Dr. Jian Luo and Dr. Michael Ellison for their valuable time.

Last but not the least, I am grateful to my friends and family for their constant support.

# TABLE OF CONTENTS

Page

# LIST OF TABLES

Table Page

# LIST OF FIGURES

Figure Page

Figure Page

Figure Page

Figure Page

Figure Page

Figure Page

Figure Page

Figure Page

# CHAPTER 1

# 1 INTRODUCTION

## 1.1 Rationale

Incorporating inorganic additives to form composites has been a very important way of synergistically improving certain properties of polymers for decades. For example, carbon black and glass fibers are used in rubbers and plastics respectively to increase their strength, mica in plastic to improve the gas barrier, and carbon black again for conducting polymers. The final properties of the composites are affected by the geometry of additive (size and shape), its arrangement and orientation within matrix, and its interaction with matrix. This can be illustrated by taking the case of glass fibers. Glass fibers can be long or short. Glass fibers for use as reinforcements in polymers are surface modified to facilitate good bonding between the two phases. Without this good interaction, load transfer from polymers to glass is poor and strength is not enhanced. The composite strength is isotropic with a lower level of enhancement when glass fibers are randomly aligned within matrix. The strength can be increased further in one or more directions by controlling the orientation and arrangement of the glass fibers. But this increase in stiffness comes at a loss of toughness. In general, longer or higher the aspect ratio of the fibers, stronger is the interfacial bonding between the fibers and the matrix, and greater is the reinforcement of the polymer matrix. This holds true for all inorganic reinforcements used in a polymer matrix.

Nano-additives gained importance at the beginning of the last decade when Toyota researchers, Okada et al. (1990) found great enhancement in strength, thermal and barrier

properties of nylon-6/nanoclay composite at a very low loading. This better performance compared to their micron-sized counterparts is due to higher surface area for interaction and larger aspect ratio at the same mass or volume. Also, their hindrance to the ductility of matrix is much less due to their size. At this length scale, the additives also affect the matrix at the molecular level leading to dramatic changes in the matrix itself (Li and Shimizu, 2006; Usuki at al., 2005). A variety of nano-scale reinforcements like carbon nanotubes, nanoclay, synthetic mica and graphite have been investigated for use in polymeric matrices for more than a decade now. Among these, polymer/nanoclay system is one of the widely studied. The major advantages of clays over other nano-reinforcements are their abundant availability in nature and minimal effect on optical transparency (at the low loadings typical of a nanocomposite) compared to carbon nanotubes and graphite. When well-exfoliated, the platelets have a thickness of 1 nm while the length can vary from 100-1000 nm depending on the type of clay. Concerted efforts in modifying the surface chemistry of clays and different incorporating techniques have led to successful intercalation and exfoliation of the clay agglomerates into nano-platelets in a few hydrophilic polymers like polyamides.

As with conventional composites, the properties of polymer nanoclay composites depend on the degree of orientation of clay platelets and their arrangement within the matrix, i.e., the internal structure of the nanocomposite. The popular processing techniques currently used for producing thermoplastic nanocomposites are twin-screw extrusion and injection molding. Twin-screw extrusion is a mixing-based process utilized to intercalate or exfoliate nanoclay and homogenously disperse them in a polymer matrix. The melt-intercalated nanocomposites thus obtained are then shaped to the required form by either passing through a die or by employing a molding technique like injection molding. Both the

processes utilize high shear rates and complex geometries leading to complicated flow patterns that are difficult to control. Hence these conventional methods offer little or no control over the final structure of the composite in terms of controlled arrangement and orientation of additives in the polymer matrix. This has impeded a detailed documentation and validation of the effect of these major influencing parameters on the matrix and nanocomposite properties (Ray and Okamoto, 2003). Also, the lack of control over internal structure has proved to be a stumbling block to achieve the potential properties that these nano-additives offer. Theoretical models have shown the importance of orientation of platelets on the gas barrier properties of clay nanocomposites (Bharadwaj, 2001). The schematic in Fig. 1.1 shows how diffusion path length (tortuosity) is increased by the alignment of platelets. The tortuosity can be further increased by decreasing the spacing between the platelets. This would typically, with a conventional mixing-based process, mean increasing the clay content.

In an attempt to produce structured materials, a new polymer processing technique was invented in about 1991 by D. Zumbrunnen and his research group at Clemson University. The first publication appeared in 1994 (Zumbrunnen, 1994). This new processing technique was based on a fundamental fluid mechanics principle articulated by Aref (1984). Aref reported that the motion of passive particles in fluids can be chaotic even in simple flows and termed this phenomenon '*chaotic advection*'. The new processing technique based on this phenomenon was appropriately called *'chaotic advection blending'*. It was successfully employed to controllably produce novel structures in polymer blends and composites and is now also known as smart blending due to a novel ability to control structure in polymer blends and composites (Zumbrunnen et al., 2006).

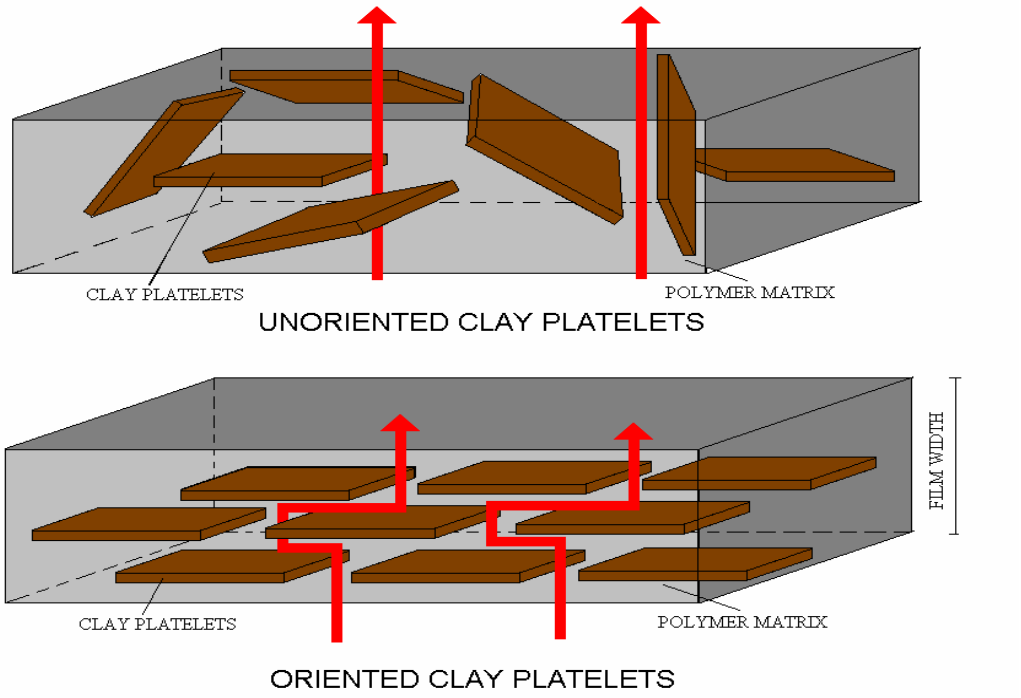


**Fig. 1.1: Schematic illustrating the effect of orientation of platelets on tortuosity of diffusion pathways**

An inherent feature of chaotic advection utilized in smart blending is the stretching and folding of the minor polymer melt component in response to a set of periodic motions. Recursive stretching and folding of the melt components within the blender produces a multi-layered structure with progressively thinner layers. When high aspect ratio additives such as clay platelets are present within one of the melt components, the shear forces within the blender, and also those associated with stretching, can cause the additives to orient in the direction of flow while the repetitive folding shuffles the melt to give rise to volumetric orientation of additives through out the matrix. This mechanism of aligning high aspect ratio additives via horse-shoe mapping (a fingerprint of chaotic advection) is shown schematically in Fig. 1.2.

The current generation chaotic advection blender operates in a continuous mode and is enabled with online process control. It is possible to control the amount of chaotic advection and hence the extent of structuring of the polymeric system online by keying in the processing parameters required. The in-situ structured melt coming out of the blender can be shaped into any required form using the appropriate die attachment.

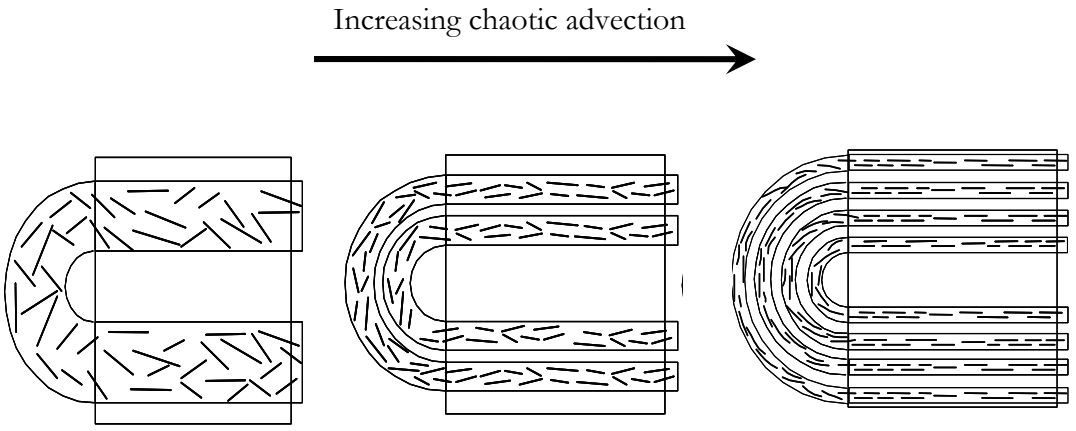


**Fig. 1.2: Schematic representation of the mechanism of multi-layering and progressive volumetric alignment of platelets in a continuous chaotic blender**

The continuous chaotic blender can be operated in 2 distinct modes. The transient mode enables visualization of different structures and structural transitions of the polymeric system as a function of chaotic advection. The steady state mode produces continuous lengths of extrusions with a single controlled structure. Hence, continuous chaotic blender is both a powerful academic tool, and an industrially relevant processing technique to investigate structure-property relationship, and produce polymeric materials with desired structure respectively

With its unique features discussed above, chaotic advection blender is capable of controlling the orientation and placement of the clay platelets. It is enabling to study the

effect of structural arrangement of nanoclay platelets on the matrix and its properties. Localizing the platelets in layers as shown in Fig. 1.2 could create high barrier walls that could lead to nanocomposites with ultra-low gas permeability.

## 1.2 Literature review

In this section, an overview of the prior art on polymer composites and nanocomposites, current processing techniques, and material properties is provided. It also contains a brief background on chaotic advection, its basic features and applications to lay the foundation for the understanding of the novel processing technique employed in the course of this research work.

### *1.2.1* Chaotic advection and smart blending

Though the everyday dictionary meaning of the word 'chaos' is 'a state of utter disorder; confused disorderly mass', in mathematics and science, 'chaotic system' refers to a non-linear dynamic system governed by deterministic laws whose long term behavior is unpredictable (Crownover, 1995). The phrase '*chaotic advection*' was coined (Aref, 1984) to denote the chaotic motions of passive particles, the positions of which cannot be predicted in the long term that can arise in a moving fluid under certain conditions. This is understood better by the following example. A fluid within a cavity is subjected to a periodic motion by the sequential rotation of the upper bounding surface and the lower bounding surface for a specified time period. The position of a single particle in that fluid is traced at the conclusion of each pair of surface motion and shown in Fig. 1.3 (Miles et al., 1995; Liu and Zumbrunnen, 1999). It follows a fixed pathline when the time period of each pair of motion is short and becomes unpredictable or chaotic with increase in time period. The time period

is proportional to the parameter, μ in the figure. When a group of particles instead of a single particle is subjected to a simple and periodic motion of the bounding surfaces, a layered structure of very fine scale is attained as shown in Fig. 1.2. Thus chaotic advection proves to be an effective means to achieve a very fine structure throughout the bulk of the fluid through controlled mechanical stirring. As a consequence, the concept was mostly initially applied in the fields of turbulence and mixing in fluid mechanics (Aref, 1984; Ottino, 1989; Aref, 2002). For the first time beginning about 1991, chaotic advection principle was employed to produce structured materials (Zumbrunnen, 1994) which led to invention of a new polymer processing technique now known as smart blending (Zumbrunnen and Kwon, 2004; Zumbrunnen et al., 2006). The amount of chaotic advection induced was characterized in terms of number of pairs of bounding surface motions, N and perturbation strength, μ (a measure of the angular displacement of the moving surfaces during each N). The characteristic features of chaotic advection significant to smart blending are shown schematically in Fig. 1.4. The first is the stretching and folding of the minor component in response to a set of periodic motions. This happens repeatedly to give rise to progressively finer layers. The second characteristic is the sensitivity to initial position. This is demonstrated here through a cluster of particles in which each particle, sensitive to its precise initial location, follows a unique and different trajectory leading to striations that can have filamentary features as shown in the schematic.

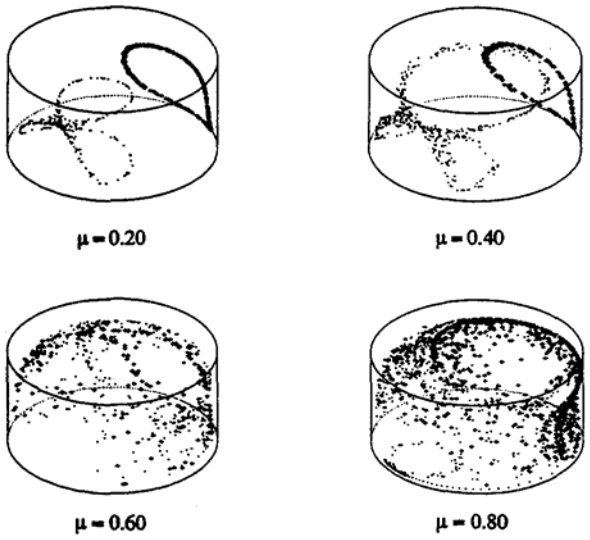


**Fig. 1.3: Chaotic motion of a particle in melt in response to a simple periodic motion [Miles et al., 1995]**

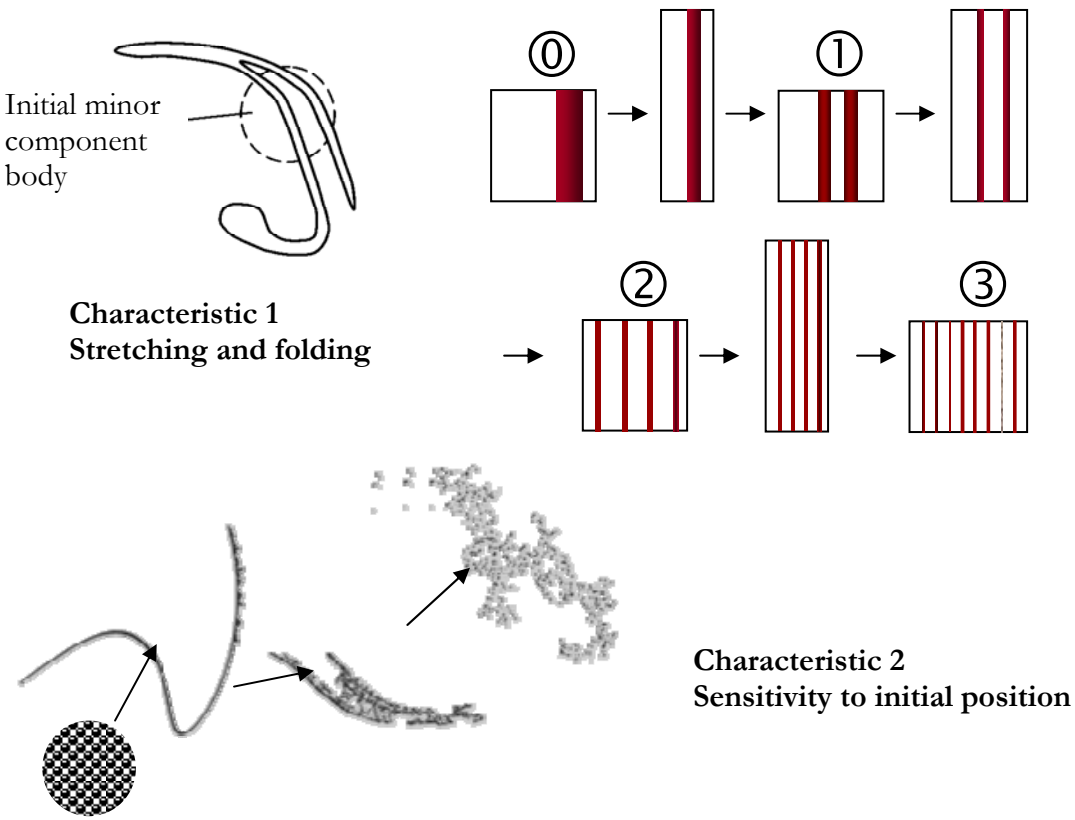


**Fig. 1.4: Characteristic features of chaotic motion employed in smart blending [Zumbrunnen et al., 2006]**

The earliest work by Miles et al. (1995) involved the development and investigation of a three-dimensional chaotic blender which was designed so as to have practical applications to batch processing of polymer melts. Solidification of melts occurred in a cavity having no impellers or stir rods. So the castings could be extracted and sectioned for examination. The chaotic motion was induced within the cylindrical cavity of the batch apparatus by the sequential motion of the upper and lower bounding surfaces. As part of this study, the conditions for global chaotic behavior for the specific geometry were also documented. The experience gained from this study was then employed by Zumbrunnen et al. (1996) to investigate the processing-structure relationship of polyolefin blends in the batch chaotic advection blender. Successive shearing and reorientation, characteristic of chaotic advection, was induced in the melt domains leading to a multi-layered morphology. The striation or layer thickness decreased exponentially with increase in N. The potential of chaotic advection blender to produce in-situ layers with thicknesses of nanoscale dimensions in the absence of interfacial tension was first described. The layered morphology served as a parent structure for derivative blend features such as ribbons, platelets, fibers and droplets.

Structural evolution and its dependence on parameters known to affect polymer blend morphology in conventional processing methods like interfacial tension and composition/ phase viscosity ratio were studied systematically to identify their influence in a chaotic advection process. The numerical model of two-dimensional chaotic mixing of two immiscible fluids by Zhang and Zumbrunnen (1996a) suggested that very fine structures (thin multi-layer structures) were possible at low interfacial tensions and the morphological evolution to ribbons, fibrils and droplets were delayed. It also indicated a degradation of basic stretching and folding during chaotic advection as the interfacial tension increased.

This model also showed that for low interfacial tensions and prior to onset of interfacial instabilities, the viscosity ratio $C_\mu$ between the phases had negligible effects within the range $0.2<C_\mu<2.0$. The results of another numerical modeling of two-dimensional chaotic mixing by Zhang and Zumbrunnen (1996b) indicated that the presence of a dissimilar minor phase body can disrupt regions of poor blending that can arise in flows stirred by chaotic advection. The changes to morphologies of fibers with three-dimensional interfaces due to an imposed shear flow in the surrounding fluid were determined through a numerical model by Zhang et al. (1998). One of the specific interests of this model was to look into the possibility of extruding fibers with an internal fibrous morphology evolved from layers. The results from these models proved to be practical importance to any melt processing of blends where a fibrous morphology of the minor phase is desirable for enhanced strength and toughness.

The computational studies (Zhang and Zumbrunnen, 1996a & 1996b; Zhang et al., 1998) were supported by experimental results. Minor phase of a blend with negligible interfacial tension presented itself as layers whereas layers transformed to other shapes such as fibers in blends with interfacial tension at similar chaotic processing conditions (Zumbrunnen et al., 1996). Similar morphologies were obtained for both LDPE/EVA and PS/LDPE blends when the composition (and hence the viscosity ratio) was inversed (Liu and Zumbrunnen, 1996). This suggested that chaotic advection is a robust process. Liu and Zumbrunnen (1999) further investigated PS/LDPE blends and mapped its processing-structure-property relationship. The batch chaotic blender was able to produce blends with different morphologies like lamellar, fibrillar and droplets at the same composition. Blends with lamellar morphology demonstrated high impact toughness which improved further with

the formation of fibrillar morphology while the blends with droplet morphology showed little improvement or decrease in toughness. This study revealed that the droplet morphology, a typical microstructure obtained at low compositions by conventional polymer processing techniques was possibly not the optimal morphology for property improvements. Impact toughness showed the maximum improvement for specimens with the finest extended microstructure and impact toughness improvement in PS of 69% with the addition of 9 vol% PE over pure PS was reported for the first time. All these studies emphasized the potential of chaotic advection and its ability to produce polymeric systems with desirable structure, independent of composition.

Danescu and Zumbrunnen (1998, 2000) suggested and investigated the potential of chaotic advection to form percolating networks of particles residing in melts. In lieu of chance interactions between particles that led to percolating conditions in conventional carbon black composites, the percolating network was constructed in the form of filament striations and their small branches (refer to Fig. 1.2, Characteristic 2) by stretching and folding. Both two-dimensional chaotic advection (Danescu and Zumbrunnen, 1998) and three-dimensional chaotic advection (Danescu and Zumbrunnen, 2000) led to significantly lower percolation thresholds for electrically conducting PS with carbon black.

With the proven ability of chaotic advection blenders to produce structured polymeric materials in batch process, attention turned to the development of an industry-relevant processing machine which could be operated in a continuous mode. A continuous flow chaotic advection blender capable of producing fine multiple layers of sub-micron thickness in a blend was reported (Gomillion, 2000; Zumbrunnen and Inamdar, 2001). In addition, batch chaotic blender with chaotic conditions similar to continuous chaotic blender

was employed initially for the better understanding of structure/morphology evolution in continuous chaotic blender as a function of processing parameters (Kwon and Zumbrunnen, 2001) and compositions (Zumbrunnen and Chhibber, 2002). The multi-layered morphology evolved into other morphologies like inter-penetrating blends (IPB), platelet, fibrous and finally droplet morphologies due to interfacial tension between the blend components. Fig. 1.5 illustrates a qualitative summary of morphologies and their transitions as a function of N or inter-changeably melt residence time. Zumbrunnen and Chhibber (2002) showed that IPBs could be formed in a wide compositional range (35-90% PS in PS/LDPE). They proposed that the rupture of thinnest locations of the layers and their subsequent growth led to formations of IPBs over the range of compositions. As the ruptures or holes grew, dual phase continuity was lost and led to formation of platelets. Also, undulations in layers developed to form fibers and capillary instabilities in these fibers gave rise to droplets.

Such effects of interfaces and the resulting instabilities on the evolution of morphology were also observed in earlier computational models (Zhang and Zumbrunnen, 1996b). Joshi and Zumbrunnen (2006) investigated in further detail the mechanism of evolution of blend morphology due to chaotic advection. They simulated the morphology development due to formation and growth of random and organized ruptures (holes) in layered melts between successive time intervals on a uniform three-dimensional grid using lattice Boltzmann method (LBM). The geometry of the model was based on values obtained from experimental data. In the case of single phase continuity where minor component layers were separated by large distances, growth of holes led to droplets or fibers. Droplets were formed when the holes were equidistant in both directions, X and Y, along the plane of a layer while different spacing between the holes along X and Y caused adjacent holes of a

single layer to coalesce in the direction of smallest spacing to form fibers. In the event of dual phase continuity or in the presence of layer interactions, droplet formation was suppressed and instead, IPBs were produced which then evolved into fibrous structures. This mechanism explained the ability of chaotic advection blender to controllably produce stable IPBs at compositions other than the intermediate compositions usually necessary in conventional blending techniques.

Chaotic advection was shown to be capable of producing in-situ nanoscale structures (Zumbrunnen et al., 1996) as well as influence the arrangement of solid additives indirectly (Dansecu and Zumbrunnen, 1998 & 2000; Zumbrunnen et al., 2002). While Danescu and Zumbrunnen (1998 & 2000) demonstrated formation of in-situ percolation networks with carbon black composites as discussed earlier, Zumbrunnen et al., (2002) were able to manipulate an initial cluster of single wall nanotubes (SWNTs) within PP to form alternate layers of PP and SWNT-rich PP in a batch process due to stretching and folding action of chaotic advection. The confinement of SWNTs within the layers of decreasing thickness caused them to orient along the direction of stretching. Similar internal structure was attained using continuous chaotic blender in clay-PP composites where the clay existed as sub-micron tactoids (Parulekar, 2003; Mahesha et al., 2005).

The advent of continuous chaotic advection blender made processing-structure-property relationship study easier. Continuous chaotic blender could be operated in the mode (Zumbrunnen et al., 2006) so as to obtain a continuous length of extrusion of any shape. The morphology and morphology development could then be followed by examining the extrusion along its length. Fig. 1.6 shows scanning electron microscopy images so obtained to discern the morphology and morphology transition of a polymer blend (Dhoble

et al., 2005). The properties were also measured in a continuous fashion to observe the influence of structure. For example, a single phase continuous layered platelet structure was recognized to be effective for an optimum combination of barrier, tensile strength, ductility and impact strength in a LLDPE/EVOH blend (Chougule et al., 2005). On similar lines, Chougule and Zumbrunnen (2005) used continuous chaotic blender to produce carbon black composites with desired resistivity and directionality. Also, their study suggested extrusions with periodic or gradient structures could be produced by online control of chaotic blender process parameters. Continuous chaotic blender has proved to be an effective tool to observe the range of structures attainable, their effect on properties and hence identify the optimum structure for a polymeric blend or composite.

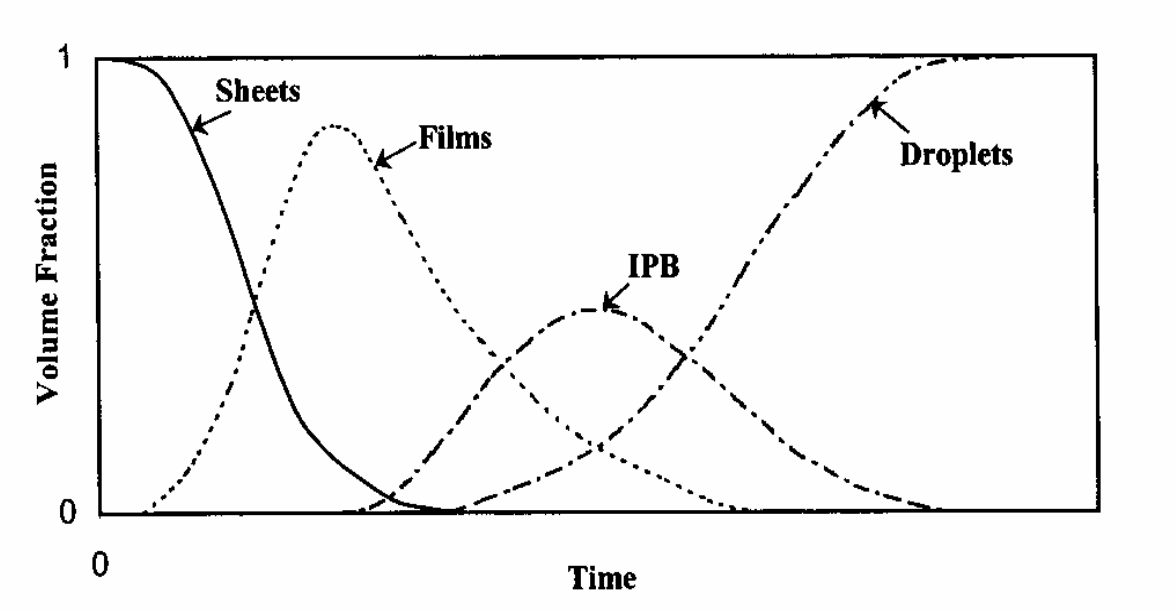


**Fig. 1.5: Qualitative summary of morphologies and morphology transitions of a blend produced by continuous chaotic blender [Kwon and Zumbrunnen, 2001]**

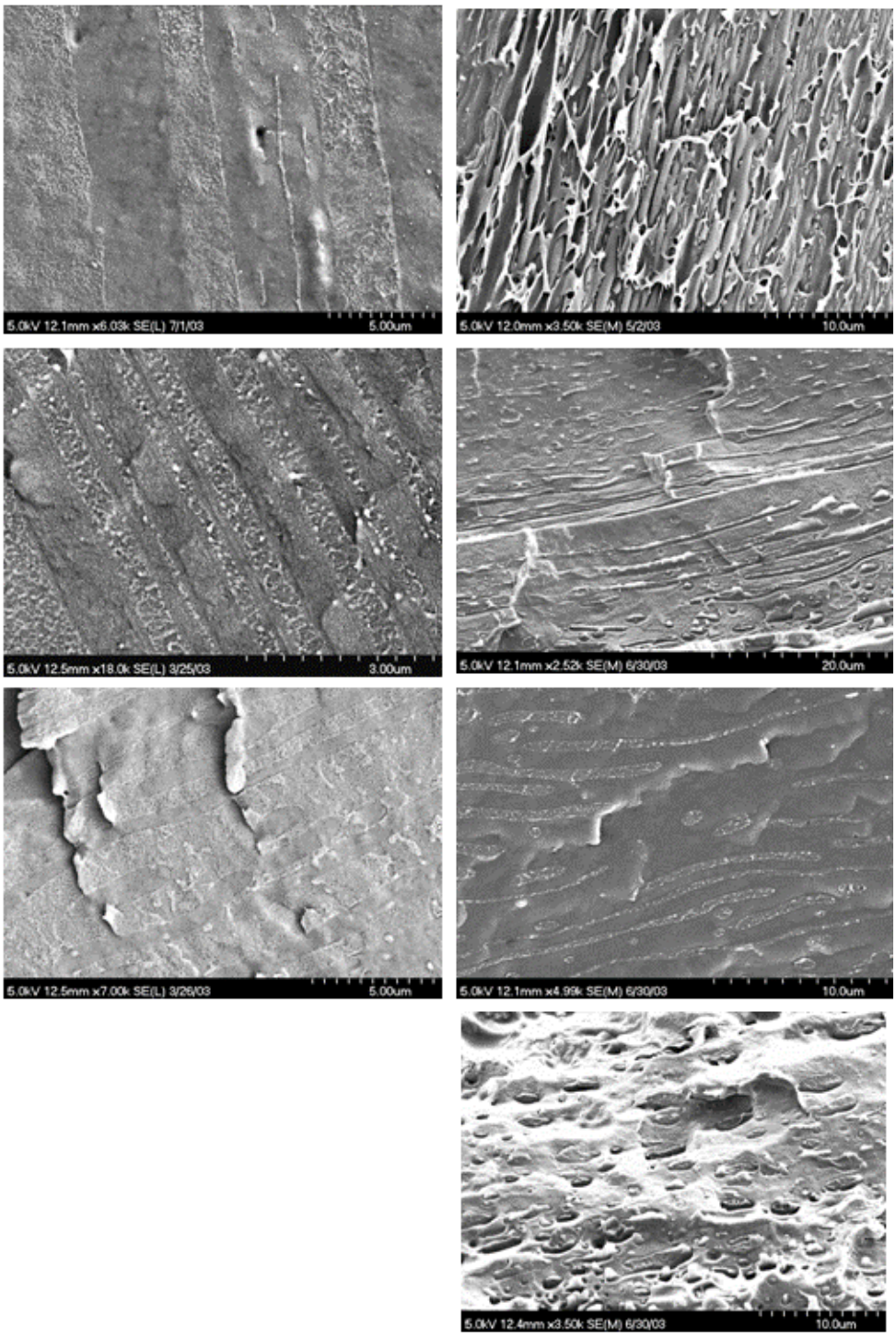


**Fig. 1.6: Progressive morphology development attained using a continuous chaotic blender shown here for a 70/30 PP/LDPE blend [Dhoble et al., 2005]**

### *1.2.2* Polymer nanocomposites

Polymer composites are a combination of two (or more) components in which typically a solid additive is incorporated within a continuous polymer matrix to obtain synergistic properties. The property enhancement depends on the shape, size, orientation and interaction of the additive with the polymer matrix. When the additive has one of its dimensions in the nanoscale (<100 nm), it is called a polymer nanocomposite. Polymer nanocomposites have gained importance as they may achieve greater enhancements in matrix properties like modulus, thermal stability and conductivity at very low concentrations of the nano-additives. Also, such property improvements, in most cases, is not accompanied by trade-offs in ductility, specific gravity, surface finish or visual appearance.

The nano-additives can be in the form of particles, fibers, tubes or platelets. Some of the widely-investigated nano-additives are carbon nano-tubes, layered silicates or clays (natural and synthetic) and graphite. They have gained significance due to their high aspect ratio which can impart better strength, stiffness and other specific functionalities like conductivity, barrier properties depending on the particular additive. Of these, the platy layered silicates or nanoclays are very popular as they have the potential to offer most of the above properties without affecting the optical clarity of the polymer matrix. Also, they are easily available in abundant both naturally and synthetically.

The commonly used nanoclays in polymer composites are montmorillonite (MMT), hectorite and saponite. These belong to the same general family of 2:1 phyllosilicates. Their crystal structure consists of layers made up of two tetrahedrally coordinated silicon atoms fused to an edge-shared octahedral sheet of either aluminum or magnesium hydroxide. The layer thickness is about 1 nm and the lateral dimension varies depending on type of clay.

Although hectorite has the largest aspect ratio among the three and hence provides better enhancement in properties to the matrices (Sherman, 2007), the use is limited compared to MMT as MMT is more easily and widely available than hectorite. MMT has a high surface area (~750 $m^2/g$) and an aspect ratio greater than 100 when dispersed as a single platelet (Dennis et al., 2001; Ray 2003). They exist in their natural forms as aggregates of platelets or tactoids of micron and sub-micron size. They must be dispersed as individual platelets in the matrix to take maximum advantage of their aspect ratio and surface area. But the clays are hydrophilic while most of the polymers are hydrophobic. Hence, in order to achieve compatibility between the two, the hydrated $Na^+$ or $K^+$ ions of clay are replaced with primary, secondary, tertiary and quaternary alkylammonium or alkylphosphonium cations. Such organic modification lowers the surface energy of the clays and increases wettability of the polymers. In some cases, these organic cationic surfactants can also contain functional groups capable of reacting with polymer matrices, thereby increasing miscibility.

The extent of miscibility and interactive forces between the polymer and modified clay determines the type of nanocomposite: *intercalated nanocomposite or exfoliated nanocomposite* (Fig. 1.7). An intercalated nanocomposite is one in which matrix polymer diffuses into the gallery spacing between clay platelets in a tactoid pushing the platelets less than 2 nm to 3 nm apart (Dennis et al., 2001; Ray and Okamoto, 2003). Nanocomposites where clay is dispersed as individual platelets separated by a distance of atleast 10 nm (Dennis et al., 2001) and act independent of each other (interactive forces between platelets no longer exists) are called exfoliated nanocomposites.

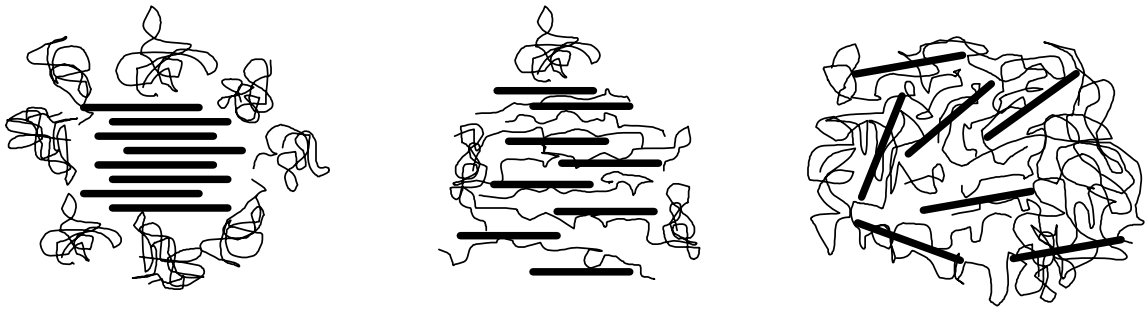

**(a) Tactoid** **(b) Intercalated** **(c) Exfoliated**

**Fig. 1.7: Structures of different types of polymer-clay composites (a) Clay exists as tactoids or clusters of platelets in conventional clay composite (b) Clay platelets are separated by diffusion of polymer chains but still have interactive forces between one another in intercalated clay nanocomposite (c) Clay platelets dispersed and independent of each other in exfoliated clay nanocomposites**

Polymer nanoclay composites caught the attention of industry and academia when a polyamide nanocomposite and their enhanced mechanical properties at very low loadings of MMT were reported by a research group at Toyota (Okada et al., 1990). They were able to achieve exfoliation by swelling clay tactoids with ε-caprolactam, a monomer used to make nylon 6 (Usuki et al., 1993a) such that the clay platelets were uniformly dispersed and then polymerizing the monomer to yield the nanocomposite (Usuki et al., 1993b). This method is known as monomer intercalation or in-situ polymerization. Another finding by Vaia et al. (1993) that polymer and nanoclay can be melt-compounded to produce nanocomposites revitalized interest, especially in the industrial community, in nanoclay composites. In this melt intercalation method, the clay tactoids and the polymer mixture are heated to a temperature above the softening point of the polymer. The diffusion of polymer chain into the gallery spacing of the clay platelets occur at this temperature either in the presence or

absence of shear. Most of the current melt intercalation methods employ medium shear rates to facilitate separation of clay platelets. For this method to be effective there must be sufficient interactive forces between polymer and clay. An effective intercalation method but not very amenable from the commercial point of view due to environmental and economic concerns was first reported by Aranda and Ruis-Hitzky (1992). This method, known as solution intercalation, utilizes a common solvent for polymer or pre-polymer and clay. The clay platelets are exfoliated in the common solvent followed by introduction of polymer into this clay suspension. The polymer is then adsorbed onto the platelets. Finally, the solvent is evaporated from the system to obtain the nanocomposite. Driving force for this kind of exfoliation is the entropy gained by desorption of the solvent, which compensates for the entropy reduction due to confinement of the polymer chains within the clay gallery spacing (Vaia et al, 1997; Ray and Okamoto, 2003; Zeng et al., 2005).

Each method has its own benefits and drawbacks. The main disadvantage of the solution intercalation method is involvement of solvents which are usually environmentally unfriendly unless the polymer is water-soluble. Melt intercalation method is industrially viable as it uses existing polymer processing techniques. This also allows modification of the thermoplastic polymer properties by end-use manufacturers to their requirements at the final product stage rather than at polymer manufacturing stage as in the case of in-situ polymerization method. The downside is the possible breakdown of clay platelet length due to mechanical shearing and degradation of some of the organic surfactants on the clay at the processing temperatures. This negative effect is not present in the case of in-situ polymerization method. Usually, nanocomposites prepared by this method exhibit slightly better properties (Cho and Paul, 2001) due to the preservation of large aspect ratio and

organic modification of clays and absence of thermal history. This method is very popular in industries handling thermoset nanocomposites (Zeng et al., 2005). Melt intercalation is the most industrially friendly method for thermoplastic composites, which are utilized in commodity and engineering products.

Thermoplastics of interest with regards to their bulk usage are polyolefins, polystyrenics, polyethylene terephthalate (PET) and polyamide-6 (PA6) and polyamide 6/6. Recently, Poly(lactic acid) (PLA) has also gained considerable importance in the area of packaging applications due its biodegradable nature. PET, polyamides, PLA, ethyl-vinyl alcohol (EVOH) being slightly polar due to their functional groups are more compatible/miscible with modified nanoclays than the polyolefins and polystyrenics. Efforts are being made to exfoliate nanoclays in polyolefins and polystyrenics (Ray and Okamoto, 2003) as they form the bulk of the plastics utilized in most of the commodity plastics and to a certain extent in engineering products because of their low cost. At the moment, the most widely studied and documented polymer-nanoclay system is PA6/MMT composites. This is because PA6 is a relatively low cost plastic with high performance and with a variety of potential and actual applications. In addition, it forms a well-exfoliated nanocomposite even at considerable higher loadings of clay (about 10 wt %). So, most of the concepts and theories about nanoclay composites have been tested with this system and many publications reviewing this system of nanocomposites are available (Ray and Okamoto, 2003; Usuki et al., 2005; Gupta et al., 2006). In the succeeding paragraphs, various important aspects of PA6/MMT are reviewed.

PA6/ MMT nanocomposites were produced for the first time by in-situ polymerization and their potential property enhancement reported by Toyota Central

Research Laboratories (Usuki et al., 1993b). Early investigations by Toyota scientists illustrated that MMT performed better compared to other platy silicates mentioned previously due to better bonding of nylon with MMT (Usuki et al., 1995). Following this result, they pursued work on PA6/MMT composites. Investigations on the effect of clay on nylon-6 showed formation of crystallites whose chain axes were parallel to the clay platelets which in turn had planar orientation to the surface of a cast-extruded film but were randomly oriented in the plane (Kojima et al., 1994). Similar studies with injection-molded bar demonstrated that the degree of orientation of the clay platelets and the nylon crystallites varied across the depth of the bar (Kojima et al., 1995). This variation in alignment of platelets and crystallites is explained by the dependence of degree of orientation of these anisotropic bodies on the applied shear forces and their aspect ratio. At mold walls or bar surfaces, the magnitude of shear force is very high and hence both platelets and crystallite orient parallel to the force applied. At intermediate layers, the shear forces are reduced but the platelets still maintain a certain degree of orientation due to their high aspect ratio while crystallites revert to their original stable orientation perpendicular to the platelets. In the middle layer, the shear forces are very low and platelets assume random orientation along the flow axis with the crystallites perpendicular to them. In the course of their research with in-situ polymerized PA6/ clay nanocomposites, the Toyota researchers found that nanocomposites showed significant enhancements in modulus with, 90% in tensile and 126% in flexural modulus at 8% clay, and heat distortion temperature (2.5 times), but slightly reduced improvements in strength, 40% for tensile strength and 60% for flexural at 8% clay. These property enhancements were accompanied by a loss of flexibility/ductility evident by the drastic decrease in impact strength and tensile elongation. They concluded that PA6

reinforced with 5 wt % organically modified MMT provided an optimum combination of properties. All the above results were compiled in a review by Usuki et al. (2005).

In 1999, nylon nanocomposite was successfully produced by melt-intercalation process using a twin-extruder (Liu et al., 1999). The properties of these nanocomposites though were mostly in tandem with those of the in-situ polymerized nanocomposites of Toyota. The major deviation was in the retention of the impact properties by the nanocomposite up to about 17 wt % clay. Also, the enhancement in heat distortion temperature was less than 2 times that of PA6.

Once it was discovered that nylon nanocomposites produced by the melt intercalation process had properties comparable to that of in-situ polymerized nanocomposites, work progressed to optimization of materials and processing conditions to achieve the maximum enhancement in properties. A collaborative study by Dennis et al. (2001a & b) found that degree of exfoliation of clay platelets in PA6 depended on the clay chemical treatment, type of extruder and screw design. They found that Cloisite 30B (organically modified clay with methyl bis-2-hydroxyethyltallow quaternary ammonium chloride) supplied by SCP, Gonzales, TX exfoliated and dispersed better than SCP's Cloisite 15A (clay modified with dimethyldihydrogenatedtallow quaternary ammonium chloride) in all extruders because of better interaction between the functional groups of Cloiste 30B with PA6. The best exfoliation and dispersion was achieved at medium shear intensities and not at high shear rates in each extruder. Amongst the different kinds of extruders, twin-screw extruders operating in a non-intermeshing mode provided the best delamination of the platelets. It was also reported that dispersion and exfoliation improved with mean residence time of the melt-nanoclay system in the extruder. Another study comparing the effect of

molecular weight of PA6 showed that exfoliation increases with molecular weight and hence the nanocomposite produced with high molecular weight nylon yielded the best properties (Fornes et al., 2001). In a related study, Cho and Paul (2001) compared the properties of clay nanocomposites with that of conventional clay and glass fiber composites. Nanoclay composites showed superior mechanical properties, especially modulus, compared to conventional composites. Also, nanocomposites retained their ductility and toughness as opposed to the loss of both in conventional composites. In addition, the nanocomposite properties were found to be independent of processing temperature in 230°C -280°C range.

In summary, numerous studies on the effect of nanoclay on mechanical properties of PA6 nanocomposites prepared by in-situ polymerization or melt-intercalation with twin-screw extrusion and subsequently shaped by injection molding found that the modulus, and to a lesser extent strength increases monotonically with clay content as long as clay is well exfoliated but impact strength and ductility reaches an optimum at a certain clay content. Though incorporation of nanoclay changes the crystalline nature and degree of crystallinity of the PA6 matrix (Kojima et al., 1994; Medellin-Rodriguez et al., 2001), they do not seem to play any major role in reinforcing the matrix. The improvement in strength of PA6 nanocomposites is attributed to the larger interfacial area due to the nanoscale dimensions of clay and superior interaction at the interface between PA6 and clay via the formation of hydrogen bond (Usuki et al., 1995). This fact is further proved by very slight increases reported for PP and PS nanocomposites without compatibilizers (Ray and Okamoto, 2003; Zeng et al., 2005). The enhancement in modulus is due to the high aspect ratio of clay platelets and their inherent superior rigidity (Ray and Okamoto, 2003).

Some mechanical properties contradictory to the above results were reported for PA6/MMT nanocomposites formed as films by cast extrusion (Ranade et al., 2003; Russo et al., 2006). Ranade et al. (2003) reported an initial sudden decrease in modulus of nanocomposite films at 1% clay loading. The modulus then gradually increased with clay content and returned to that of base resin at clay concentration of 3 wt% and showed a meager 8% increase at 5 wt% clay loading. They attributed this to the presence of smaller crystals in the nanocomposite whose negative reinforcement effect was counteracted by the increased concentration of stiffer clay platelets. Their accompanying yield strength and tensile strength data matched that of the injection molded specimens. Russo et al. (2006) on the other hand reported increased modulus for a PA6 nanocomposite film with 3 wt% clay which increased further at 6% clay loading. But the tensile strength decreased with clay content. The yield strength exhibited negligible change with clay content.

Another major factor which drove the nanocomposite research was its potential gas barrier properties. Despite its importance, little literature is available on barrier properties of nanocomposites, especially on barrier properties of polyamide nanocomposites. Hence to get an overview of nanoclay and its effect on permeability characteristics of the matrix, the discussion here is broadened to include all relevant polymer matrices and not just PA6.

Excellent resistance to water permeation and a reduction of more than 70% in permeability coefficient of water vapor in PA6 at organic clay loading of about 1.5 wt% was reported for injection-molded plates made from in-situ polymerized nanocomposite (Kojima et al., 1993; Usuki et al., 2005). Nanoclay also proved effective in reducing oxygen, helium and water vapor permeability of polyimide (PI) films cast from solution (Yano et al., 1993). Permeability coefficients of all three permeants were reduced drastically to less than half the

value of pristine PI at a loading of 2 wt% clay and reached near zero values at the highest loading of 8 wt%. Similar reductions were reported for carbon dioxide ($CO_2$) diffusing through PI cast films reinforced with organoclay (Lan et al., 1994). The trend was revealed to be same for water vapor transmission rate of poly(ε-caprolactone) cast films filled with modified MMT (Messersmith et al., 1995). Further studies revealed that as the aspect ratio of the clay platelets increased, the barrier property improvement was better (Yano et al., 1997). Fluorinated synthetic mica reduced the water vapor permeability coefficient by an order of magnitude of PI at 2 wt % loading. Apart from the aspect ratio (~1200), the authors proposed that the fluorine in mica repelled the water molecules and further enhanced the barrier improvement.

The first known findings of oxygen barrier property of PA6-clay nanocomposites were published by Liang et al. (2001). They reported an improvement of ~80% in oxygen barrier of the cast nanocomposite films with 8 wt %. As before, the permeability followed an exponential relationship with clay content. A similar reduction was also observed for water vapor transmission. Other reports announcing some commercial products utilizing nylon nanocomposite as a core layer in PET bottles appeared around the same time (Plastics Technology, 2000; Leversuch, 2001). Imperm, a nylon-based nanoclay composite developed by Eastman Chemical Co., TN was claimed to have a three to six fold oxygen and $CO_2$ barrier enhancement over typical nylons (Plastics Technology, 2000). A nylon-6 nanocomposite with 3 times the oxygen barrier at 2 wt% and 6 times at 4 wt % under the trade name Aegis NC was reported by Honeywell (Leversuch, 2001). Leversuch also reported a new kind of barrier material based on nylon-6 with active oxygen scavengers (Aegis OX, Honeywell) which took the permeability to near-zero levels. In the same article,

Leversuch mentioned a cast film from a pre-commercial compound by Bayer using nanoclay with a 50% reduction in OTR with respect to a nucleated nylon-6. Unfortunately, no further details about the process employed or raw materials involved are available for these commercial products. Recently, a research publication by Russo et al. (2006) reported oxygen barrier properties of cast extruded films of nylon-6 and two copolymers of nylon-6 with similar structure but of different molecular weights compounded with Cloisite 30B, an organically modified MMT. The PA6 film showed only ~28% reduction in permeability at 6 wt% clay while the high molecular weight copolymer showed about 55% reduction at the same clay content. The gas barrier was the lowest for the low molecular weight copolymer. Comparative analysis showed that clay was in general exfoliated but for a few tactoids at 6 wt% clay loading in both nylon-6 and its high molecular weight copolymer with the copolymer having a lower fraction of tactoids. Also, the orientation of clay platelets was better in the copolymer than the PA6 matrix. They explained the better enhancement in the high molecular weight copolymer matrix to be a direct effect of better exfoliation and orientation of the clay platelets within the matrix.

Many studies followed on different polymer-clay systems like polyurethane (Xu et al., 2003; Osman et al., 2004a), vinyl ester (Shah and Gupta, 2002), epoxy resin (Osman et al., 2004a & 2004b), PLA (Ray et al., 2002; Ray and Okamoto, 2003) and HDPE (Osman et al., 2005). All systems exhibited improved barrier properties similar to earlier publications discussed here.

It was established that the major contributor to the reduction in permeability is the high aspect ratio of additives in systems with a mixed morphology of exfoliated and intercalated clays irrespective of the basal spacing within the tactoids (Gusev and Lusti, 2001;

Osman et al., 2005). Apart from the high aspect ratio of clay platelets, the changes that occur in polymer matrices due to inclusion of clay platelets like mobility of chains in amorphous phase, change in degree of crystallinity, crystalline forms and orientation of crystalline lamellae also were reported to contribute to the permeability characteristics (Russo et al., 2006). Significant effort has gone into understanding the fundamental changes in the polymer matrix that the incorporation of clay platelets causes.

PA6 can exist in two crystalline forms, monoclinic (α-form) and pseudo-hexagonal (γ-form) (Holmes et al., 1955; Arimoto et al., 1965). The α-form is formed when hydrogen bonding exists between anti-parallel polymer chains and the γ -form by hydrogen bonding among parallel chains (Fig. 1.8).

The α-form is the thermodynamically stable crystalline form of pure PA6 at room temperature (Maiti and Okamoto, 2003), where as γ-form manifests itself in the case of an elongational flow field (Samon et al., 1999), quench cooling (Kyotani and Mitsuashi, 1972) or restricted chain mobility (Miltner et al., 2005). Many authors reported that incorporation of clay platelets leads to a predominant formation of γ-crystals over α-form (Kojima et al., 1994; Medellin-Rodriguez et al., 2001; Lincoln et al., 2001; Maiti and Okamoto, 2003; Fornes and Paul, 2003) due to restricted chain mobility induced by the strong interaction between clay platelets and PA6 chains (Miltner et al., 2005). Studies on extruded films and injection molded bars indicated that clay platelets also induced preferred orientation in PA6 crystallites and the degree of orientation depended on clay content as well as the magnitude of shear stress acting on the system (Kojima et al., 1994 and 1995; Medellin-Rodriguez et al., 2001; Fornes and Paul, 2003; Weon et al., 2005). The crystalline lamellae were found to grow on both sides of an exfoliated clay platelets leading to a sandwiched structure (Maiti and

Okamoto, 2003) with the chain axes perpendicular to the clay platelets. These crystalline lamellae in turn had branches growing on them leading to a 'shish-kebab' structure. Recently, it was reported that not only does the orientation of clay determine the orientation of polymer crystallites but also the spacing between clay platelets has a pronounced effect (Li et al., 2006). Li et al. found that the perpendicular orientation of crystalline lamellae was changed to parallel orientation at clay platelet spacing less than 30 nm. This is schematically shown in Fig.1.9.

The crystallization kinetics is also affected, with clay increasing the overall rate of crystallization up to a certain clay content compared to pure PA6 (Maiti and Okamoto, 2003; Fornes and Paul, 2003). The higher nucleation rate in nanocomposites compared to virgin PA6 was because clay particles act as heterogeneous nucleating agents for the matrix (Maiti and Okamoto, 2003). Clay also has some deterring effects on PA6 matrix. First, presence of clay may disrupt formation of crystallites and hence lead to less ordered crystals (Lincoln et al., 2001). Second, the degree of crystallinity may be changed (Fornes and Paul, 2003; Weon et al., 2005) although there is no consensus on the trend. Finally, the γ-phase formed in nanocomposites is a softer phase than α-form due to the lesser interaction between chains in the γ-form (Maiti and Okamoto, 2003).

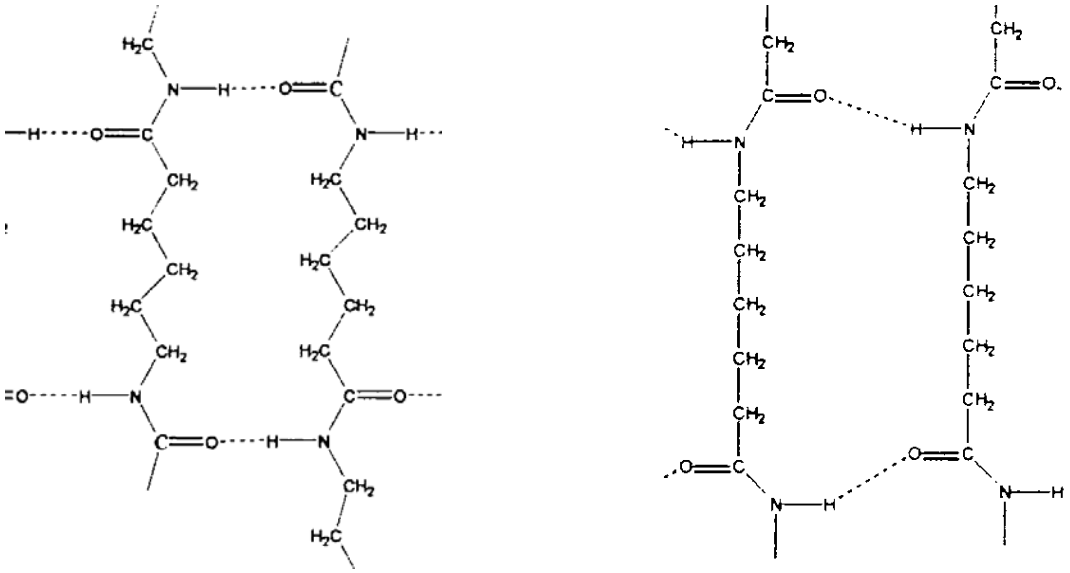

**(a)** **(b)**

**Fig. 1.8: Crystalline forms of PA6 (a) the α-form and (b) the γ-form [Zheng et al., 2003]**

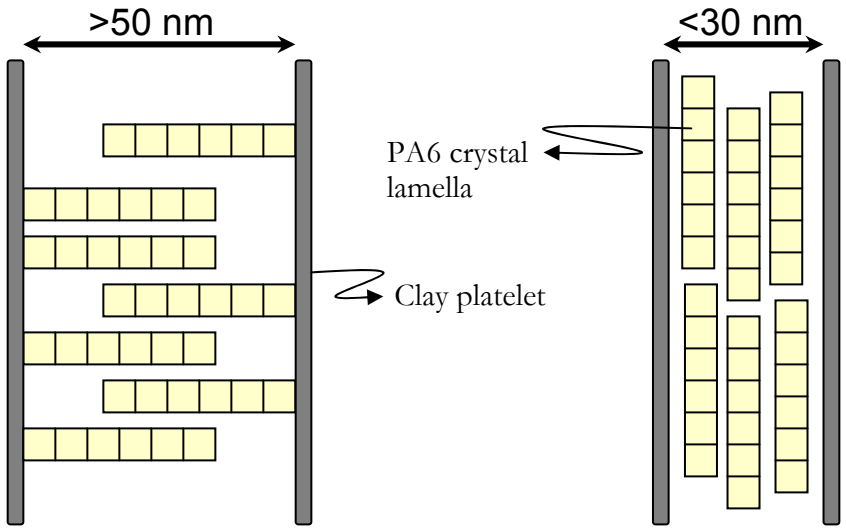


**Fig. 1.9: Schematic showing the effect of clay spacing on orientation of PA6 crystals [Li and Shimizu, 2006]**

### *1.2.3* Nanocomposite processing techniques

At present, melt-intercalation of thermoplastic nanocomposites is achieved using conventional processing techniques like batch mixers and twin-screw extruders. As mentioned in the previous section, studies on processing conditions in a twin-screw extruder have been done and the parameters optimized for the best exfoliation characteristics in PA6-clay nanocomposites (Dennis et al., 2001a & b; Fornes and Paul, 2001; Cho and Paul, 2001). So far, twin-screw extruders, especially of the non-intermeshing types, operating at medium shear rates have proved to be the best tool to produce exfoliated nanocomposites. These are widely used to produce nanoclay- polymer concentrates or masterbatches.

The exfoliated masterbatches are used as raw materials in subsequent processing steps to produce various products like sheets, films, films, fibers by extrusion, injection molded automotive parts and blow-molded bottles. For small scale productions such as in academia, solution casting and spin casting methods are utilized to form nanocomposite films.

The main advantage of the conventional melt-processing techniques is the fact that no major changes are required to be made to the machineries by the manufacturing industries. The major disadvantage, especially to the research community, is the difficulty to control the internal structure or morphology of the polymeric system (blend or a composite) in an organized manner. This difficulty is mainly due to the complex flow fields and mixing focus involved in these processes (Zumbrunnen et al., 2006). So composition-structure-property optimization is not practically achievable. The final morphology or internal structure of a polymeric blend or composite to the most part is hence determined by its composition and material characteristics like relative viscosities (Sperling, 1997). This failure

to control structure/morphology leads to inability to attain optimum functional properties of the polymer system. Due to this drawback, the enhancement of properties of a nanocomposite and its real dependence on the internal structure of clay nanocomposites like orientation and placement of clay platelets and the changes in polymer matrix thereof has not been well documented (Ray and Okamoto, 2003) although it has been shown by some theoretical models that orientation and arrangement of high-aspect ratio additives affects the properties significantly. Chaotic advection blenders, discussed in detail in the previous section, have been able to control the structure of the polymeric system at the order of micron, submicron and nanoscale dimensions (Zumbrunnen and Kwon, 2004).

### *1.2.4* Permeability models

Permeability (P) of a polymer is a function of diffusion and sorption properties of the material. It is defined as the product of diffusion constant D and solubility constant S for a polymeric system. The solubility constant is almost the same for all polymers (Osswald et al., 2006) and hence permeability depends on the diffusion process. Based on Fick's first law of diffusion and considering unidirectional concentration gradient, generally true for a thin homogenous polymer film or membrane of density ρ, the rate of permeation $\dot{m}$ through a film of thickness *l* and area of cross-section A with concentration difference ($c_1$-$c_2$) in the direction of diffusion given by

$$\dot{m} = -DA\rho\frac{c_1 - c_2}{l} \qquad \textbf{1-1}$$

The equilibrium concentration at each surface due to Henry's law is given by c=Sp where p is the partial pressure of permeating gas. Hence permeability is given by the below equation.

$$P = \frac{\dot{m} l}{\rho A (p_1 - p_2)} \qquad \textbf{1-2}$$

In this section, a few theoretical models relevant to the diffusion of a permeable matrix filled with impermeable particles are briefly reviewed. Much insight can be derived from a simple diffusion model designed for conventional filled composites. This model includes tortuosity effects (Nielsen, 1967). He defined tortuosity factor τ as the ratio of the distance a molecule travels through the film to the thickness of the film. Fig. 1.10 illustrates a diffusion pathway assuming maximum possible tortuosity factor.

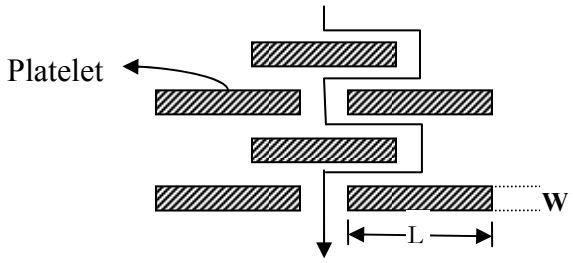


**Fig. 1.10: Schematic showing the pathway of a diffusing molecule through a filled composite [Nielsen, 1967]**

The permeability of the composite, P relative to that of matrix, $P_m$ was thus predicted as a function of aspect ratio, α (=L/W) and volume fraction of the filler, φ by this model.

$$\frac{P}{P_m} = \frac{1-\varphi}{\tau} \qquad \textbf{1-3}$$

$$\tau = 1 + \frac{\alpha}{2}\varphi \qquad \textbf{1-4}$$

The denominator of right-hand side of the Equation 1-3 is the average tortuosity factor, τ and is defined by Equation 1-4. This model was derived with for a dilute system or a system with very low loadings of the filler. Aris (1986) derived an equation for diffusion of a solute

through a composite material for the general case of an array of impermeable obstacles of irregular shape and size dispersed parallel to the plane of a membrane using statistical probability. He incorporated a geometric factor μ to account for the fraction of the diameter of the obstacle which on the average is added to the path length of the permeating molecule. He then solved a special case of diffusion of a permeant through a two-dimensional periodic array of obstacles using conformational mapping methods to obtain exact solutions for μ. Using these analytical values for μ, he concluded that for cases where the spacing between the obstacles along the direction of diffusion is large compared to their lateral spacing, the diffusion is hindered to a very small extent until the area fraction of the obstacles approaches close to 1.

Another paper discussed simple models predicting the permeability of membranes as a function of volume fraction of flakes (φ), their aspect ratio (α) and their shape (Cussler et al., 1988). Here, the authors deduced expression for total flux through barrier membrane. The actual general geometry of a barrier membrane (Fig. 1.11A) was modeled in three different ways (Fig. 1.11B-D). The first two ideal cases were solved in similar manner considering a unit cell. For the geometry in Fig. 1.11B, the total flux through the unit cell, $J_1$ of area 2dW rearranged as a resistance to diffusion across the membrane of thickness 'l' and a concentration gradient of Δc was deduced and is as given below.

$$\frac{D\Delta c}{J_1} = \frac{l}{2dW} + \frac{b}{dW}\ln\left(\frac{b}{2s}\right) + \frac{a}{2sW} \qquad \textbf{1-5}$$

The first term of the right-hand side of the Equation 1-5 accounts for the resistance without flakes, second term the constriction into and out of the slit and the third term corresponds to the resistance of the slit itself. The resistance to diffusion was then extended to a

multilayer membrane with n flakes to obtain the following equation. Similar general expression was derived for case C of Fig 1.11.

$$\frac{D\Delta c}{J_N} = \frac{l}{2dW} + \frac{b}{dW}\ln\left(\frac{b}{2s}\right) + \frac{na}{2sW} + \frac{1}{2}(n-1)\frac{d}{bW} \qquad \textbf{1-6}$$

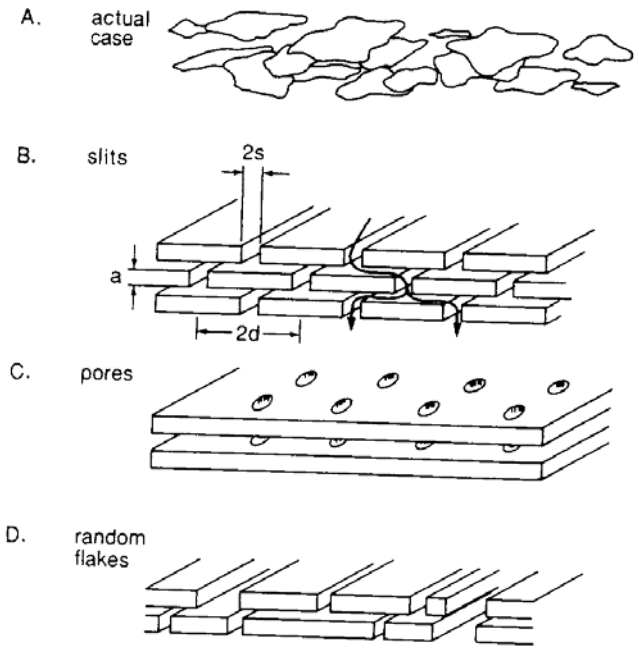


**Fig. 1.11: Various geometric models of barrier membranes. (A) Actual membrane with particles of irregular shape and size randomly dispersed. Diffusion occurs through regularly spaced (B) slits and (C) pores (D) Diffusion through randomly spaced slits [Cussler, 1988]**

The expression developed by Cussler et al. (1988) for the particular case of diffusion through a three-dimensional, random array of flakes (Fig. 1.11D) can be considered to be an extension of two-dimensional equation deduced by Aris (1986). This expression known as Cussler-Aris equation is given below.

$$\frac{P}{P_m} = \frac{1}{1 + \mu\alpha^2\varphi^2/(1-\varphi)} \qquad \textbf{1-7}$$

The factor, $\mu$ as defined earlier is an unknown constant that depends on the geometric shape, size and extent of positional disorder.

Another theoretical model based on a multiple scattering expansion (Fig. 1.12) was formalized to predict the diffusion of a composite with 'n' randomly dispersed, perfectly aligned discs of radius 'R' in dilute ($nR^3<<1$) and semi-dilute ($nR^3>>1$, $\varphi<<1$) regimes (Fredrickson and Bicerano, 1999). In the diagram circles denote discs, dots represent the scattering events and directed arrows represents unperturbed diffusion. The scattering matrix of all the incoming and outgoing vectors of the vertices was extracted from the Green's function solution to diffusion equation $G(\mathbf{q})=1/[\mathbf{q}.\mathbf{D}(\mathbf{q}).\mathbf{q}]$, where $\mathbf{D}(\mathbf{q})$ is a generalized diffusion tensor. The denominator of this equation was re-expressed as $\mathbf{q}.\mathbf{D}(\mathbf{q}).\mathbf{q}= D_m q^2-\sum(\mathbf{q})$ where $\sum(\mathbf{q})$ denotes "self-energy". This self energy term was evaluated from the scattering matrices of all the 'n' discs to the second order to obtain the relative diffusivity of the composite. This model predicted that in the dilute regime, "randomly oriented disks were only one-third as effective in reducing penetrant diffusion when compared with perfectly aligned disks." Also, the expression reduced to that of 'modified-Nielsen' equation (Nielsen's expression with a geometric factor) in the dilute regime where $\alpha\varphi$ is much greater than one and to that of 'modified Cussler-Aris' equation in the semi-dilute region.

Finite-element calculations were presented for the first time for three-dimensional periodic models comprised of random dispersion of perfectly aligned non-overlapping platelets by Gusev and Lusti (2001). For the geometry and adaptive-meshes shown in Fig 1.13, Laplace's equation (Equation 1-8) for the local chemical potential, $\eta$ was solved with a

position-dependent local permeability co-efficient, P(**r**). P(**r**) was assigned values of 0 inside the platelets and $P_m$ everywhere in the matrix.

$$\text{div } P(\mathbf{r}) \text{ grad } \eta = 0 \qquad \textbf{1-8}$$

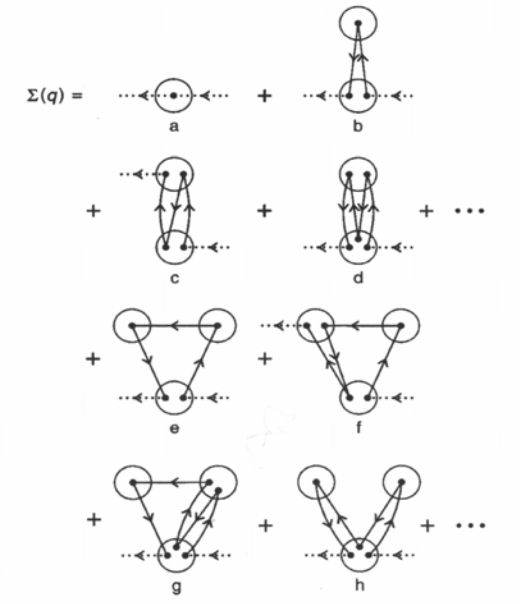


**Fig. 1.12: Diagram explaining expansion of the self-energy function ∑(q) involved in multiple scattering formalism [Fredrickson and Bicerano, 1999]**

The overall permeability coefficient was calculated from the overall flux and chemical potential gradient. The flux and the potential gradient were considered to have a linear response relationship. The permeability coefficient was shown to depend on the factor $\alpha\varphi$ with the relative permeability changing very slightly for values of $\alpha\varphi$ lesser than 1. The reduction in permeability was dramatic after that point (Fig 1.14). Comparing the results from this model simulating actual three-dimensionality involved in the problem to the earlier models described above (Nielsen, 1967; Cussler et al., 1988; Fredrickson and Bicerno, 1999), the authors found that the simple diffusion model by Nielsen assuming one-dimensional diffusion gave accurate predictions matching theirs upto $\alpha\varphi \sim 10$.

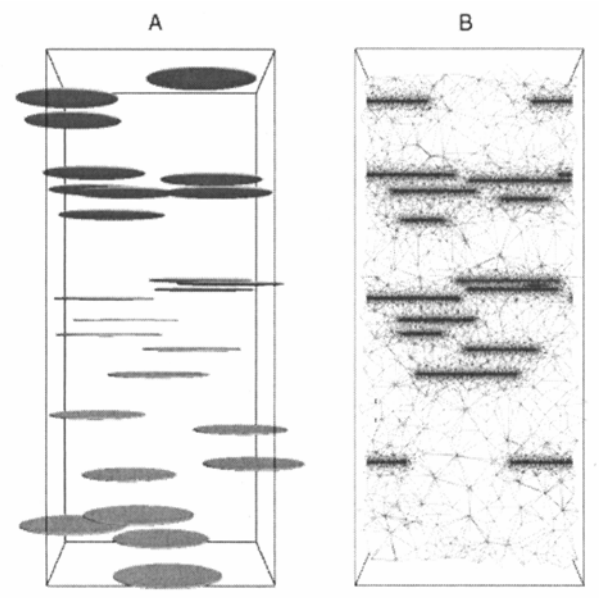


**Fig. 1.13: (A) Sketch of a periodic multi-inclusion model containing randomly dispersed, perfectly aligned non-overlapping platelets. (B) Cross-section through a periodic morphology-adaptive quality mesh employed for predicting permeability coefficient [Gusev and Lusti, 2001]**

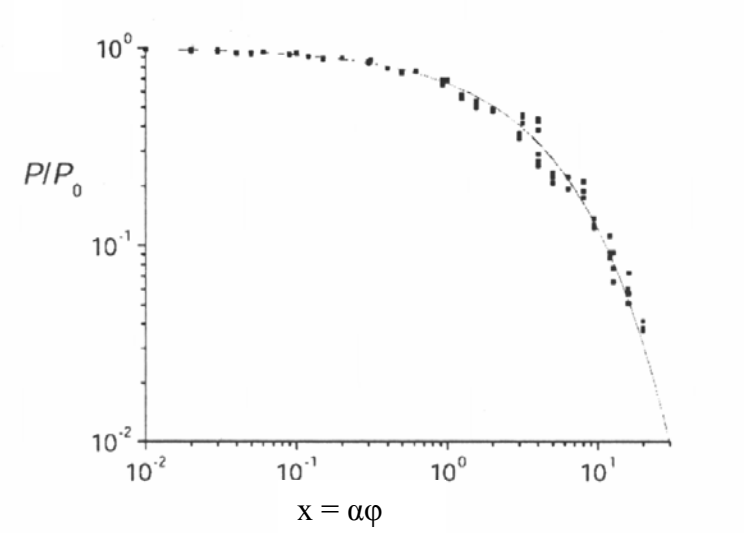


**Fig. 1.14: Relative permeability coefficient predicted by finite element model [Source: Gusev and Lusti, 2001]**

The most recent theoretical model which aims to calculate the permeability of a polymer-nanoclay composite addresses the effect of degree of orientation of the clay platelet, its aspect ratio and the extent of exfoliation (Bharadwaj, 2001). The deduced equation is a modified form of the Nielsen's expression (Equation 1-3 and 1-4) which incorporates an order parameter, S (Equation 1-9), to account for the degree of orientation of the clay platelets. This equation now known as Bharadwaj-Nielsen model is given by Equation 1-10.

$$S = \frac{1}{2}\left\langle 3\cos^2\theta - 1 \right\rangle \qquad \textbf{1-9}$$

$$\frac{P}{P_m} = \frac{1-\varphi}{1+\alpha\varphi(\frac{2}{3})(S+\frac{1}{2})} \qquad \textbf{1-10}$$

The physical meaning of the order parameter is shown by Fig. 1.15. This model predicted that an increase in permeability by a factor of four with a decrease in aspect ratio by a factor of seven and hence extent of exfoliation as the major factor which controls the barrier property of a clay nanocomposite. Also, orientation was shown to have a significant effect on the permeability characteristics of the nanocomposite, especially in the lower aspect ratio range of 50-250 (the typical range of aspect ratio exhibited by MMT).

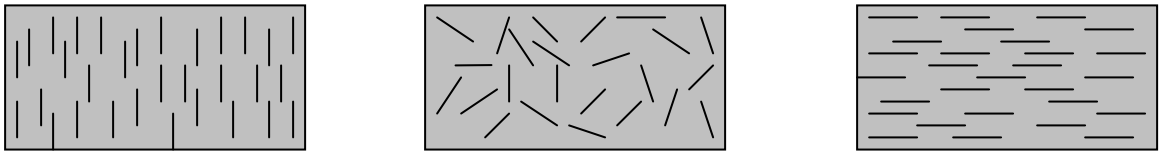

**S= -1/2** **S=0** **S=1**

**Fig. 1.15: Schematic explaining the physical meaning of order parameter, S used to quantify the degree of orientation of platelets in Bharadwaj-Nielsen model [Bharadwaj, 2001]**

## 1.3 Objectives

Polymer-nanoclay composites have gained importance because nanoclay has the potential to improve rigidity and gas barrier properties with little effect on ductility, toughness and optical transparency. Enhancement in properties depends on the internal structure of the nanocomposite like arrangement of clay platelets, crystallinity and crystalline orientation of the matrix polymer. The gas barrier properties especially are enhanced by the increase in tortuosity effected by above stated structural factors and which is dependent on the spacing between the nanoplatelets and orientation of the clay platelets (Bharadwaj, 2003; Russo et al., 2006). Conventionally, the only way to achieve decreased spacing between the platelets and thereby increased tortuosity and decreased permeability is by increasing the overall clay content of the nanocomposite (Liang et al., 2001; Li and Shimizu, 2006; Russo et al., 2006). As expounded in the rationale (Section 1.1), decreased clay spacing could be achieved without increasing the overall clay content of the nanocomposite by localizing the platelets within numerous thin layers forming a multi-layered nanocomposite. Also, conventional mixing-based processing techniques cannot control the orientation of the clay platelets within the bulk of the nanocomposite (Ray and Okamoto, 2003; Fornes and Paul, 2003, Russo et al., 2006). On the other hand, a continuous processing technique based on chaotic advection has been able to produce blends and composites with in-situ multi-layering and a variety of different structures derived from the multi-layer structure at the same compositions (Zumbrunnen and Inamdar, 2001; Zumbrunnen et al., 2002; Chougule and Zumbrunnen, 2005). The structures are evolved in chaotic advection blending instead of broken down as in conventional methods and hence can be controlled. Chaotic advection was shown to be capable of manipulating the orientation and arrangement of particulate

additives within the bulk of the matrix (Danescu and Zumbrunnen, 1998 & 2000; Zumbrunnen et al., 2002; Mahesha et al., 2005; Chougule et al., 2005). Hence, the purpose of this study is to produce novel nanocomposites with multi-layered structure and high degree of orientation necessary to achieve reduced gas permeability. The objectives are specifically:

1. To characterize and document various internal structures of nanocomposite films produced with the continuous chaotic advection blender. .
2. To assess the ability of continuous chaotic advection blender to control the internal structure in terms of orientation and placement of the platelets.
3. To evaluate the effect of structure on oxygen permeability, mechanical and optical properties of nanocomposite films.
4. To compare the theoretically predicted permeabilities with those measured for nanocomposite films.

.

# CHAPTER 2

# 2 EXPERIMENTAL METHODS

## 2.1 Materials

Polyamide-6 (PA6) was identified as the matrix material taking into consideration its ability to form exfoliated clay nanocomposites. Capron B135QP, a cast and blown film extrusion grade nylon-6, was acquired from BASF, Mt. Olive, NJ. Cloisite 30B, which is an organically modified nanoclay compatible with PA6 was purchased from Southern Clay Products (SCP), Gonzales, TX. The two were compounded in twin-screw extruders to produce masterbatches with different concentrations of modified clay. The compounding was performed using the services of a few polymer compounding industries over the course of the study.

The initial masterbatch that was produced had a loading of 4 wt% Cloisite 30B (4% MB) and was prepared by Standridge Color Corporation (SCC), Social Circle, GA. This specific loading was used as literature available (Dennis et al., 2001) suggested that the clay could be effectively dispersed as individual nano-platelets in the matrix at this concentration. The exfoliation was essential to test the effectiveness of the chaotic advection blender to manipulate the structural arrangement of nano-platelets which is one of the objectives of this study. To study influences of clay concentration, a set of additional masterbatches with 7%, 8% and 10% Cloisite 30B were produced at 21$^{st}$ Century Polymers, Fort Worth, TX, a compounding service suggested by SCP.

Table 2.1 lists the masterbatches used. These masterbatches along with virgin Capron B135QP served as the starting resins for nanocomposite film production using the continuous chaotic advection blender.

**Table 2.1: List of various PA6-nanoclay masterbatches used during this study**

| Sample ID | PA6 grade | Clay type | Manufacturer |
|---|---|---|---|
| 4% MB | Capron B135QP | Cloisite 30B | Standridge Color Corp. |
| 7% MB | Capron B135QP | Cloisite 30B | 21st Century Polymers |
| 8% MB | Capron B135QP | Cloisite 30B | 21st Century Polymers |
| 10% MB | Capron B135QP | Cloisite 30B | 21st Century Polymers |

## 2.2 Film Processing

### *2.2.1* Drying

PA6 has a tendency to absorb moisture from the air. At high temperatures employed during processing, any moisture present causes degradation of the polymer (Brydson, 1982). Hence, both virgin PA6 and PA6-nanoclay masterbatch pellets were dried at 80°C under 30 in-Hg vacuum (Cho and Paul, 2001). The time for drying varied from one to three days depending on the amount of moisture in the material, which was monitored by drop in vacuum of the system. Once the vacuum stabilized indicated by a steady vacuum reading of 30 in-Hg, the heating was turned off. The material was then allowed to cool to room temperature and stored under vacuum. Required amount of the material was retrieved from the vacuum oven and transferred to the feed hoppers having a continuous nitrogen purge for processing.

### *2.2.2* Continuous chaotic advection blending

A photograph of the laboratory set up of a chaotic advection blending in operation is shown in Fig 2.1. The assembly consisted of two identical single screw extruders on each side of the blender, each having a length to diameter ratio of 24. The screw extruders are not clearly seen in Fig. 2.1 due to the process control panels. Hence a schematic of the set up with the important parts of assembly is shown in Fig. 2.2. As shown in the schematic, the feed hoppers of the extruders were purged with high purity nitrogen to prevent resins from absorbing atmospheric moisture. The screw extruders discharged to geared metering pumps which in turn were connected to the chaotic blender through a transfer flange. The basic design of the continuous chaotic blender is illustrated in Fig. 2.3. A detailed mechanical design and construction of the continuous chaotic blender and its principles of operation have been described in earlier publications (Gomillion, 2000; Zumbrunnen and Inamdar, 2001; Dhoble et al., 2005; Chougule and Zumbrunnen, 2005; Zumbrunnen et al., 2006). The blender by itself was an assembly of an oval shaped barrel with two cylindrical stir rods and melt distribution blocks. Dimensions of blender components are given in a recent publication (Zumbrunnen et al., 2006). The stir rods were connected to stepper motors through a gear box with computer programmable controls. Zonal electric heaters with precise process control and display units (Fig. 2.1) were attached to the entire set up and wrapped with insulation to prevent heat loss. The blender was connected to a die with a simultaneous linear taper and transverse expansion to shape the melt. The coat-hanger film die used in this study is shown in Fig. 2.3. It had a die lip of 150 μm and a width of 23 cm.

**Fig. 2.1: CCB laboratory setup shown here in operation. Also seen is a closer view of the film exiting the die onto a chill roll**

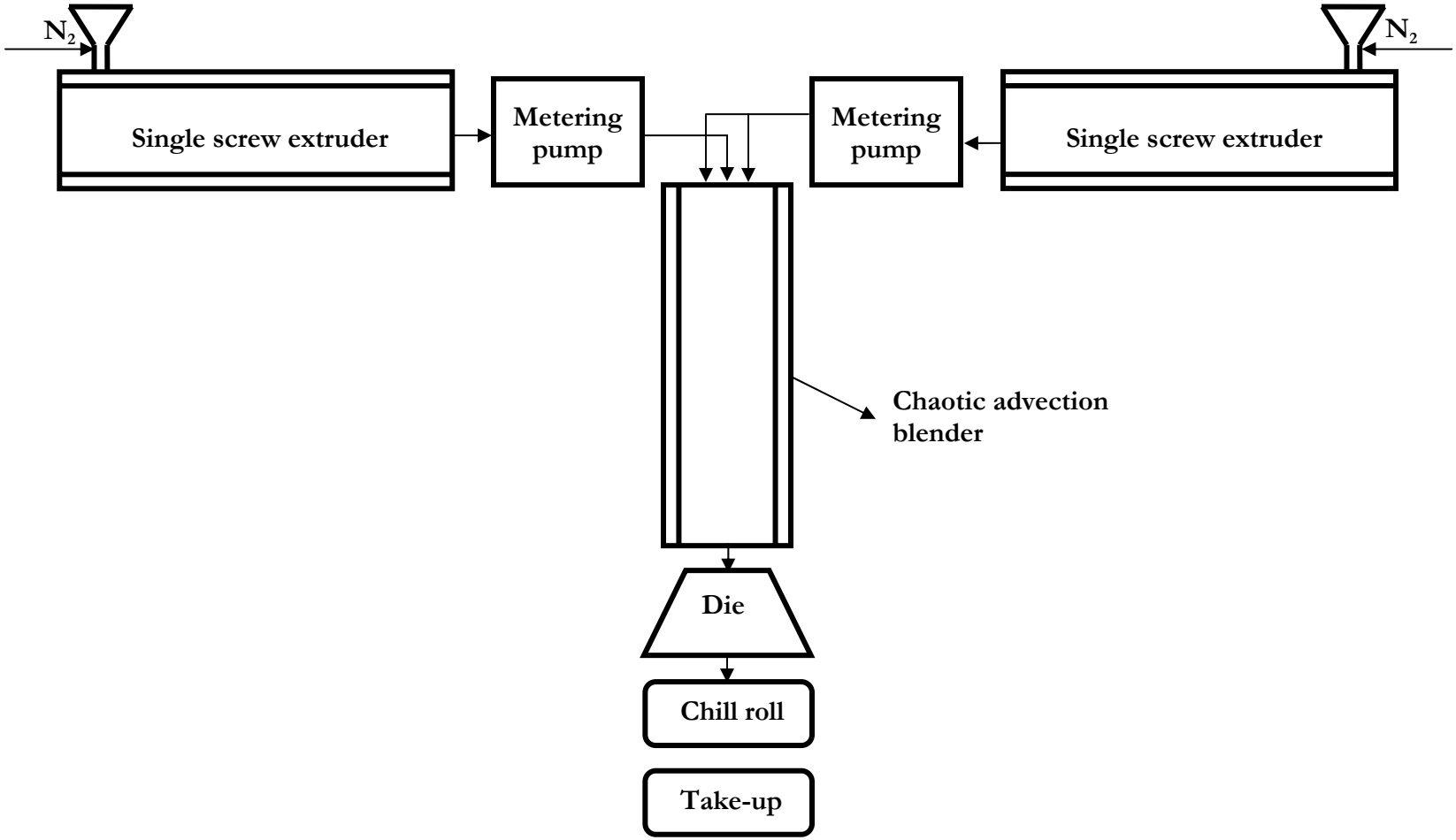


**Fig. 2.2: Flow schematic of the chaotic advection blending process. The schematic shows the different units the resins pass through before being taken up as films.**

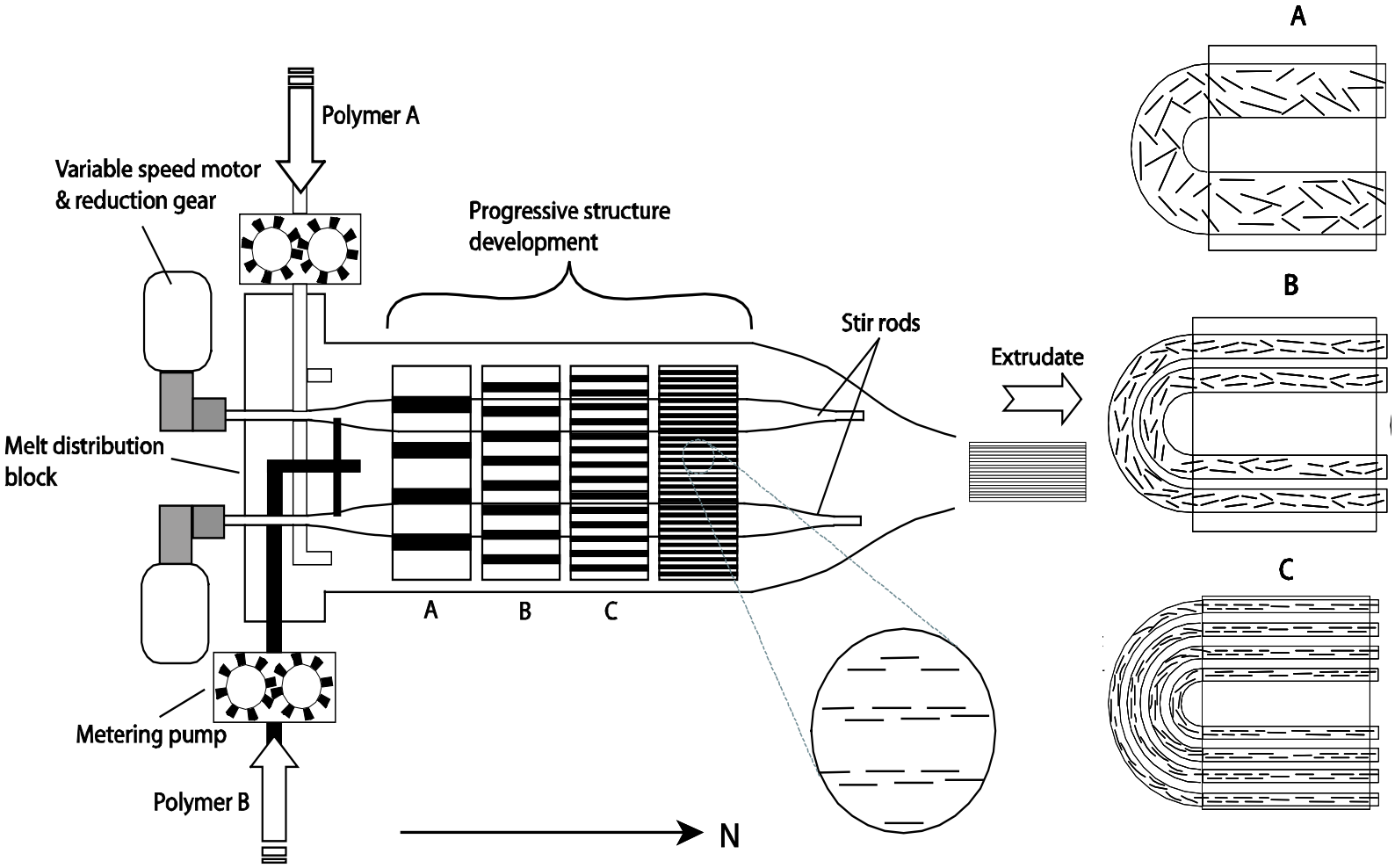


**Fig. 2.3: Schematic of the continuous chaotic blender showing progressive structure development and resulting platelet alignment.**


**Fig. 2.4: Photo showing the faces of the coat-hanger die used in this study**

To obtain structured nanocomposite films, vacuum oven-dried pellets of PA6 and masterbatch were fed separately into the single screw extruders through hoppers. Depending on the extruder into which the material was fed, the melt could either be injected through a central port or through peripheral distributed ports (white melt domain or dark melt domain respectively in Fig. 2.3). The metering pumps at the end of the extruders controlled the volumetric feed rates of the melts into the continuous chaotic advection blender. The required metering pump speeds for major and minor components were calculated from the required volumetric throughput, Q and input into the controls. The melt inside the blender was subjected to chaotic advection by sequential rotational motion of two stir rods (Zumbrunnen and Inamdar, 2001; Zumbrunnen et al., 2002; Dhoble et al., 2005). The rods

were first rotated at a relative rotational speed of ratio 1:3. The relative rod rotation speed was then reversed, so that the previously faster rotating rod now rotated at the slower speed. One pair of rod speed alterations constituted one 'N', a measure of amount of chaotic advection. The sequence of the two stir rods and the relative speed ratio, known as the perturbation strength ($\mu$=3), was chosen so as to attain chaotic advection through out the volume of blender (Dhoble et al., 2005). The stir rod sequence and speed were controlled by two stepper motors (gear ratio of 1:10). The speed of rotation of the stir rods was a function of the melt residence time within the chaotic advection blender t and the final steady state N and was calculated as follows. The average melt speed through the blender was $v = Q/A$ where 'A' was the area of cross-section of the chaotic blender. The melt residence time was thus, $t \approx L/v$ where L is the effective length of the barrel where chaotic advection is induced. Since each N consisted of a pair of stir rod rotations with a perturbation strength $\mu$, the input value of faster rotating rod ($\omega_f$ , RPM) was evaluated by the total number of rod $2N/\mu t$. The speed of the slower rotating rod was then calculated as one third of $\omega_f$.

The melt flowing through the blender was structured in response to chaotic advection. The two melt domains were recursively stretched and folded as shown by the horse-shoe mapping intrinsic to chaotic advection on the right hand side of Fig. 2.2. This repetitive stretching and folding can lead to a multi-layered structure as shown in Fig. 2.2 (rectangular insets within the blender with alternating black and white bands) with progressively finer layers (Zumbrunnen and Inamdar, 2001; Zumbrunnen et al, 2002; Kwon and Zumbrunnen, 2003). Also, of interest to this study, shear forces present in the blender may cause orientation of platelets and the inherent shuffling action of chaotic advection within the blender may concurrently lead to volumetric orientation in the bulk of the film.

The structured melt coming out of the blender was passed through the coat-hanger die of Fig. 2.4 to obtain nanocomposite films. Films exiting the die were cooled by contacting a pair of chilled rolls and taken up on the winding roll. A typical temperature profile employed during the film processing is given in Table 2.2.

**Table 2.2: Temperature profile of continuous chaotic advection blending system**

| Location | Extruder zones | | | Metering pump | Transfer | Blender zones | | | Die | Chill roll |
|---|---|---|---|---|---|---|---|---|---|---|
| | 1 | 2 | 3 | | | 1 | 2 | 3 | | |
| Tempera-ture, ˚C | 255 | 265 | 265 | 265 | 265 | 265 | 265 | 265 | 265 | 34-35 |

Nanocomposite films in steady state and transient operating modes (Zumbrunnen, 2005 & 2006) with compositions listed in Table 2.3 were produced. In the transient mode, as explained in Chapter 1, films have a continuously evolving structure along the length of extrusion. In this mode, the stir rods were kept stationary until a steady flow of both melt components of the run was observed coming out of the die as coarse, continuous streaks. Then the stir rod motors set to required speed were started and the transient films were collected in a continuous fashion. The N values corresponding to each pair of rod rotations were marked with an indelible marker on the films as they exited the die. These films were produced to investigate transition of structure of nanocomposite films in terms of orientation and arrangement of clay platelets within the matrix, to characterize the different structures attainable using continuous chaotic advection blender, and to relate processing parameters to the structure. From this initial characterization, a few different structures and corresponding processing parameters were identified to produce long lengths of films with

similar structure (steady state mode). In the steady state mode, films were collected, once the parameters were set and the stir rod motors were started, after waiting for atleast 3 melt residence times. These films were then utilized for property testing.

**Table 2.3: List of films produced using continuous chaotic advection blender**

| Total clay (wt %) | N values | Central melt injection port (left extruder) | Peripheral melt injection ports (right extruder) |
|---|---|---|---|
| **0** | Transient: 1-25<br>Steady: 0, 25 | 50% of Capron B135QP | 50% of Capron B135QP |
| **2** | Transient: 1-25 | 50% of Capron B135QP | 50% of 4% Cloisite 30B MB |
| **2** | Transient: 1-22<br>Steady: 6, 10, 12, 14, 18, 22 | 50% of 4% Cloisite 30B MB | 50% of Capron B135QP |
| **2.8** | Steady: 8, 10, 12,15, 20, 25 | 70% of 4% Cloisite 30B MB | 30% of Capron B135QP |
| **3.5** | Steady: 0 | 50:50 premixed Capron B135QP and 7% Cloisite 30B MB | 50:50 premixed Capron B135QP and 7% Cloisite 30B MB |
| **3.5** | Steady: 7, 9, 11, 13, 20 | 50% of Capron B135QP | 50% of 7% Cloisite 30B MB |
| **5.6** | Steady: 0 | 70:30 premixed Capron B135QP and 8% Cloisite 30B MB | 70:30 premixed Capron B135QP and 8% Cloisite 30B MB |
| **5.6** | Steady: 7, 9, 20 | 70% of 8% Cloisite 30B MB | 30% of Capron B135QP |

Note that melt residence time within the blender is calculated using the average value of melt velocity ($v$) through the blender satisfying the volumetric throughput requirement, Q.

In reality, there is a distribution of melt residence time within the processing equipment due to the various flow paths (and their different lengths) followed by each stream or particle. The waiting period before the collection of films ensured that the melt with longest residence times from the prior runs of the blender exited the die. It also promoted structural uniformity of the collected steady state films. For the transient mode, waiting period was the same as above, but without the stir rod motion. In general, chaotic advection in the blender gives a narrower melt residence time distribution than occurs in pipe flows (Joshi and Zumbrunnen, 2005).

### *2.2.3* Biaxial stretching

Post-processing, the cast die films obtained from CCB were biaxially stretched in a biaxial stretcher apparatus (Model Karo IV, Bruckner, Siegsdorf, Germany) by Dr. Ajji Abdellah at the Industrial Materials Institute of The National Research Council of Canada (IMI-NRC), Boucherville, Canada. The apparatus and the sample clamping unit are shown in Fig. 2.4. A sample of dimensions 10 cm x 10 cm was used. A stretching speed of 5%/s was utilized based on industrial practice where film stretching is used. Prior to stretching, the sample was preheated for a 30 second period to the required stretch temperature to ensure uniformity of temperature across the sample. The required temperature of stretching was determined through initial trials on virgin PA6 and PA6-nanoclay films. First, a near glass transition temperature ($T_g$) of 60°C was chosen to minimize thermally induced crystallization. Though this temperature was low and close to $T_g$ some thermally induced crystallization was observed in each sample and was different leading to partial crystallization in some and complete crystallization in others. This posed difficulty in maintaining consistency and hence

a higher temperature range near melting 190°C - 210°C was screened. After some trials in higher temperature range, 200°C was found to perform well for all samples ensuring complete thermal crystallization and good reproducibility in stretching. Samples were simultaneously stretched along the machine direction and the transverse direction. Three stretch ratios (defined as the final dimension to the original dimension of the sample in each direction of stretching) of 1.5x1.5, 2.0x2.0 and 2.5x2.5 were employed for each sample.

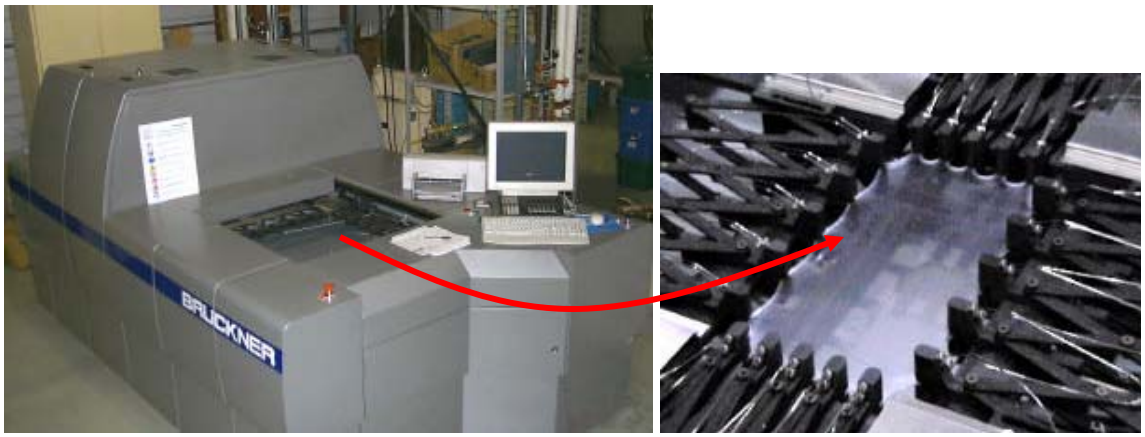


**Fig. 2.5: Bi-axial stretcher apparatus with a closer view of the stretching elements**

## 2.3 Material Characterizations

### *2.3.1* Rheology

An ARES rheometer (TA instruments, New Castle, DE) was used to measure the viscosity of all resins prior to chaotic blending. This was a precautionary step to determine whether viscosities were below an acceptable level that would not result in exceeding torque limits of motors used to rotate the stir rods (Fig. 2.2 and 2.3). Also, it enabled documentation of viscosity ratio of the materials and observation of its effect, if any, on the final films obtained

from the blender. Initially, measurements of PA6 and 4% clay masterbatch in the pellet form were carried out with a standard cone and plate geometry (25 mm plate, 0.056 mm gap and 0.1 rad cone angle). The measurements were made in a steady state, strain-controlled mode. The viscosity data of Capron B135QP and 4% clay masterbatch are plotted in Fig. 2.6. The shear rates within the blender ranges from $0.5s^{-1}$ to $1.5s^{-1}$. The viscosity ratio was about 4 for virgin PA6 and 4% masterbatch in this shear rate range.

The increased clay content in the subsequent 7%, 8% and 10% masterbatches presented difficulties in compressing the sample to the required small gap of a cone and plate geometry. Hence a switch to parallel plate geometry (25 mm plates) was made. For the parallel plate rheometric experiments, discs of diameter 25 mm and thickness 3 mm were prepared by compression molding. The discs were placed between the plates of the rheometer and compressed to the lowest gap possible (~ 2mm), before starting the viscosity measurements. Even with this procedure, viscosity measurements were not possible for the higher clay content masterbatches. The increase in clay content appeared to increase the stiffness of the melt making it difficult to compress without exceeding the torque limits of the rheometer. It is well known that increasing the clay content increases the shear stress and the zero-shear viscosity but exhibits shear thinning and viscosities similar to the matrix at high shear rates (Krishnamoorti et al., 1996; Aalaie et al., 2007). Considering this and the excessive shear thinning demonstrated by the 4% MB, decision was made to use the masterbatches. The 7% and 8%masterbatches were successfully processed but 10% MB could not be melted and processed satisfactorily by the system.

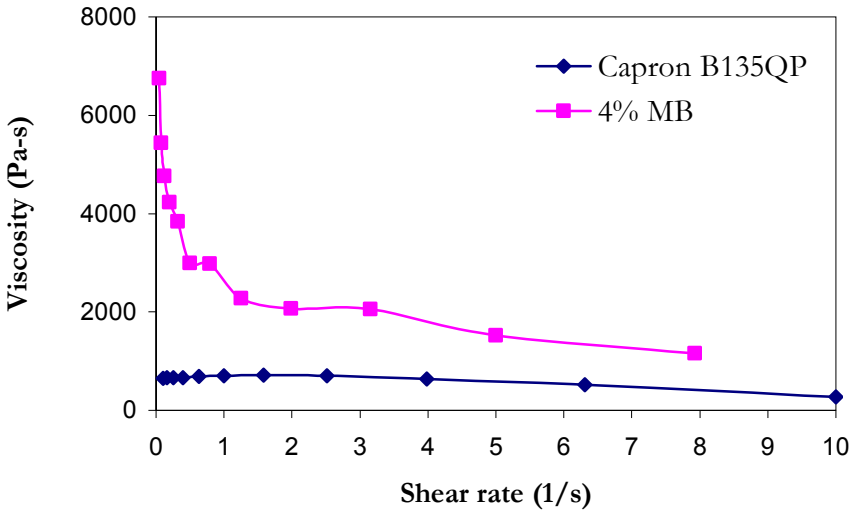


**Fig. 2.6: Comparison of viscosities of virgin PA6 and PA6-4% nanoclay masterbatch**

### *2.3.2* Thermal analysis

**Thermo-gravimetric analysis (TGA):** 2950 Hi-Res Thermogravemetric Analyser (TA instruments, New Castle, DE) was used to determine thermal stability of PA6 and thereby identify the processing temperature which can be employed in the chaotic blender. A 10-15 mg sample of PA6 was placed on a standard Indium pan in a closed furnace and heated in the presence of nitrogen at a rate of 20°C/min to different temperatures above the melting temperature. Both PA6 and the PA6-nanocaly masterbatches were shown to be stable up to 275°C under nitrogen atmosphere for a prolonged time of 3 hrs. A temperature of 265°C was utilized in processing taking into account shear heating within the extruders of the processing machine.

This method was also utilized for initial estimate of clay content in the masterbatches by heating a sample of about 10 mg of the masterbatch at a rate of 20°C/min from 25°C to 800°C with an air purge. An average of residue of 3.669% was obtained from heating three

samples of the masterbatch. This test provided only a rough estimate of the clay content in the masterbatch.

### *2.3.3* Ash content

The masterbatches were subjected to ash content test to determine and confirm the percentage of clay present in them. The tests were carried out according to ASTM 5630-01. Porcelain crucibles were fired at the operating test temperature of 900°C for 20 minutes to burn off any residue and then cooled to room temperature. The empty crucible was weighed and its weight noted ($w_1$). The required amount of sample (ASTM 5630-01) was placed in the porcelain crucible and the combined weight of sample with crucible recorded ($w_2$). Then it was placed in a furnace set at 900°C for 30 minutes for complete ignition of the organic material. The crucibles were then allowed to cool to room temperature in a desiccator and weight of the cooled crucible with the residue was recorded ($w_3$). Ash content, its corresponding inorganic clay content (% MMT) and organic clay content (%OC) were calculated using the following equations (Fornes et al., 2001).

$$\%\,ash = \frac{w_3 - w_1}{w_2 - w_1} \qquad \textbf{2-1}$$

$$\%MMT = \frac{\%\,ash}{0.935} \qquad \textbf{2-2}$$

$$\%\,OC = \%\,ash\left[\frac{30}{70} - 0.065\right] + \%MMT \qquad \textbf{2-3}$$

The factor 0.935 in Equation 2-2 accounts for the structural water loss from MMT. The expression for % organic clay content (Equation 2-3) accounts for the 30% organic content of Cloisite 30B. The data obtained from this test showed that all the masterbatches produced

had final clay contents close to that of the specified amount of Cloisite 30B as shown in Table 2.4.

**Table 2.4: Clay content of masterbatches determined by ash content experiment**

| Masterbatch | % ash | % MMT | % OC (Standard deviation) |
|---|---|---|---|
| **4% MB (SCC)** | 2.791 | 2.987 | 4.002 (0.070) |
| **7% MB (21CP)** | 4.593 | 4.913 | 6.623 (0.045) |
| **8% MB (21CP)** | 5.379 | 5.752 | 7.707 (0.104) |

### *2.3.4* Film thickness

Thicknesses of each of the steady state film rolls were measured using a micrometer (Digimicro MF-501, Nikon Instruments Inc., Melville, NY) with an accuracy of 1 μm. Thicknesses at 100 different locations of the film across its width and along a length of ~0.5 m were recorded for each roll of film. These measurements were recorded to observe the variation in thickness between films as thickness variation is known to affect physical properties like impact strength, tear strength and haze. An average value of these readings is presented for each film in Table 2.5.

**Table 2.5: Thickness variation among the different rolls of films produced and tested**

| Clay (wt%) | N value | Average thickness (μm) | Standard deviation (μm) |
|---|---|---|---|
| **0** | **0** | 111.05 | 10.00 |
| | **25** | 114.84 | 6.50 |
| **2.8** | **8** | 115.87 | 6.28 |
| | **10** | 114.32 | 7.63 |
| | **12** | 115.55 | 7.81 |
| | **15** | 98.85 | 5.61 |
| | **20** | 99.41 | 6.32 |
| | **25** | 115.99 | 6.20 |
| **3.5** | **0** | 145.24 | 37.05 |
| | **7** | 144.059 | 13.95 |
| | **9** | 136.22 | 16.80 |
| | **11** | 128.10 | 16.08 |
| | **13** | 118.20 | 16.78 |
| | **20** | 138.86 | 21.46 |
| **5.6** | **0** | 131.63 | 18.83 |
| | **7** | 129.54 | 25.60 |
| | **9** | 118.14 | 25.57 |
| | **20** | 117.14 | 36.29 |

## 2.4 Structural Investigation

### *2.4.1* TEM

The internal structure of the nanocomposites in terms of nanoclay platelet orientation and arrangement was visually characterized by transmission electron microscopy. H-7600T, (Hitachi, Japan) located in the electron microscopy facility at Clemson University was used for this purpose. The instrument consists of a TEM column, CCD camera and TV camera system with an image processing unit and a control PC (Fig. 2.7). Operating accelerating voltages ranges from 40 to 120 kV for this instrument. Thin specimens of about 100 nm were cut from film samples at -80 °C using a cryomicrotome (RMC Powertome X, Boekler Instruments, Tuscon, AZ) shown in Fig. 2.8 and placed on copper grids with a thin carbon coating. For preliminary investigation of the first set of films, sections were extracted randomly from different regions of the film. For further detailed structural documentation, different regions were marked along the width of the films as shown in Fig. 2.9 with L and R denoting the left and right side of the film as it exits the die. Sections were extracted from any 3 non-symmetrical regions (L3, L1 and R2 or R3, R1 and L2) in the plane perpendicular to imaging direction (Fig 2.9). The grids were placed in a grid box with proper identifications. The grid box was then placed in a desiccator to remove any moisture. This prevented contamination of the TEM vacuum chamber and destabilization of specimens during examination under the scope. The specimen was examined under the electronic scope by placing the grid on a single specimen holder. An accelerating voltage of 120kV and beam current of 21 μAmp were used for imaging. The image was captured by the TV camera attached to the scope and stored on the computer attached to the system.

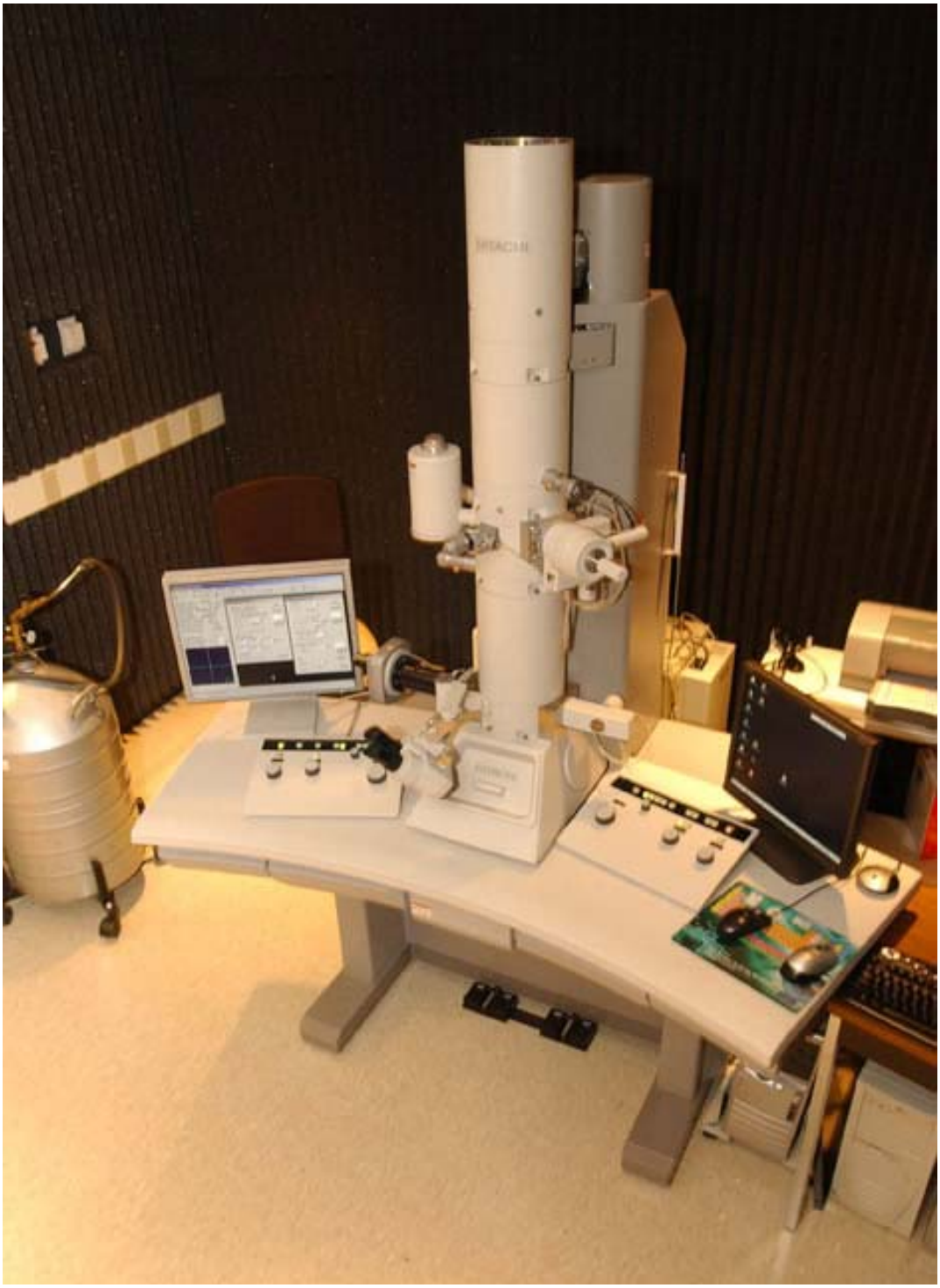

**Fig. 2.7: Model H-7600T electron microscope (Hitachi, Japan) used during the course of this study**

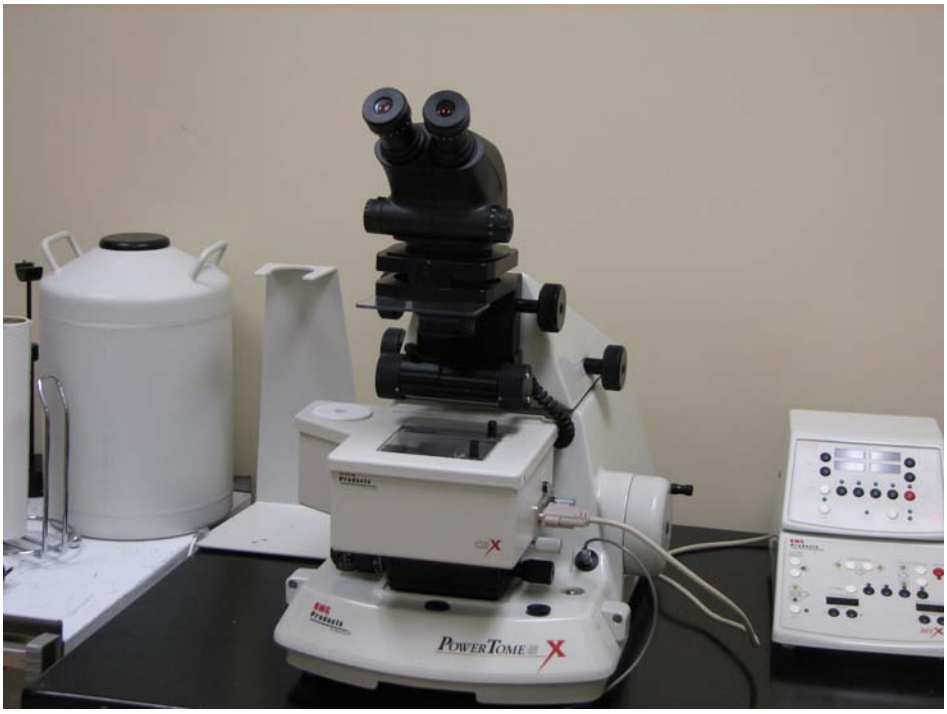


**Fig. 2.8: Cryomicrotome utilized to cut thin specimens for observation under TEM**

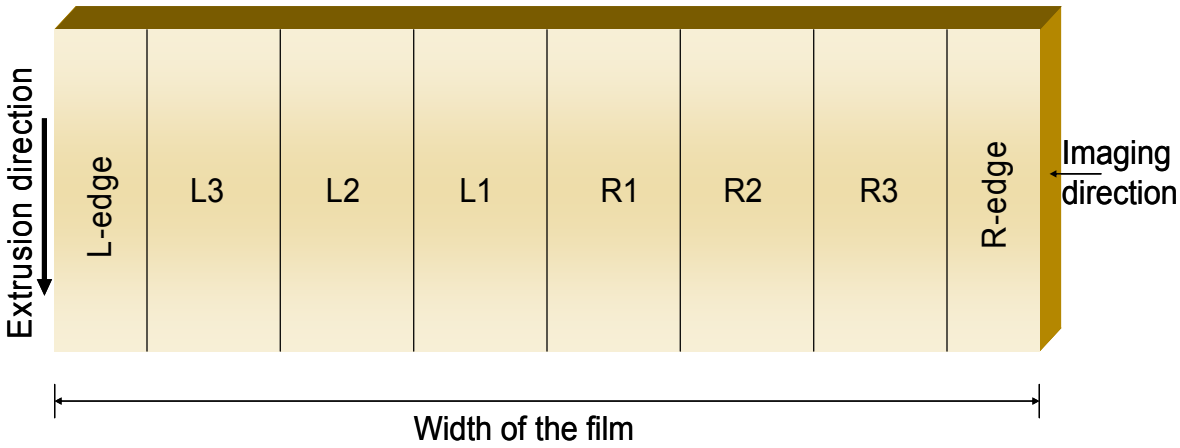


**Fig. 2.9: Schematic showing a layout of different locations of films examined under TEM**

### *2.4.2* X-ray diffraction

X-ray diffraction techniques were employed to characterize the crystallinity and crystalline morphology of virgin PA6 and the PA6 matrices of the nanocomposites. (X-ray characterizations were carried out by Mr. Dilru Ratnaweera and Dr. Dvora Perahia at Dept. of Chemistry, Clemson University as part of collaborative work.) A powder diffractometer operating at CU kα (λ=1.54Å) provided information on structural features in the 0.1nm to 10nm range, such as the crystalline to amorphous ratio and the crystal forms of PA6 (Li, 2006; Fornes, 2003; Arimoto, 1965). Another X-ray instrument with a single crystal setup equipped with CCD detector and a molybdenum radiation operating at λ=0.7Å was used to determine the orientation of polymer crystals.

### *2.4.3* Differential scanning calorimetry (DSC)

TA instruments Q1000 DSC (New Castle, DE) was used to estimate crystallinity levels of films. For this, a sample of about 10 mg was weighed into a standard DSC pan, covered with a standard lid, and placed in the DSC instrument. It was then heated at a controlled rate of 10°C/min upto 265°C under nitrogen atmosphere. The degree of crystallinity was calculated as the ratio of heat of fusion per gram of PA6 in the sample to heat of fusion of a 100% crystalline PA6 reference value of 240 J/g (Fornes and Paul, 2003). At least three specimens extracted from three different regions similar to TEM were tested for each film type.

## 2.5 Property Evaluations

The nanocomposite films obtained from continuous chaotic advection blender were tested for various properties, as detailed below.

### *2.5.1* Optical microscopy

The physical properties are known to depend on the surface quality of the film. The quality of the films produced using the laboratory scale equipment was not identical for all the sets. Hence, in order to account for this variation in quality among the different sets of films on their properties, an optical microscope (Meiji Techno RZ, Japan) was employed in the transmission mode.

### *2.5.2* Oxygen transmission rate

Oxygen permeability through the film was tested per ASTM F1927 using an OX-TRAN 2/21 module SL (Mocon Controls Inc., Minneapolis, MN). A schematic of the module obtained from the manufacturer's brochure is given in Fig. 2.10. The tests were carried out at 50% RH and at 23°C and were conducted by Mr. Kyle LaDean as part of the collaborative effort with American Plastics, Rhinelander, WI. The film samples were cut using a standard template that contained a circular test area of 50 $cm^2$. The thicknesses at a minimum of 10 different locations on the film sample were measured for each specimen. Test specimens were placed within the diffusion cell, which consisted of two metal halves. A good seal was ensured by the presence of an O-ring on one side (oxygen side) of the diffusion cell. Each Ox-tran module had two such diffusion cells. Once the specimens were in place, the residual oxygen was purged using nitrogen as a carrier gas. The carrier gas was routed through the sensor until a stable zero was established. This procedure also helped to ensure that no leaks were present in the system. The test gas, 99.9% pure oxygen was then introduced into the outside chamber. The diffusing oxygen was conveyed by the carrier gas to the sensor and the

readings recorded by the software connected to the system. The test was terminated when a stable constant value of transmission rate was reached.

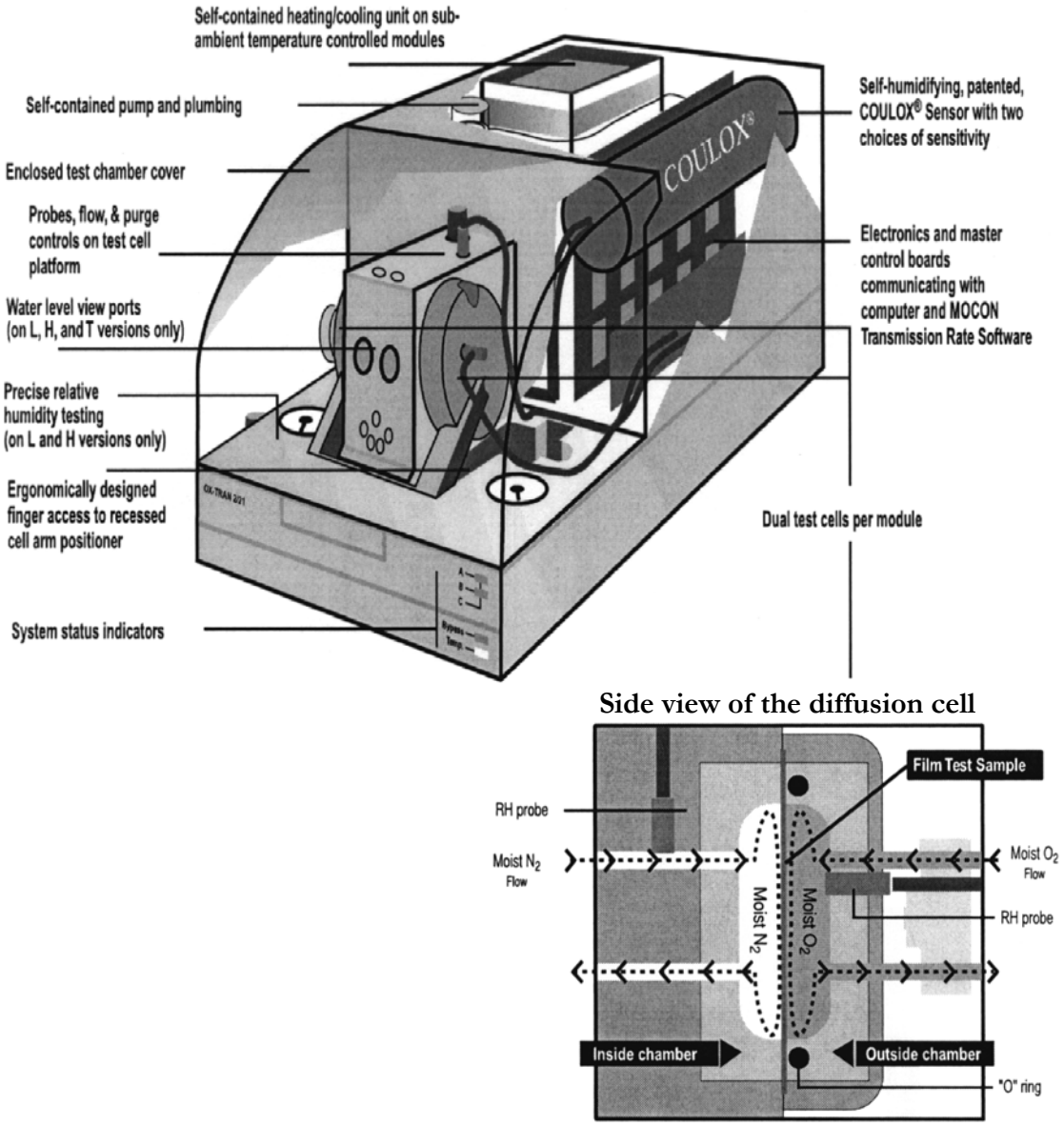


**Fig. 2.10: Schematic of an OX-TRAN 2/21 module showing the different functional parts of the unit and principle of operation of the diffusion cell [http://www.mocon.com/oxtran221.php]**

### *2.5.3* Tensile properties

Tensile properties of the films were tested on Tensile Tester 3343 (Instron, Norwood, MA) in both machine and transverse directions. Specimen size and test parameters were determined using the procedure described in ASTM D882. Rectangular specimens of width of 1 inch and length of 5 inches were cut using a specimen cutter. A gauge length of 2 inches and a constant strain rate of 500 mm/min were used for all samples. The specimen thickness was recorded from atleast 7 different points, using a micrometer, before clamping the specimen between fixed and movable grips of the testing machine. Five specimens in each direction were tested for each sample.

### *2.5.4* Tear strength

Tear strength, which is an important property for a packaging film, was determined using an Elmendorf tear tester (Thwing-Albert Instrument Co., PA) as per ASTM D1922. Test specimens were cut both in machine and transverse directions of the films samples using a template. Fig. 2.10 illustrates the specimen geometry used. The specimen of this geometry compensates for the problem of oblique tearing resulting from any deviation of the axis of maximum orientation of polymer chains from the machine direction. Average thickness from atleast seven readings was computed prior to testing. The specimen was then clamped and a slit of 20 mm made at the center of the edge, perpendicular to the direction to be tested, using a sharp knife at the bottom of and between the clamps. The test was conducted by releasing the pendulum and tearing the specimen. The force required to propagate tearing of the film was read via a pointer and a pre-calibrated scale connected to the pendulum.

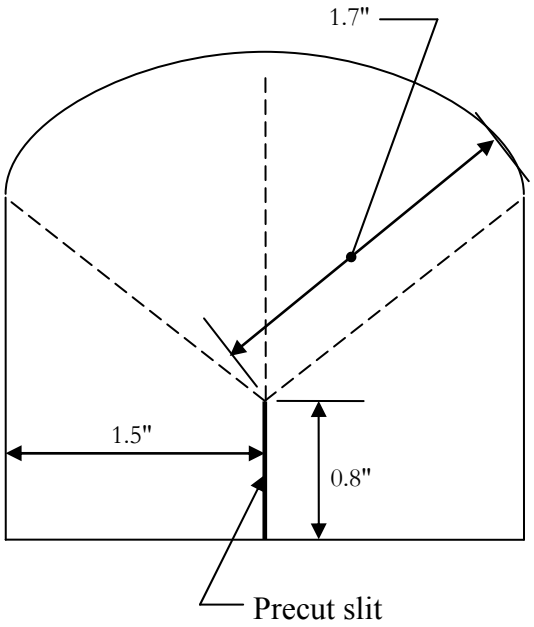


**Fig. 2.11: Constant-radius test specimen for tear resistance test with the dashed lines indicating the radius of tear**

### *2.5.5* Impact strength

A dart-drop impact testing machine (DDI-120, Dynisco, Ft. Lauderdale, FL) was used to determine the impact toughness of the film samples per ASTM D4272. The films were conditioned in a vacuum of 30 in-Hg for atleast 48 hrs prior to testing. This was done to remove the moisture present in the film samples and to ensure uniformity of all samples prior to testing. A dart weight of 1.415 kg and a drop height of 0.660 m were employed. The time for free-fall of the dart without any specimen was measured prior to the test. This was used as a baseline to calculate and record the impact energy required to rupture the films specimens. Five specimens were tested for each sample.

### *2.5.6* Haze

Optical clarity is an important factor for films for packaging applications. This was measured in terms of haze for the nanocomposite films to determine the effect of structuring. Haze is defined as "the percent of transmitted light that is scattered so that its direction deviates more than a specified angle from the direction of the incident beam". The optical clarity of the films was tested using a spherical hazemeter according to ASTM D1003. The hazemeter consisted of a light source capable of providing a unidirectional beam, a photodetector, and an integrated sphere to collect the transmitted flux. The specimen (a square of 2" side) to be tested was placed at the entrance port of the sphere. A calibrated dial in the instrument recorded the percentage haze. Again, five specimens were tested for each sample.

# CHAPTER 3

# 3 THEORETICAL MODELING

## 3.1 Unit cell permeability model

A theoretical model was formulated to study the effect of multi-layered structure and platelet orientation on the permeability of a composite with high aspect ratio and impermeable fillers like nanoclay. Permeability of a polymer as explained in Chapter 1 (Section 1.2.4) is a diffusion-controlled process (Vieth, 1991) and is governed by Fick's first law of diffusion (Equation 1-1). The diffusion across a pure polymer film or membrane can be assumed one-dimensional without much error as the concentration gradient essentially exists across the thickness of the system and is negligible along other dimensions of the film (Vieth, 1991).

Incorporation of high aspect ratio impermeable additives like clay introduces multi-dimensionality to the process. As shown in Fig.1.10, the diffusing molecule has to move along the lateral dimensions of film whenever it encounters the filler. Despite this, simple pseudo-1D diffusion models based on tortuosity arguments have been employed to predict permeabilities of composites (Nielsen, 1967; Cussler et al., 1988; Bharadwaj, 2001). The model due to Nielsen (1967) was found to predict the permeability of a composite as accurately as a three-dimensional finite element model in the range of volume fraction ($\varphi$) and aspect ratio ($\alpha$) currently employed for melt-processed thermoplastic nanocomposites ($\varphi\alpha<10$) (Gusev and Lusti, 2001). At higher values of $\varphi\alpha$, the tortuosity model underestimated the improvement in barrier properties. In order to explore the whole range

of volume fraction and aspect ratio of platelets within a multi-layered structure, the current model was formulated on the basis on the three-dimensional finite element model by Gusev and Lusti (2001).

### *3.1.1* Geometry

An idealized geometry was specified for the arrangement of platelets in the composite as shown in Fig. 3.1. The composite consists of well-defined alternating platelet-rich layers and pristine polymer layers in series along the diffusion direction. The important assumptions made about the composite structure of the model are the following:

- The composite comprises of only two distinct isotropic materials namely the platelets and the polymer matrix.
- There are equal numbers of platelet-rich and pristine polymer layers in the composite.
- All platelet-rich layers are of identical thickness $t_1$ and all pristine polymer layers are of thickness $t_2$.
- The volume fraction of the platelets $\varphi_l$ within each platelet-rich layer is the same.
- The platelets are randomly but homogenously dispersed within each layer.
- All platelets are circular discs of diameter $l$ and thickness $h$.
- All platelets are perfectly aligned within the matrix.
- Fick's law is assumed to be applicable.

For convenience, layer thicknesses were expressed as thickness fractions $\beta$ and $\lambda$. Fraction $\beta$ was defined as the ratio of the thickness of pristine polymer layer to that of

platelet-rich layer ($t_2/t_1$). Thickness fraction of the platelet-rich layer $\lambda$ was defined as the ratio of the thickness of platelet-rich layer to the sum of the thickness of the two layers i.e., $t_1/(t_1+t_2)$. By this definition and inspection of the geometry, the overall platelet composition of the composite $\varphi_c$ was given by $\varphi_l\lambda$. Table 3.1 further clarifies the relationship between these fractions and their physical meaning.

The geometry is related to the nanocomposite films produced as described in Section 2.2.2. In nanocomposite films platelets have nano-scale dimensions. However, effects stemming from nano-scales such as crystalline morphology changes were not taken into account. The thicknesses of the layers have a distribution with an average represented by the idealized geometry of Fig. 3.1. At early stages of chaotic advection, the volume fraction of platelets within the platelet-rich layer is almost equal to the volume fraction of the injected masterbatch and the average thickness fraction $\lambda$ of the layers is equivalent to the volumetric feed ratio of the virgin polymer and masterbatch into the blender. The stretching and folding mechanism of chaotic advection causes the platelets to orient (Fig. 2.3). But with increased chaotic advection, the number and thickness of virgin layers decrease as the layers become thinner and platelets from the platelet-rich layer encroach on them. This implies that $\beta$ decreases and $\lambda$ increases, and the volume fraction of platelets within the platelet-rich layer decreases ($\varphi_l = \varphi_c / \lambda$). Eventually $\lambda$ tends to 1 when the platelet arrangement approaches that of a dispersion due to fine scale structuring by chaotic advection. Hence, as chaotic advection is prolonged, the average distance between the platelets increases.

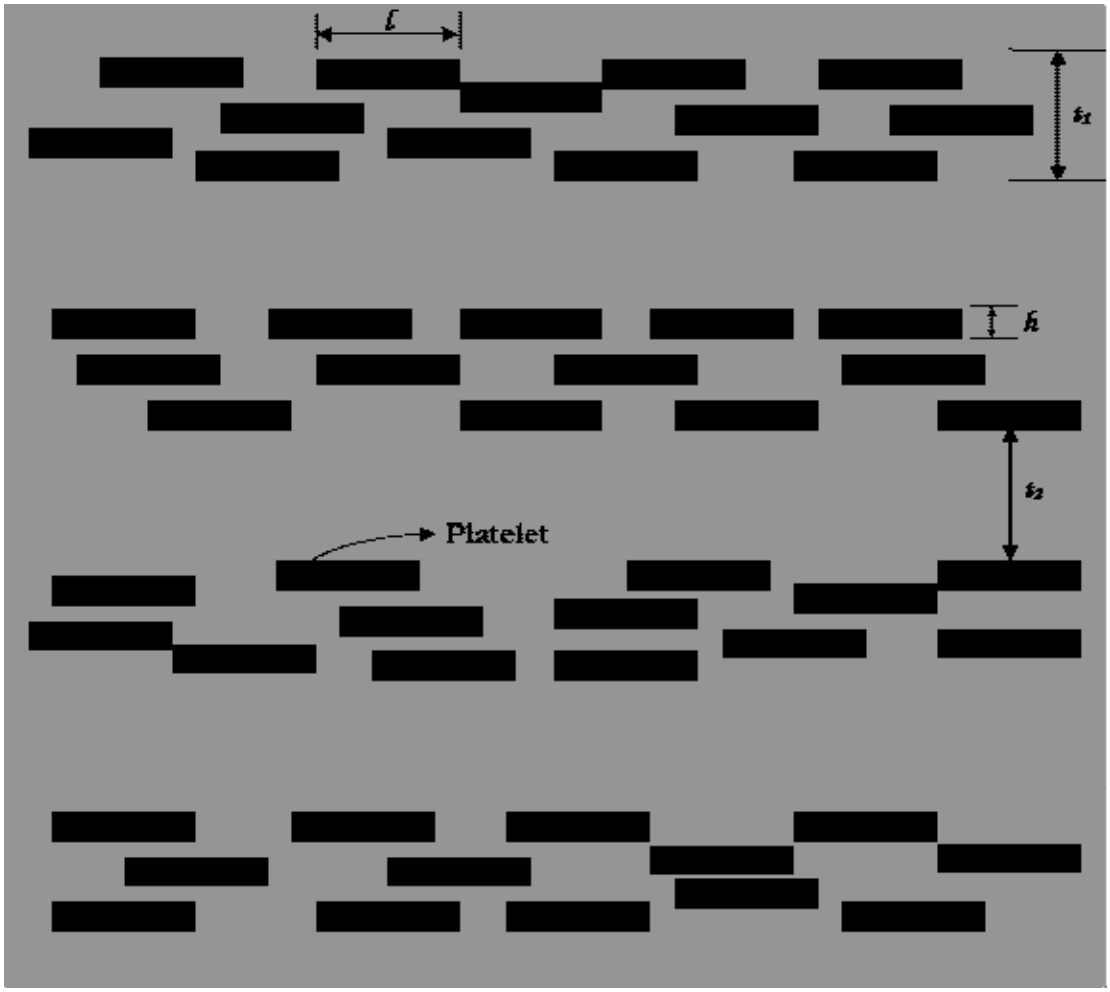


**Fig. 3.1: Characteristic geometry of the transport model employed to evaluate structural effects on the composites.**

**Table 3.1: Physical meanings of model parameters**

| λ | β | $\varphi_1$ | **Physical meaning** |
|---|---|---|---|
| 1 | 0 | $\sim\varphi_c$ | Homogenous dispersion of platelets within the matrix |
| 0.5 | 1 | $2\varphi_c$ | Platelet-rich and virgin layers of equal thickness |
| 0.1 | ~0.91 | $10\varphi_c$ | High volume fraction of platelets localized in a thin layer |
| →0 | →1 | →0 | Matrix polymer without platelets |

### *3.1.2* Governing equations

For layers containing platelets, an expression was utilized which was developed with a three-dimensional finite-element model of the permeability for a composite with randomly located round platelets which were perfectly aligned perpendicular to the diffusion direction (Gusev and Lusti, 2001). The expression was obtained by curve fitting of numerical predictions and is given in Equation 3-1 using the current model nomenclature. The permeability of the platelet-rich layer $P_p$ relative to the permeability of the matrix $P_m$ was thus given by

$$\frac{P_p}{P_m} = \exp\left[-\left(\frac{\alpha\varphi_l}{x_0}\right)^{\beta}\right] \qquad \textbf{3-1}$$

Here, $\alpha = l/h$ is the aspect ratio of the platelets, $\beta = 0.71$ and $x_0 = 3.47$ are the least-squares parameters obtained by curve fitting (Gusev and Lusti, 2001). Hence, with the inclusion of Equation 3-1, the model of this study accounts indirectly for three-dimensional transport effects within the platelet-rich layers.

By definition of the model geometry, platelet-rich layers and pristine polymer layers are arranged in series and have identical areas of cross-section. Hence from Equation 1-2, assuming the difference in densities of the two layers are negligible, permeability is a function of thickness of the layer (Kwon and Zumbrunnen, 2003; Osswald et al., 2006). Thus the overall composite permeability $P_c$ was a function of the permeabilities of the two types of layers and their thickness fractions. It was calculated using Equations 3-1 through 3-3.

$$\frac{1}{P_c} = \frac{\lambda}{P_p} + \frac{1-\lambda}{P_m} \qquad \textbf{3-2}$$

$$P_c = \frac{P_p P_m}{\lambda P_m + (1-\lambda) P_p} \qquad \textbf{3-3}$$

As indicated by the above equation, model permeability of the composite was independent of the number of pairs of layers present in the system.

The above governing equations were utilized in a MATLAB (Natick, MA) code to discern the effect of structure on the permeability of the composite. The parameters that were investigated were thickness fraction of the layers (β, λ), aspect ratio of the platelets (α) and the volume fraction of the platelets ($\varphi_l$, $\varphi_c$).

### 3.2 Modeling results

The effect of localizing aligned platelets within layers which leads to decreased spacing between the platelets at a constant overall clay content was investigated. The relative permeability of the composites with respect to permeability of the virgin polymer predicted using the mathematical expression (Equation 3-1) is plotted in Fig. 3.2 as a function of thickness fraction of the platelet-rich layers. An aspect ratio of 100 was specified for the platelets, which is a typical aspect ratio found in melt processed thermoplastic nanoclay composites (Dennis et al., 2001). Fig. 3.2 shows that the curves have large gradients at low λ and gradually become asymptotic as well dispersed condition is approached (i.e., $\lambda \rightarrow 1$ or $\beta \rightarrow 0$, refer to Table 3.1). The layer thickness fraction λ of the platelet-rich layer at which a sudden drop in relative permeability was observed corresponded to a layer fraction with very high localized clay content as shown in Fig. 4.1b.

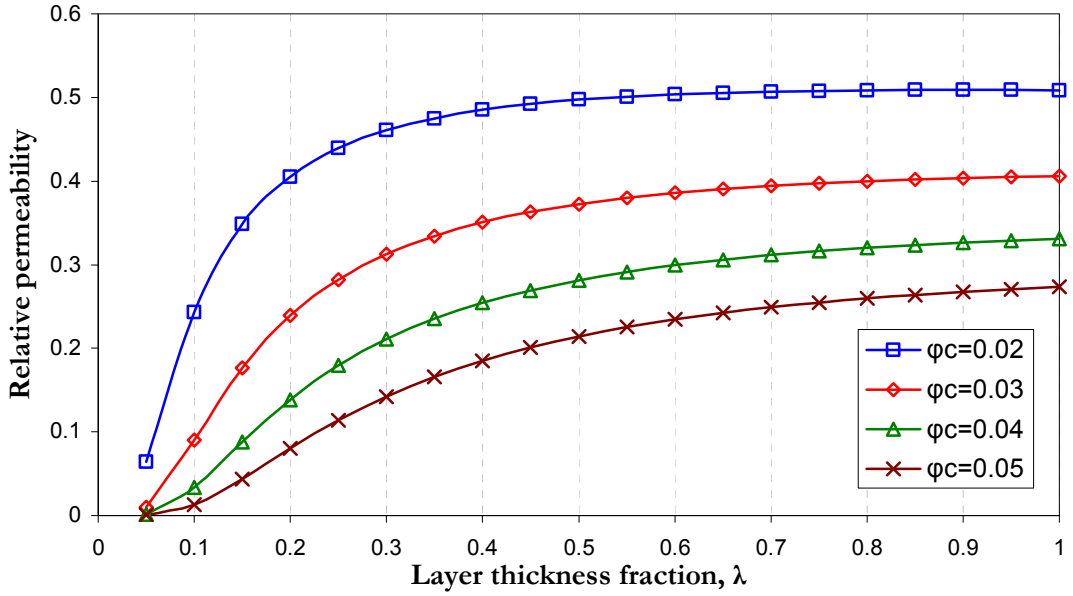


(a)

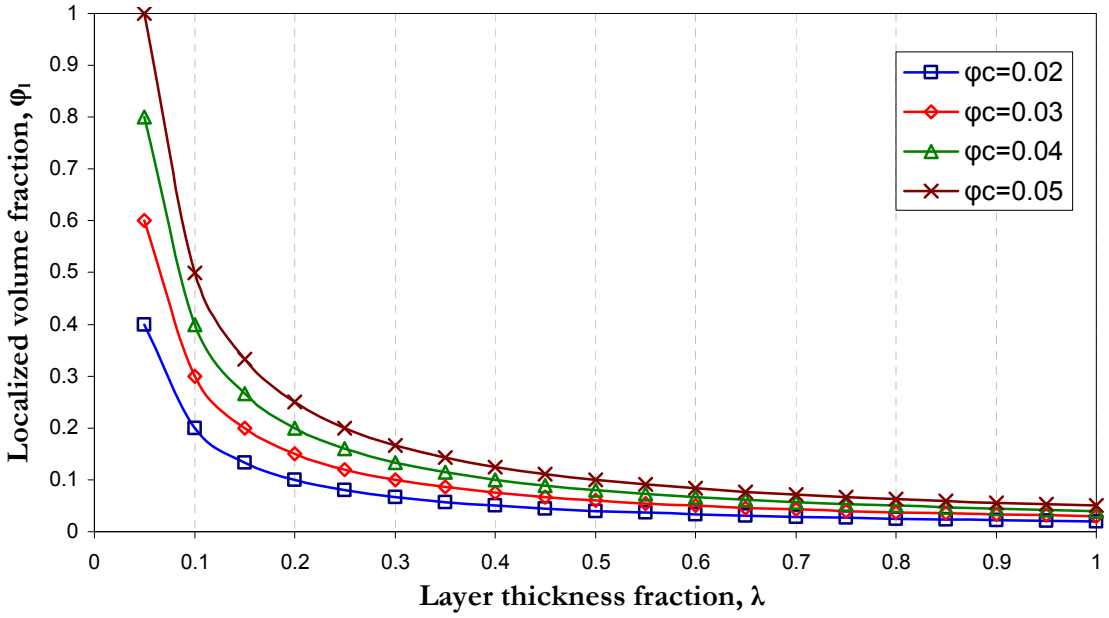


(b)

**Fig. 3.2: (a) Effect of multi-layered structure on relative permeability of the composite, (b) the volume fraction of the platelets localized in the platelet-rich layers corresponding to the layer thickness fraction of Fig. 3.2(a) for composites of different clay contents ( S=1, α=100)**

The layer thickness fraction λ required of a multi-layered structure composite to reduce the permeability by half with respect to a composite with homogenous dispersion of platelets (α=100) is given in Table 4.1. The volume fraction of platelets within the platelet-rich layer corresponding to λ is also given. The 50% reduction in permeability with a multi-layered structure was obtained when the local volume fraction of platelets was about 18%.

**Table 3.2: Thickness fraction of platelet-rich layers in a multi-layer composite required for 50% reduction with respect to a composite with homogenous dispersion of oriented platelets (S=1, α=100)**

| Net platelet content, $\varphi_c$ (vol%) | Thickness fraction, λ | Platelet content within layers, $\varphi_l$ (vol%) |
|---|---|---|
| 2 | ~0.11 | ~18 |
| 4 | ~0.24 | ~17 |
| 6 | ~0.34 | ~17 |
| 8 | ~0.43 | ~17 |
| 10 | ~0.5 | ~17 |

Hence at an aspect ratio of 100 and excluding crystalline morphology changes that may occur, the multi-layered structure was found to significantly change the permeability characteristics only when high concentration of platelets could be localized in very thin layers. Exfoliated masterbatches with such high nanoclay content are currently difficult to produce. Therefore, the effect of aspect ratio on the permeability of multi-layered structure was investigated next.

A plot of relative permeabilities for a constant overall content $\varphi_c$ but with different platelet aspect ratios (α) are given in Fig. 3.3. The volume fraction within the layers $\varphi_l$ corresponding to the layer fraction is also shown. The model shows that the effectiveness of

multi-layered structure is more significant when aspect ratio is increased. The permeability reduces almost linearly with thickness fraction at high aspect ratios as seen for $\alpha = 500$ in Fig. 3.4 where the reduction in permeability for a multi-layered structure ($P_{ML}$) in comparison to composite with homogenous dispersion ($P_H$) of aligned platelets is plotted. Thus, the model predicts that benefits of a multi-layered structure can be more effectively realized by employing low volume fraction masterbatches with high aspect ratio platelets.

Increasing the aspect ratio of the platelets increases the path length of the diffusing molecule especially when the platelets are perfectly oriented in a direction perpendicular to the concentration gradient. Localizing such high aspect ratio platelets within layers decreases the inter-platelet distance along both the direction of diffusion and the lateral directions. Thus the pathways available for permeation decrease and the permeability is reduced.

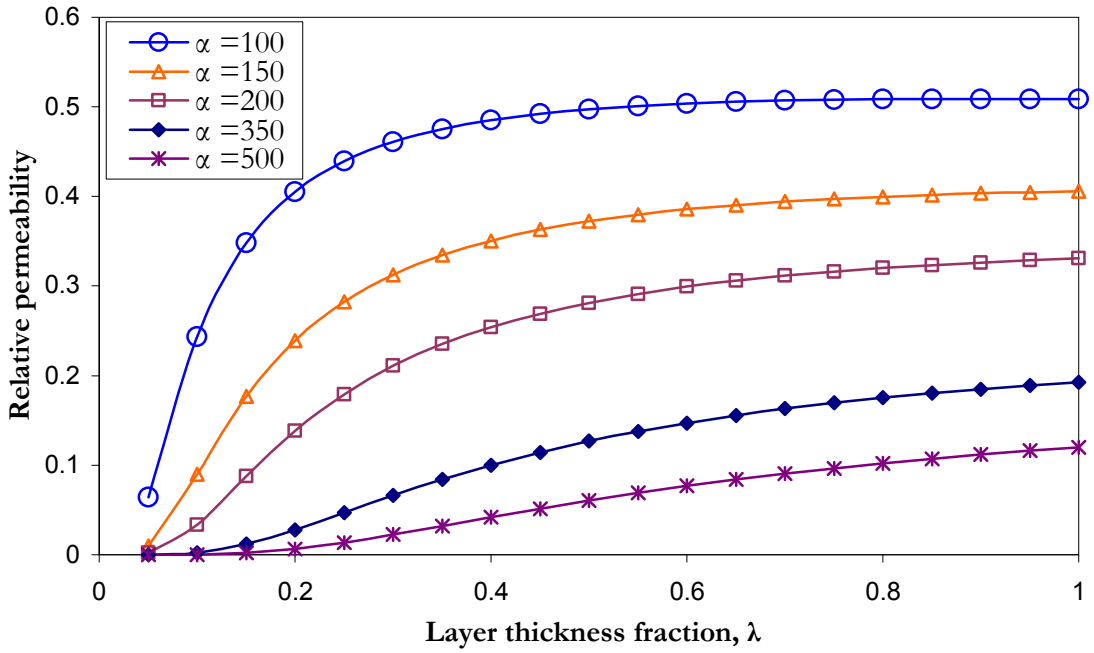


| Λ | 0.1 | 0.2 | 0.3 | 0.4 | 0.5 | 0.6 | 0.7 | 0.8 | 0.9 | 1 |
|---|---|---|---|---|---|---|---|---|---|---|
| $\varphi_l$ | 0.2 | 0.1 | 0.067 | 0.05 | 0.04 | 0.033 | 0.029 | 0.025 | 0.022 | 0.02 |

**Fig. 3.3: The significance of multi-layered structure on composites containing higher aspect ratio platelets ($\varphi_c$=0.02, S=1)**

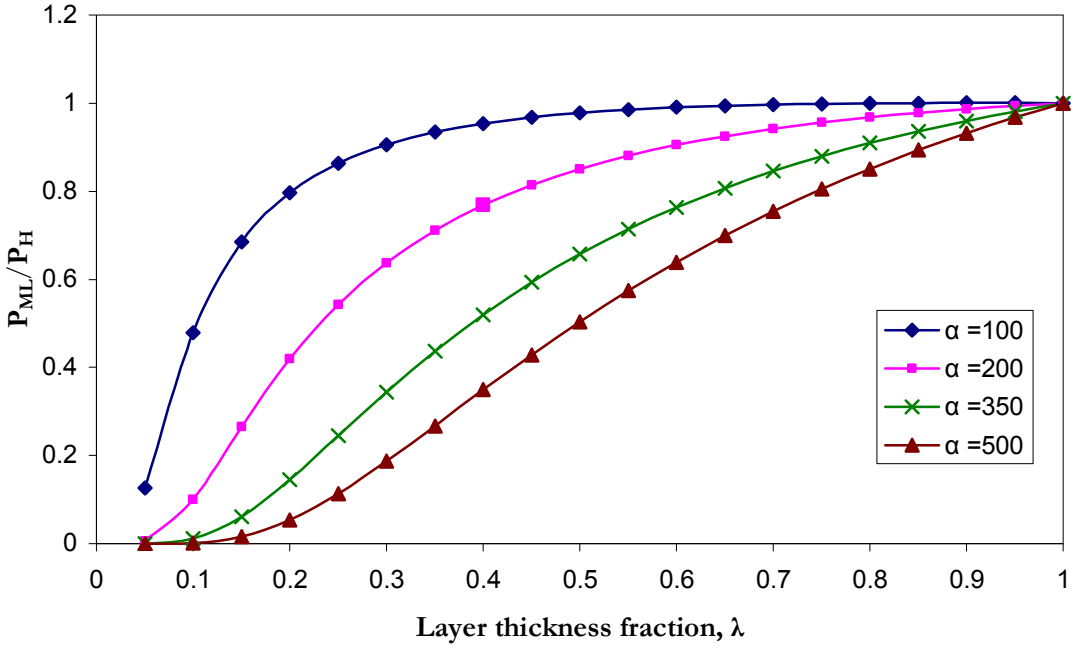


**Fig. 3.4: Influence on composite permeability of localizing platelets within layers where platelets are oriented ($\varphi_c$=0.02, S=1)**

### *3.2.1* Effect of chaotic advection on permeability

Finally, the overall advantage of localizing and orienting platelets in discrete layers was investigated in comparison to dispersion of platelets in matrix obtained through conventional processing methods. Utilization of conventional processing techniques results in nanocomposites having dispersed and unoriented platelets. So property improvements that might be derived from other structural arrangements have not been considered (Zumbrunnen, 2000; Ray and Okamoto, 2003; Zumbrunnen et al., 2006). The permeability of such a composite ($P_{S=0}$) was calculated using the mathematical model (Equation 1-10) due to Bharadwaj (2001). An order parameter S=0 was specified to account for unoriented

platelets (refer to Section 1.2.4). Since the model by Bharadwaj (2001) is based on the Fickian diffusion model by Nielsen (1967), the predictions at the range of overall volume fraction and aspect ratios investigated is identical to the permeability predicted by Equation 3.1 (Gusev and Lusti, 2001; Osman et al., 2004). The relative permeability of a structured composite produced by chaotic advection ($P_c$) in comparison to unstructured nanocomposite ($P_{S=0}$) is shown in Fig. 3.5. It is clear that both orientation and arrangement of platelets within the matrix have a pronounced effect on the barrier properties. The increase in orientation increases the lateral distance the diffusing molecule has to travel along the platelet while the multi-layering reduces the spacing between the platelets. Both lead to increased tortuosity and hence reduced permeability. The tortuosity is increased further and permeability reduced by increasing the clay content as shown by Fig. 3.5b. Being a low shear process, chaotic advection blending has an additional advantage over the high shear conventional techniques like screw extrusion. The chaotic advection blender can retain the aspect ratio of platelets during the processing and more effectively produce ultra-high barrier in-situ structured nanocomposites ($\alpha$>350 of Fig. 3.5).

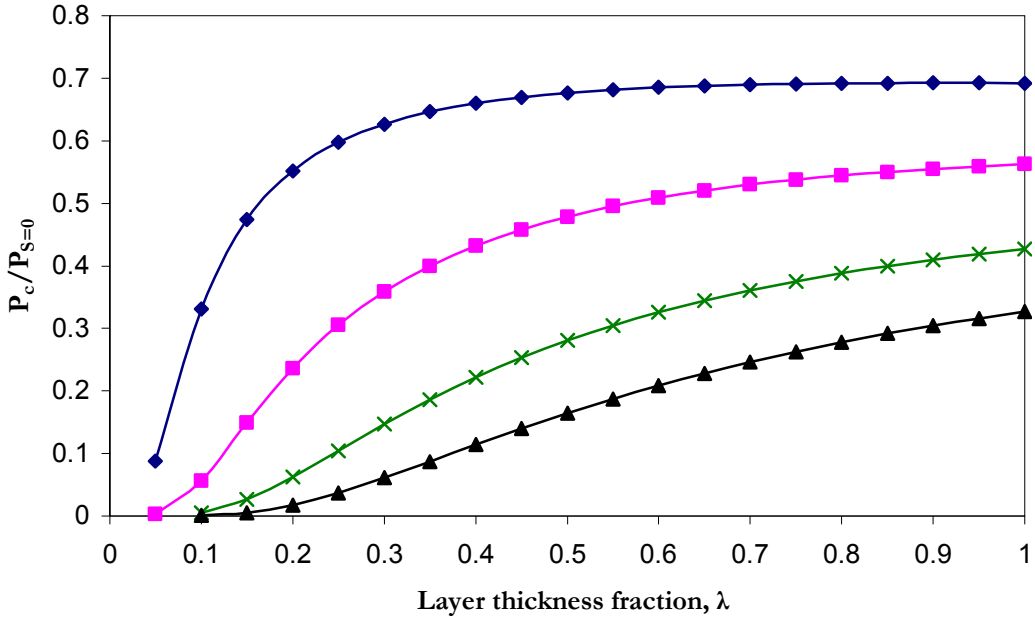


(a)

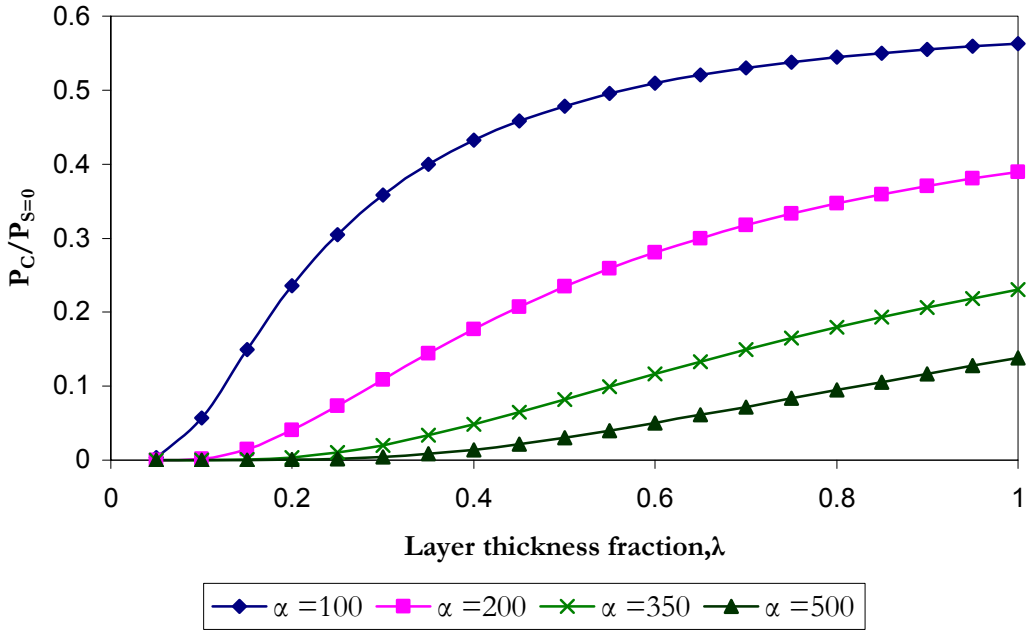


(b)

**Fig. 3.5: Theoretical permeability of a multilayer nanocomposite with S=1 in comparison to that of a nanocomposite produced by conventional mixing where S=0 for (a) volume fraction $\varphi_c$=0.02, (b) volume fraction $\varphi_c$=0.04**

# CHAPTER 4

# 4 RESULTS AND DISCUSSION

## 4.1 Structure

### *4.1.1* Structural examination by transmission electron microscopy

Fig. 4.1 shows micrographs of PA6-clay masterbatches used in the study. The clay appears as dark regions and the PA6 matrix as light grey regions. The nanoclay was observed to be well exfoliated in all masterbatches with platelets dispersed as individual platelets. Within the masterbatch, the platelets had a low degree of orientation within the bulk of the matrix as is the case typically with the mixing-based polymer processing technique like twin-screw extrusion used in masterbatch preparation.

#### 4.1.1.1 Transient films

Nanocomposite films with net clay content of 2 wt% were produced by feeding equal amounts of 4% MB and PA6 melts separately in to a continuous chaotic advection blender operated in transient mode as described in Section 2.2.2. Extruded film roll had different structures along its length that corresponded to differing extents of chaotic advection denoted in terms of the parameter N (Kwon and Zumbrunnen, 2001; Zumbrunnen et al., 2002; Dhoble et al., 2005; Zumbrunnen et al., 2006).

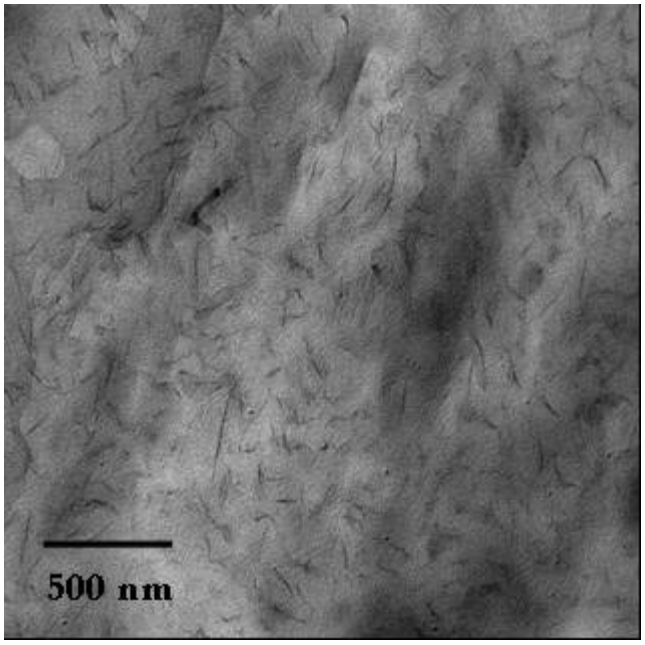


(a)

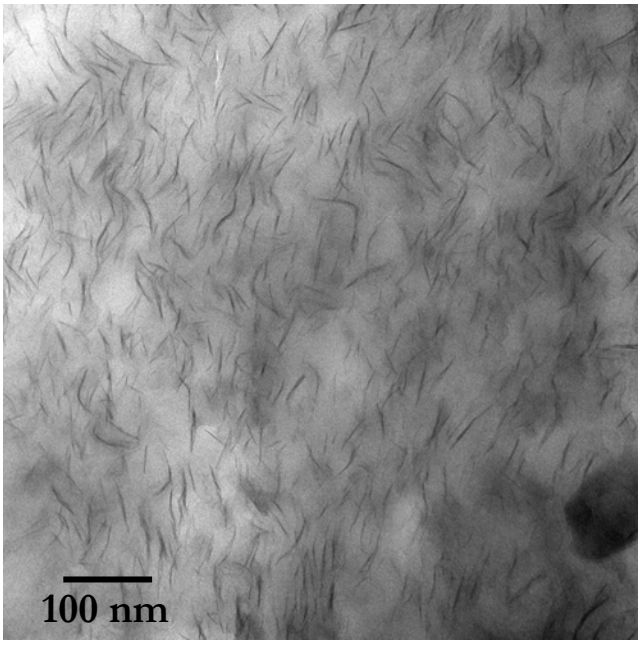


(b)

**Fig. 4.1: Images showing exfoliated and unoriented platelets in (a) 4% MB and (b) 7% MB pellets**

At the very early stages of chaotic advection like N=4, the orientation of clay platelets within the masterbatch layer were only slightly improved in comparison to the masterbatch pellets. This is illustrated by the image in Fig 4.2a. At these low values of N, the melt domains had very little time within the blender and were subjected to only small extent of chaotic advection. This is also evident in Fig. 4.2b showing thick layers of masterbatch and virgin PA6. As the melt domains experienced increasing number of stir rod rotation sequences, the stretching and folding (Fig. 1.4) which is an inherent character of chaotic advection imparted a novel in situ structure to the nanocomposite film. The nanocomposite had a multi-layered structure. The nanoclay platelets were placed in numerous discrete clay-rich layers which were separated by virgin PA6 layers as shown in Fig. 4.3a.

This novel arrangement of platelets within layers reduced spacing between the platelets at a low net clay loading. This localization of platelets and the accompanying decreased spacing could present an increased tortuosity to a diffusing molecule and improve the resistance of the nanocomposite to gas permeability as predicted by the theoretical model in Chapter 3. The reduced spacing may also lead to changes in the orientation of crystalline lamellae of the matrix polymer (Li and Shimizu, 2006) as shown in Fig. 1.9 (Chapter 1, Section 1.2.2). Hence, the physical properties of the films like tensile strength, impact strength and tear strength which are affected by the orientation of the polymer may also be affected (Sperling, 2006).

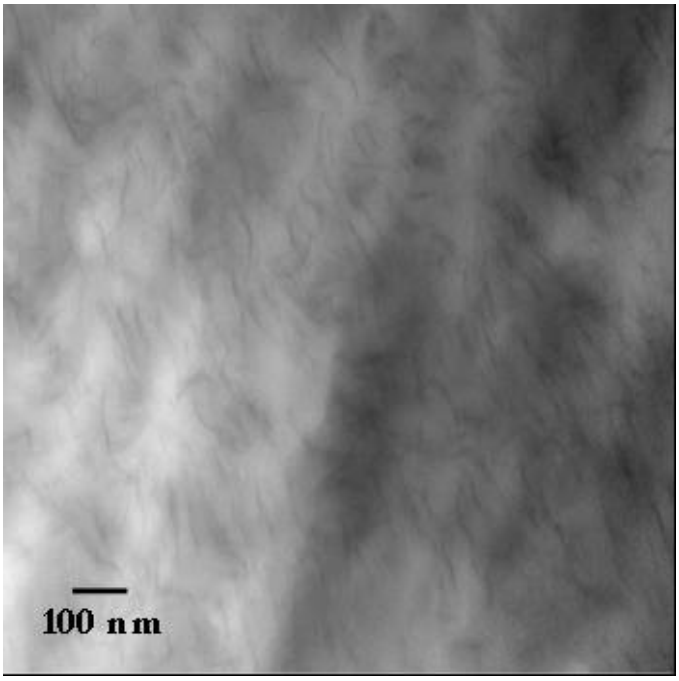


(a)

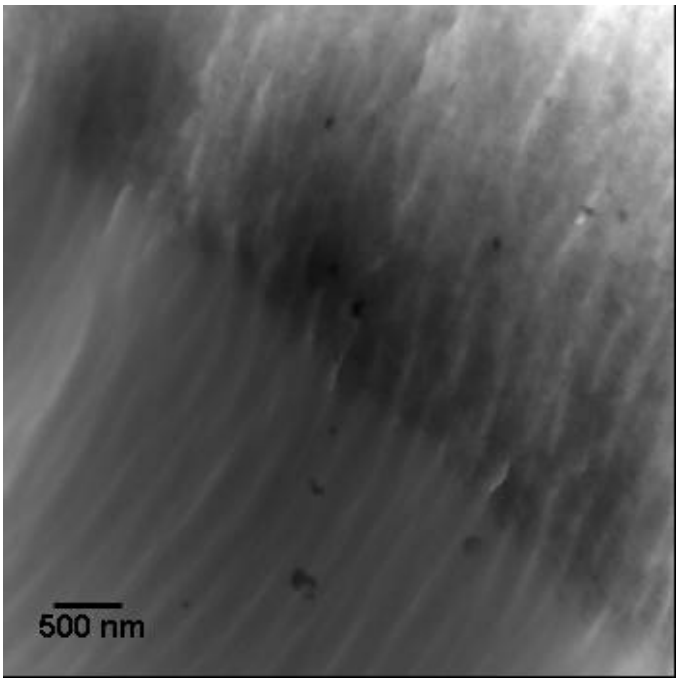


(b)

**Fig. 4.2: The internal structure of 2% nanocomposite of N=4 exhibiting (a) low degree of orientation and (b) coarse multi-layers**

Stretching of the masterbatch melt layers during chaotic advection also caused the high aspect ratio nanoclay platelets to orient along the flow direction and parallel to the film surface. The orientation mechanism due to layering was illustrated in Fig. 1.2. A physical example of this orientation is given by two micrographs of progressively higher magnification in Fig. 4.3b and Fig. 4.4. A detailed observation of the micrograph in Fig. 4.4 reveals the hierarchical nature of the nanocomposite structure produced by chaotic blender. The nanocomposite film with a thickness of ~150 μm has numerous alternating layers whose average thickness ranges from a few micrometers to a few hundred nanometers depending on the amount of chaotic advection. Within each clay-rich layer, the polymer matrix is again separated by ~1 nm thick clay platelets giving rise to a hierarchy of multiple orders of dimension. For clarity, this multiple scale of the nanocomposite is illustrated by the schematic in Fig. 4.4b.

The layer thickness reduced and the layers dissipated as the amount of chaotic advection induced on the melt domains increased. Fig. 4.5a shows a micrograph with a thin virgin layer in an otherwise clay-rich region. The alternate layering structure was no longer discernable as the thickness of the layers became comparable to the spacing between the platelets. The gradual structural evolution finally led to a nanocomposite with volumetrically aligned and homogenously dispersed nanoclay platelets in Fig. 4.5b.

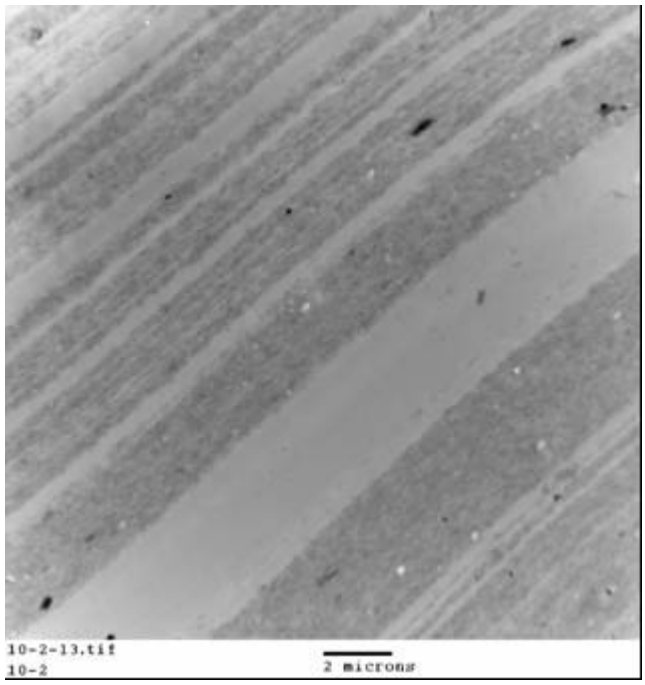


(a)

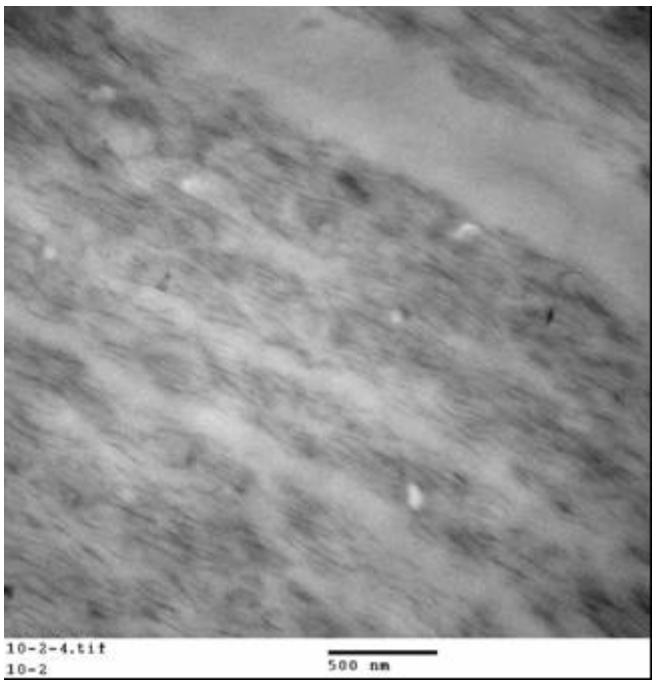


(b)

**Fig. 4.3: (a) Novel multi-layered structure formed at intermediate N of 10 and (b) high degree of orientation of the platelets along the film surface shown by a higher magnification image for same N**

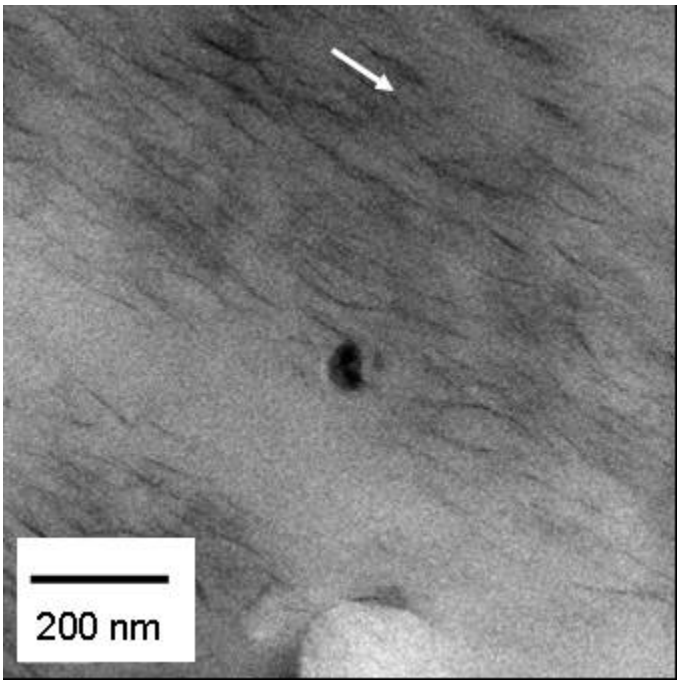


(a)

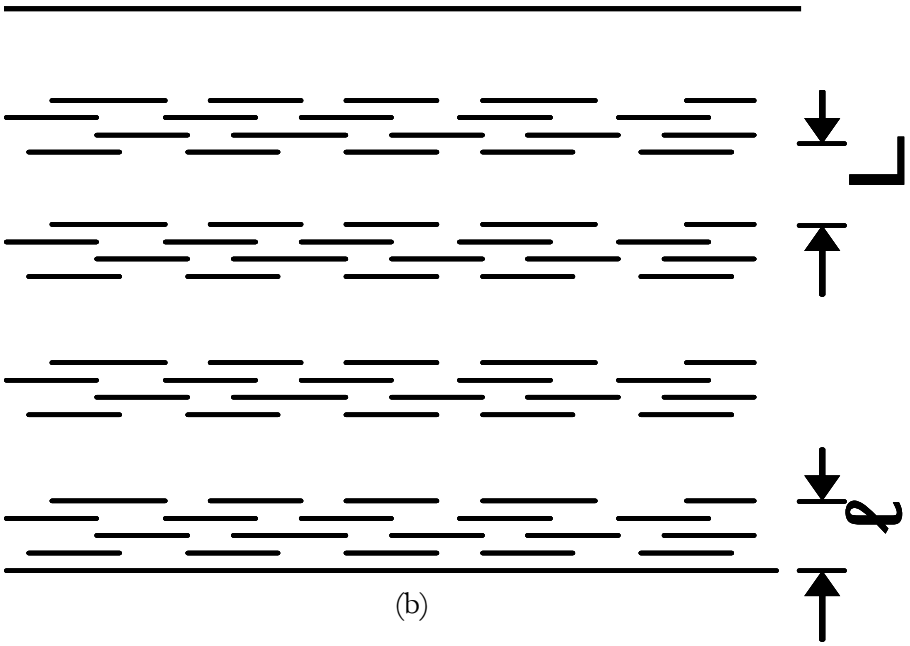


(b)

**Fig. 4.4: Hierarchical nature of in-situ multi-layered nanocomposite (a) Micrograph showing platelets oriented along the flow direction (marked by the arrow) at N=12, (b) Schematic illustrating the multiple length scales of the hierarchical structure.**

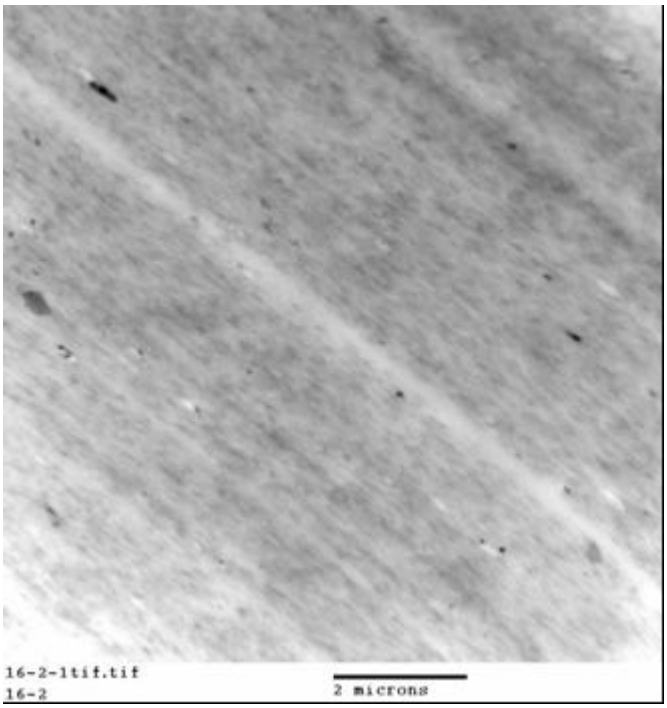


(a)

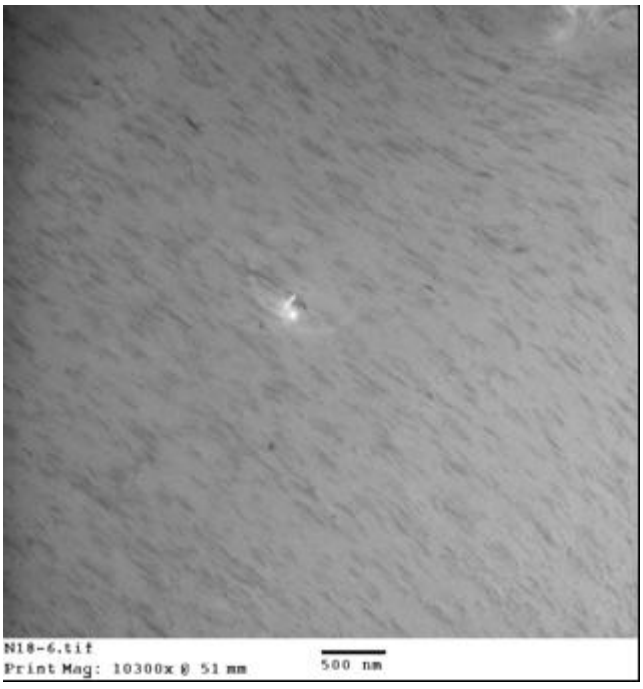


(b)

**Fig. 4.5: Increased dissipation of virgin layers with N (a) Thin and occasional virgin layers at N=16 leading to (b) homogenous dispersion of well-aligned platelets within the nanocomposite at N=18**

A computational simulation of passive particle motions in a continuous chaotic blender is shown in Fig. 4.6a (Dhoble et al., 2005). The simulation indicated that particle pathlines were predominantly tangential to the interior stir rod and barrel surfaces. The cluster of particles had a filament type geometry that oriented along the pathlines (Dansecu and Zumbrunnen, 1998). This was experimentally confirmed by the above micrographs obtained through TEM. However, simulation also predicted complex pathlines that intrinsically arise in chaotic flows where in-flow and out-flow manifolds of hyperbolic points intersect transversely (Ottino et al., 2000). Such complex pathlines may be indicated by the encircled regions in Fig. 4.6a. Anomalous structures, such as shown in the TEM micrograph of Fig. 4.6b, resulted in such regions where platelets were oriented to a lesser extent than in the other regions. As seen in the simulation, such areas are few and form a small percentage of the otherwise well-structured composite.

In summary, structural investigation of the nanocomposite films produced in the transient mode revealed that chaotic advection was capable of orienting the nanoclay platelets along the films surface. Also, the continuous chaotic blender created a novel in situ multi-layered nanocomposite, represented in Fig. 4.4, in which the average layer thicknesses was controlled as a function of amount of chaotic advection or equivalently N. This enables control of spacing between the platelets without changing the overall clay content of the nanocomposite and hence makes it possible to investigate its effect on crystalline morphology of the PA6 matrix (Li and Shimizu, 2006). Concentrating clay platelets within thin layers can increase gas barrier property of the composite drastically as demonstrated in Chapter 3. Hence, a detailed documentation of the internal structure envisaged for steady state films produced for property measurements is provided next.

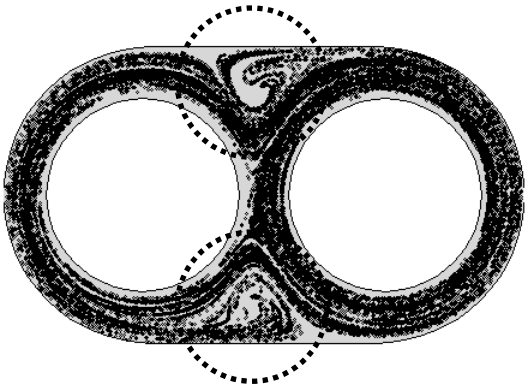

(a)

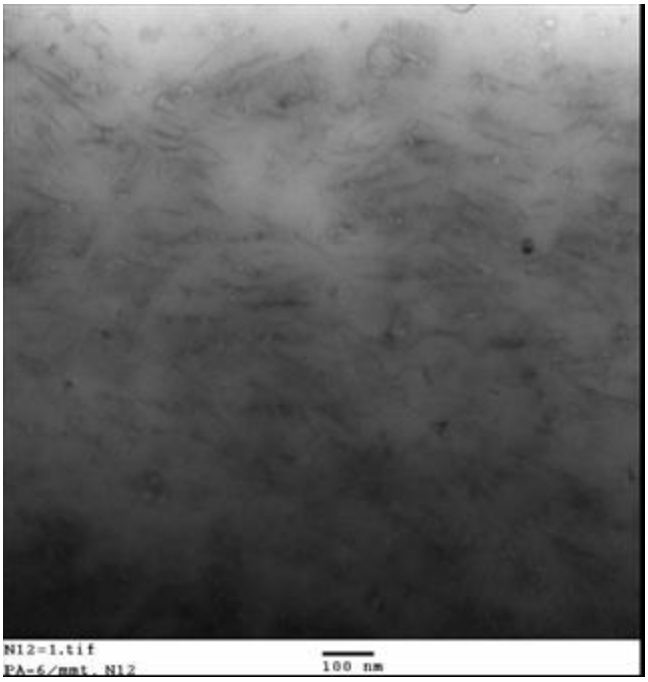


(b)

**Fig. 4.6: Anomalous regions (a) Complex particle pathlines (circled regions) of chaotic advection as demonstrated by a computational simulation led to (b) regions in the nanocomposite where platelets were oriented to a lesser extent.**

#### 4.1.1.2 Steady state films

Films for property measurement were produced in the steady state mode to improve the structural uniformity along the length of the films. Earlier studies (Liang et al., 2001, Ranade et al., 2003) and the theoretical model results presented in the last chapter indicated that the improvement in gas barrier properties is more significant at higher clay contents. Since an objective apart from producing nanocomposites with novel structure was to achieve high barrier properties, films with higher clay content were produced in the steady state mode.

Virgin PA6 and 4% MB were fed in the ratio of 30 to 70 to the chaotic advection blender operating in the steady state mode to obtain films with higher net nanoclay content of 2.8%. Steady state mode was adopted to produce a film with uniform structure through out its length necessary to conduct all the physical property measurements. The clay content was increased to assess compositional effects. Six different sets of films, each subjected to certain N were produced (Table 2.3). Observation of sections from these films elucidated their internal structure and is shown by the micrographs in Fig. 4.7. The nanoclay platelets are oriented along. Since the sections were extracted along a plane perpendicular to the flow direction and the film surface (Fig. 2.9), the orientation of the platelets corresponded to the flow direction along the film surface. The degree of orientation was slightly less at N=8 (Fig. 4.7a). N=12 showed better orientation as shown in Fig. 4.7b. (The upper left corner is dark in the image due to overlap of a two microtomed sections.) Films of higher N showed a very high degree of orientation. No evidence of multi-layered structure was evident for any of the films. The lower percentage of virgin polymer in the feed may have led to the dissipation of the virgin layers at N values lower than that observed in the transient 2% films described before leading to a nanocomposite with aligned platelets homogenously distributed and

dispersed within the matrix for all films. Even in the absence of multi-layering, the nanocomposite structure of these films produced with the chaotic advection blender was significant due to overall higher degree of orientation of clay platelets within the PA6 matrix compared to films produced by conventional processing methods (Russo et al., 2006; Li and Shimizu, 2006; Ray,2002). Simple image analysis of the micrograph in Fig. 4.7c using ImageJ (Public domain, National Institutes of Health, Washington DC) showed that variation in the angle of orientation of the clay platelets from the flow direction was less than $\pm 5°$ in the films from the chaotic advection blender. This corresponded to an average order parameter S (Bharadwaj, 2001) of 0.98 compared to an order parameter of 0.57 and 0.15 reported by Russo et al. (2006) for their nanocomposite films. A higher order parameter suggests better degree of orientation of the platelets perpendicular to the direction of diffusion, an increased tortuosity of the diffusing molecule and hence a reduction in permeability of the nanocomposite as shown by the model in Chapter 3 and other theoretical models of the past (Bharadwaj, 2001; Osman et al., 2004).

In order to achieve multi-layered structure with higher clay content, films with a 50:50 feed ratio of virgin PA6 and 7% Cloisite MB in PA6 were obtained with chaotic advection blender. Keeping the previously described structural results in mind, a set of steady state films with N=7, 9, 11, 13 and 20 were produced as indicated in Table 2.3. Only two sets of steady state films, N=13 and N=20 were produced and investigated in the higher N range since the results from 2% transient films showed that the layers were considerably dissipated and gave way to structures with almost homogenous or homogenous dispersions by N=16. The lowest value of N=7 was chosen so as to be able to obtain multi-layered structure in the nanocomposite.

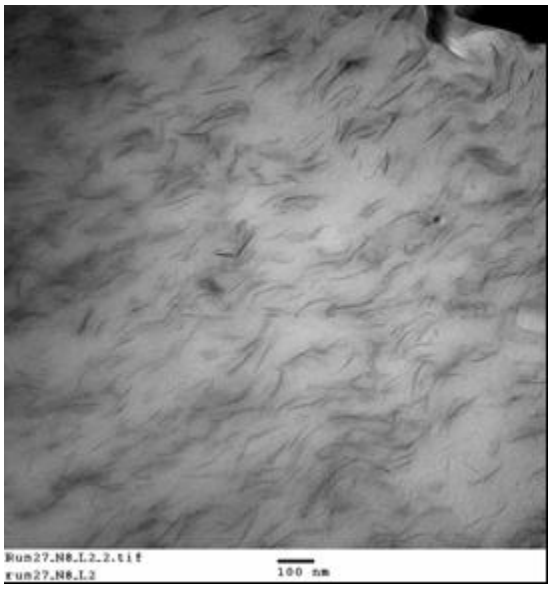


(a)

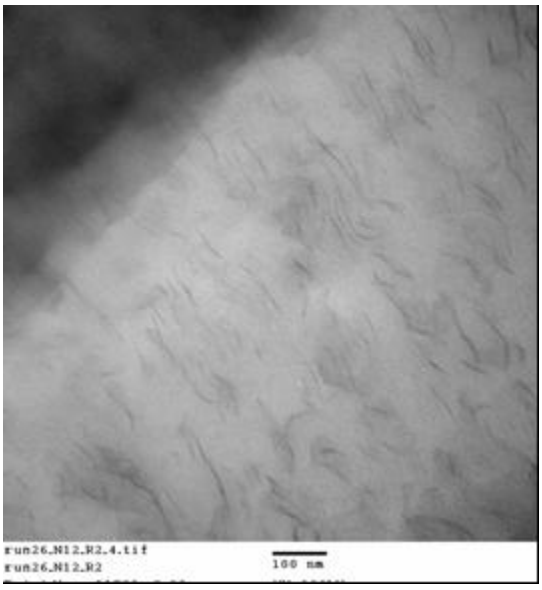


(b)

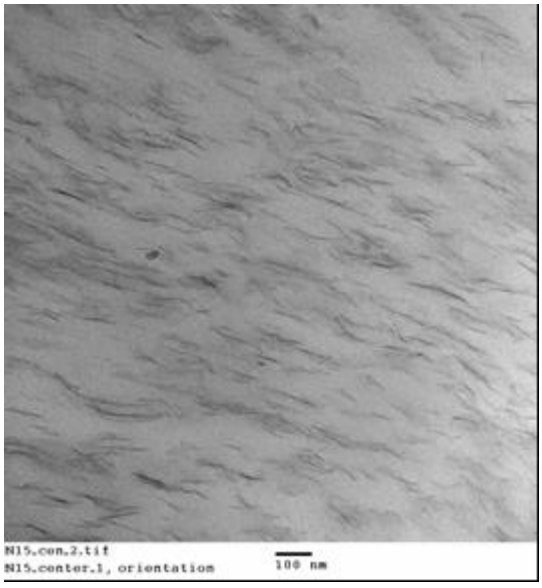


(c)

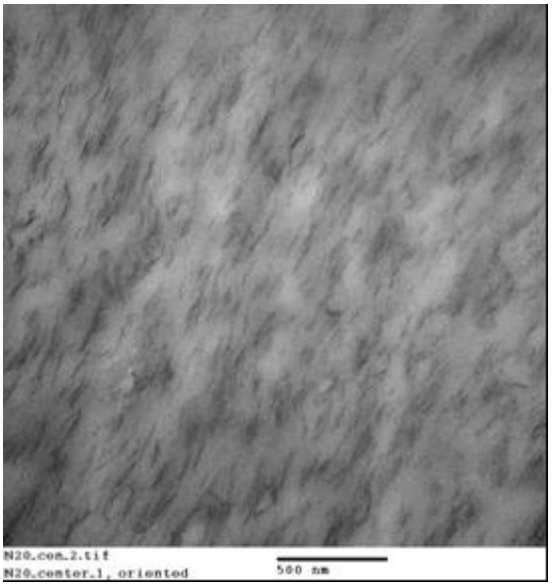


(d)

**Fig. 4.7: Homogenously dispersed platelets with good degree of orientation which increased with N as shown here by the 2.8% clay steady state films of (a) N=8, (b) N=12, (c) N=15 and (d) N=20**

Figure 4.8a shows a discrete virgin PA6 layer between two platelet-rich layers observed in a thin section taken from a film with N=7. The micrograph in Fig. 4.8b exemplified the degree of orientation across this nanocomposite film. Both these images show that the film at N=7 had a degree of orientation closer to that of N=10 (Fig. 4.3b) than that of N=4 (Fig. 4.2a) of the transient 2% films. An example of the overall structure of the film showing thin virgin layers amidst large platelet-rich regions of the nanocomposite is provided by Fig. 4.8c. The number and thickness of the virgin layers reduced further at N=9 as shown by the image in Fig. 4.9a. An individual layer from N=9 film at higher magnification is shown in Fig. 4.9b. The overall degree of orientation of this film was better than the lower N film and was exemplified by the image in Fig 4.9c.

With further increase in chaotic advection, the layers started dissipating as seen by the images in Fig. 4.10. At N=11, the number of layers decreased and only an occasional layer as seen in Fig. 4.10a was observed across a 100μm section. In general, the structure was that of almost homogenous dispersion of platelets with hardly discernible virgin layers as shown in Fig. 4.10b.

A similar structure but with better alignment of platelets was observed for N=13 films (Fig. 4.11). The platelets were found to be well aligned along the flow direction parallel to the film surface (Fig. 4.11a). There were no discernible virgin layers but some virgin-rich regions as shown in Fig. 4.11b were present. (Some TEM images like in Fig. 4.11a show the microtomed sections folding unto themselves. This was because the sections from microtoming were too thin causing the sections to curl and fold.)

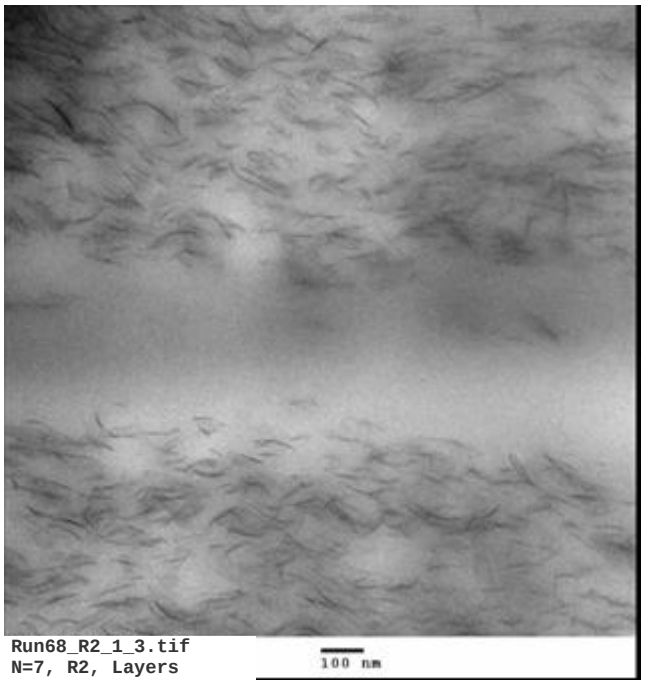


(a)

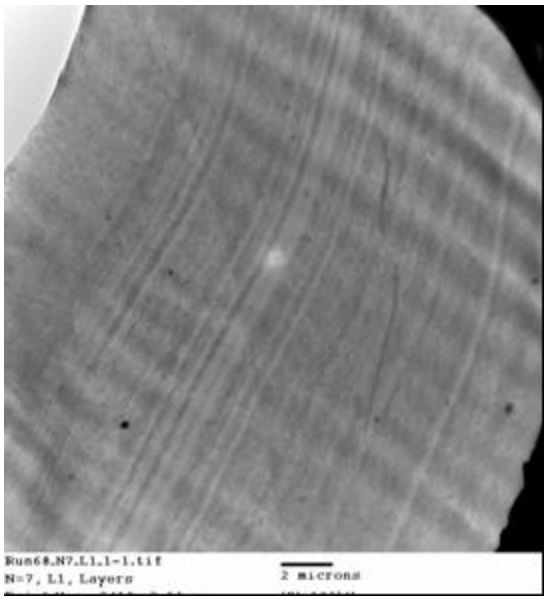


(b)

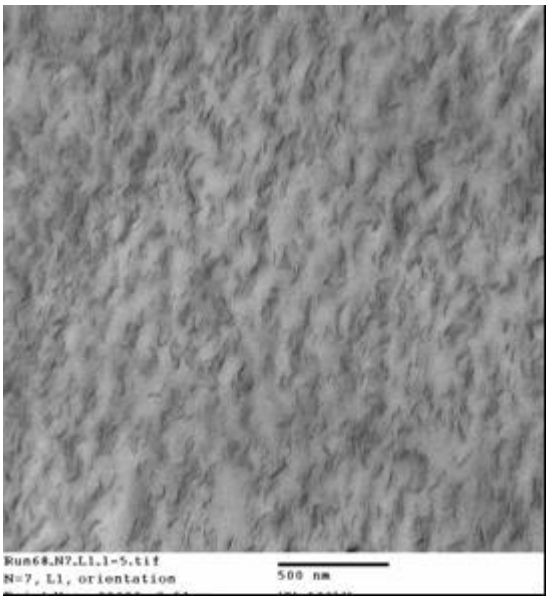


(c)

**Fig. 4.8: Images of 3.5% films at N=7 exhibiting their (a) multi-layer structure, (b) overall structure across its thickness and (c) degree of orientation**

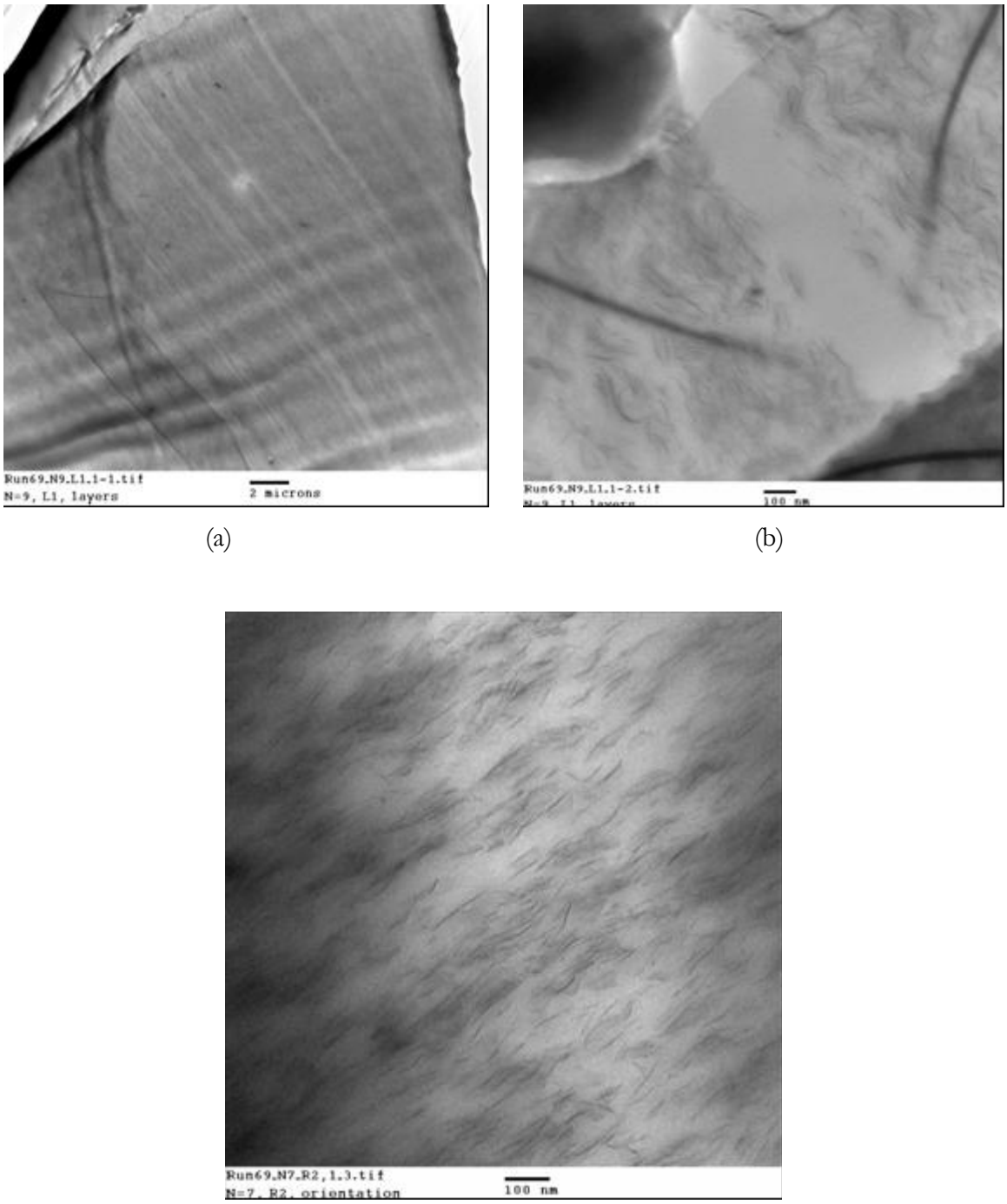


(a) (b)

(c)

**Fig. 4.9: N=9 films with 3.5% clay showing (a) an overall reduced number of layers, (b) reduced virgin layer thickness and (c) a good degree of orientation of the platelets along the film's surface**

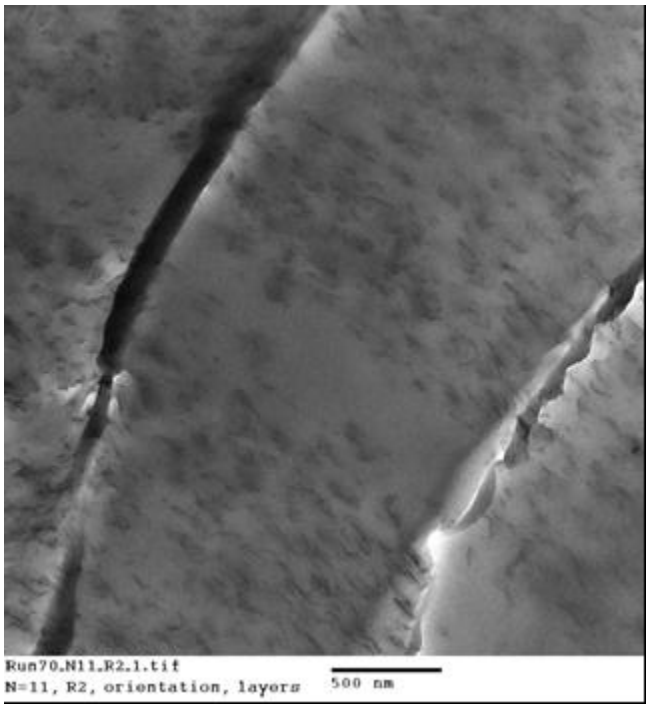


(a)

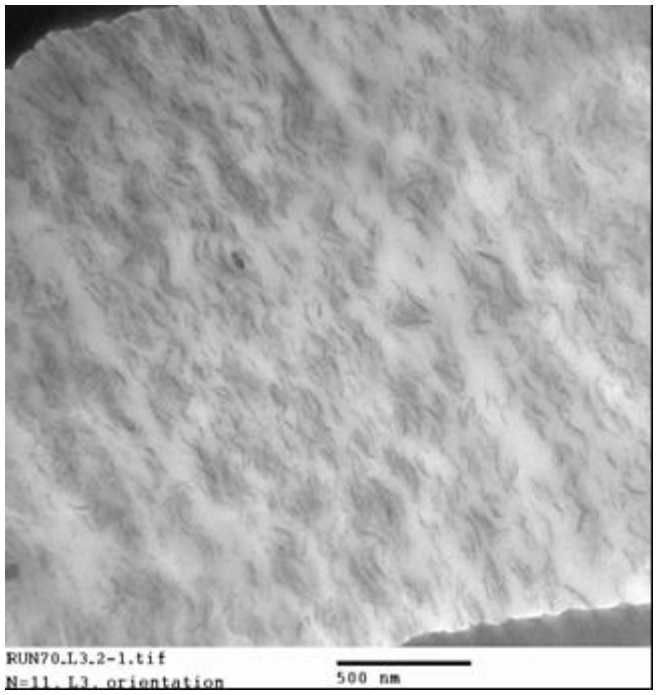


(b)

**Fig. 4.10: TEM of films at N=11 showing (a) a single virgin layer found across the thickness of the film and (b) well aligned platelets with some hardly discernible virgin layers**

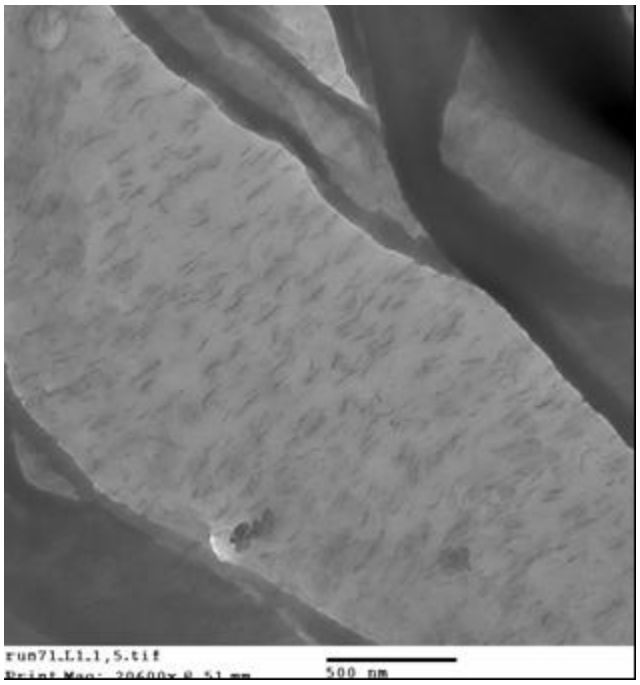


(a)

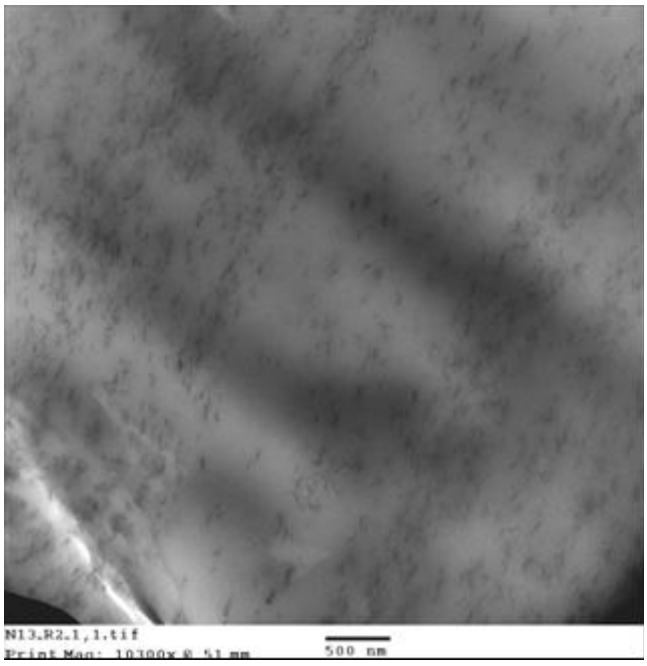


(b)

**Fig. 4.11: N=13 films with 3.5% clay revealing a structure of (a) volumetrically aligned platelets (b) with some virgin-rich regions**

Finally with increased chaotic advection the structure of the nanocomposite evolved into that of a homogenous dispersion of volumetrically aligned platelets. An example of such a structure obtained for the 3.5% films with N=20 is shown by the micrograph in Fig.4.12. This structure was similar to that exhibited by the 2% transient films at N=18 (Fig. 4.5b).

To establish that the high degree of orientation of the nanoclay platelets occurred in-situ due to chaotic advection and was not due to high shear forces within the die, a 3.5% nanocomposite film not subjected to chaotic advection was extruded out. This was done by pre-mixing the virgin PA6 and 7% MB pellets in equal amounts by weight and feeding these pre-mixed pellets to both the extruders of the chaotic advection assembly (Fig. 2.1). The melt domains were then passed through the blender without stir rod rotation and shaped by the die into a film. Micrographs indicating the structure of such a nanocomposite are shown in Fig. 4.13. The film had platelets homogenously dispersed within the matrix of the composite similar to high N films of 3.5% but did not show a high degree of orientation. This result confirmed that chaotic advection is responsible for imparting a high degree of volumetric alignment to the clay platelets of the nanocomposites and the structuring occurs upstream of the die. Hence, it is fair to conclude that nanocomposites with platelets aligned along the flow direction through the bulk of the material can be produced by the chaotic advection blender.

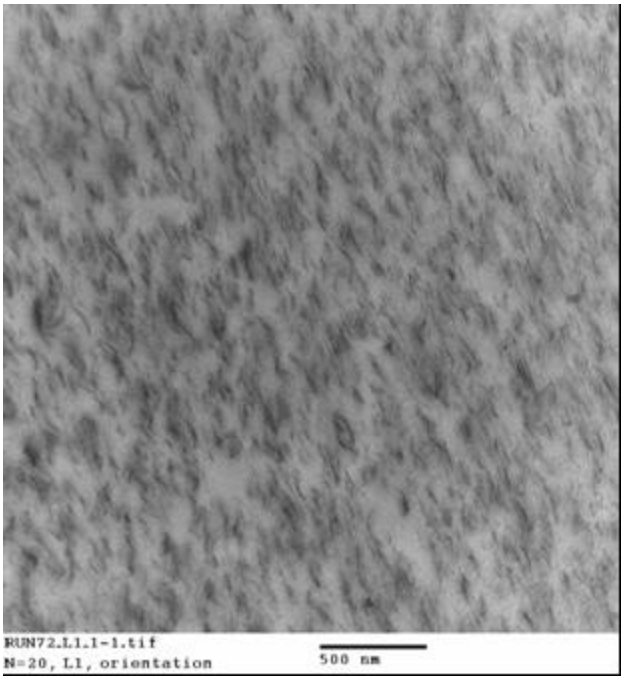


**Fig. 4.12: Clay platelets aligned and dispersed uniformly within the bulk of the 3.5% nanocomposite at N=20**

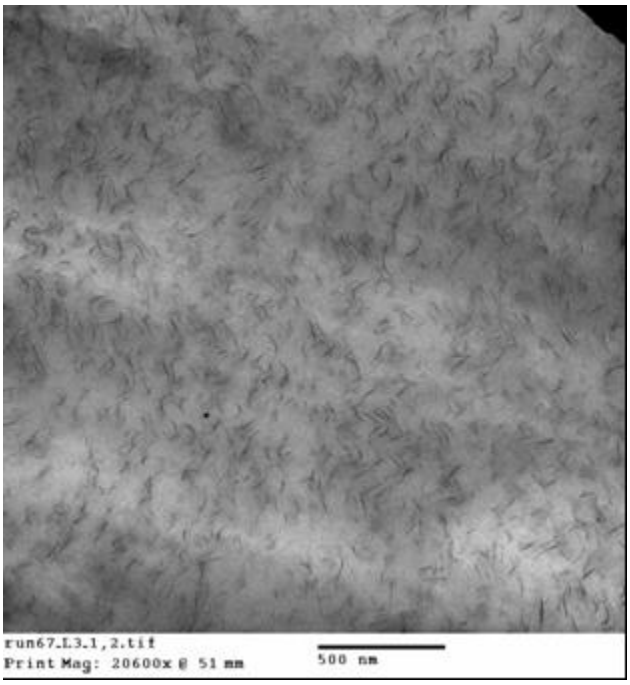


**Fig. 4.13: 3.5% films produced without chaotic advection with the other processing parameters identical to N=20 above exhibiting a low degree of orientation**

A few steady state films (N=7, 9, 20) with an even higher clay content of 5.6% were obtained by feeding 8% MB and virgin PA6 in the ratio 70:30. Layers were evident in both N=7 and N=9 films as shown in Fig. 4.14a and Fig. 4.14b respectively. But their thickness was lower than the corresponding films of 3.5% clay loading due to the feed ratio. The structure was contrary to what was observed with 2.8% films produced with a similar feed ratio where even N=8 films did not show any kind of multi-layering. This difference might be explained by the significantly higher viscosity of the 8% MB (Section 2.3.1). The high viscosity melt poses a higher resistance to shear deformation and reduced the rate of refinement caused by chaotic advection. A lesser number of layers were found for films at N=9 than for films at N=7. At N=20, the layered structure of low N's had given way to a homogenous dispersion of clay platelets consistent with the earlier films of similar N's. All films displayed a high degree of orientation along the flow direction and parallel to the film surface as shown in Fig. 4.15. The high degree of orientation even at the earlier stages of chaotic advection (Fig. 4.15b and 4.15c) was attributed to the high clay content. The decreased spacing between the high aspect ratio clay platelets restricted lateral movement of one another and led to increased orientation along the flow direction. This was further confirmed by the observation of high degree of orientation in films produced by pre-mixed pellet feed into the blender without chaotic advection.

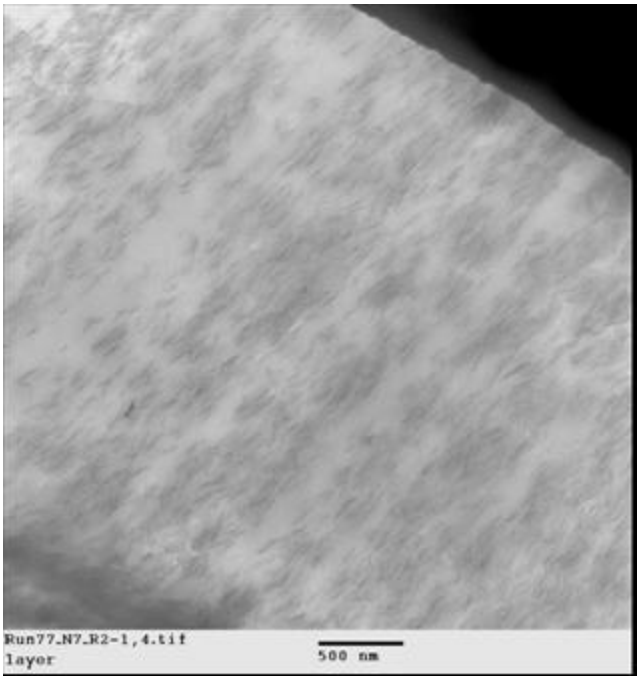


(a)

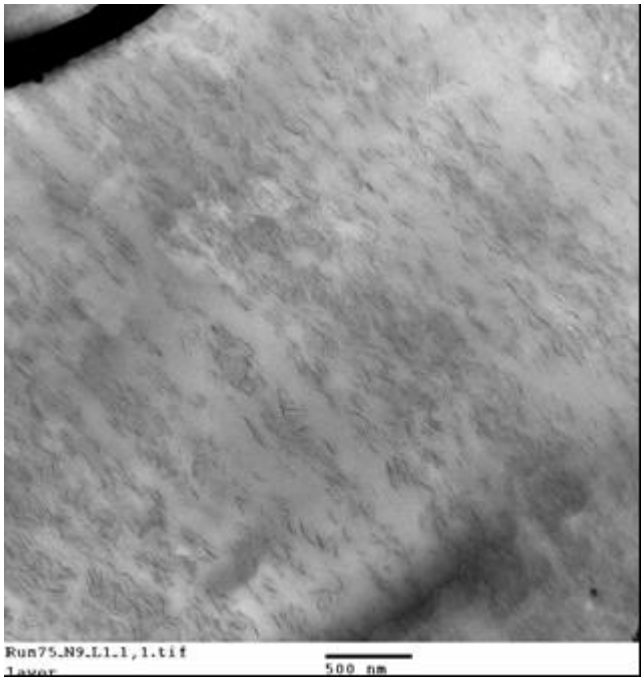


(b)

**Fig. 4.14: Very thin virgin layers contributing to the multi-layered structure of the 5.6% nanocomposite at (a) N= 7 and (b) N=9**

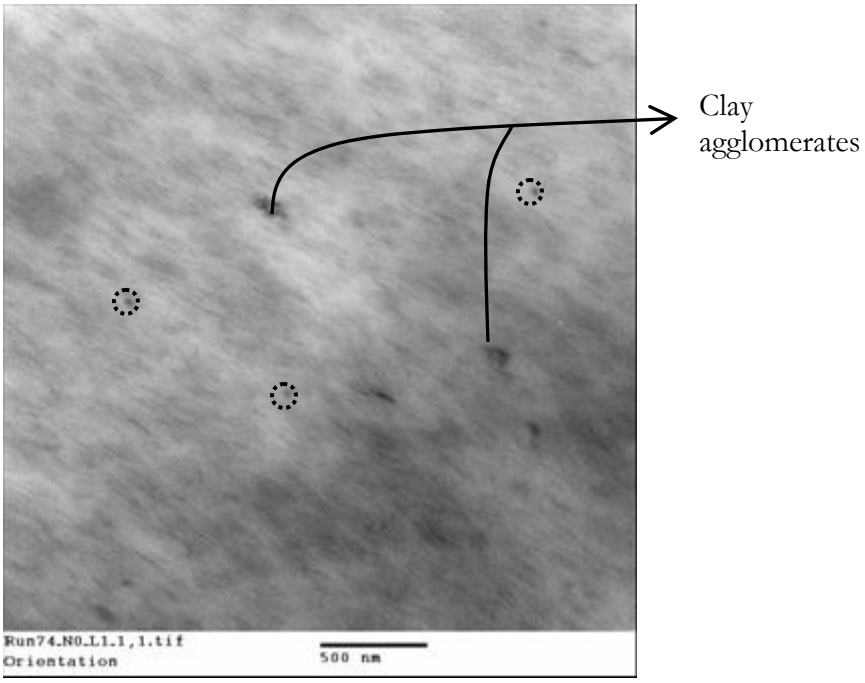


(a)

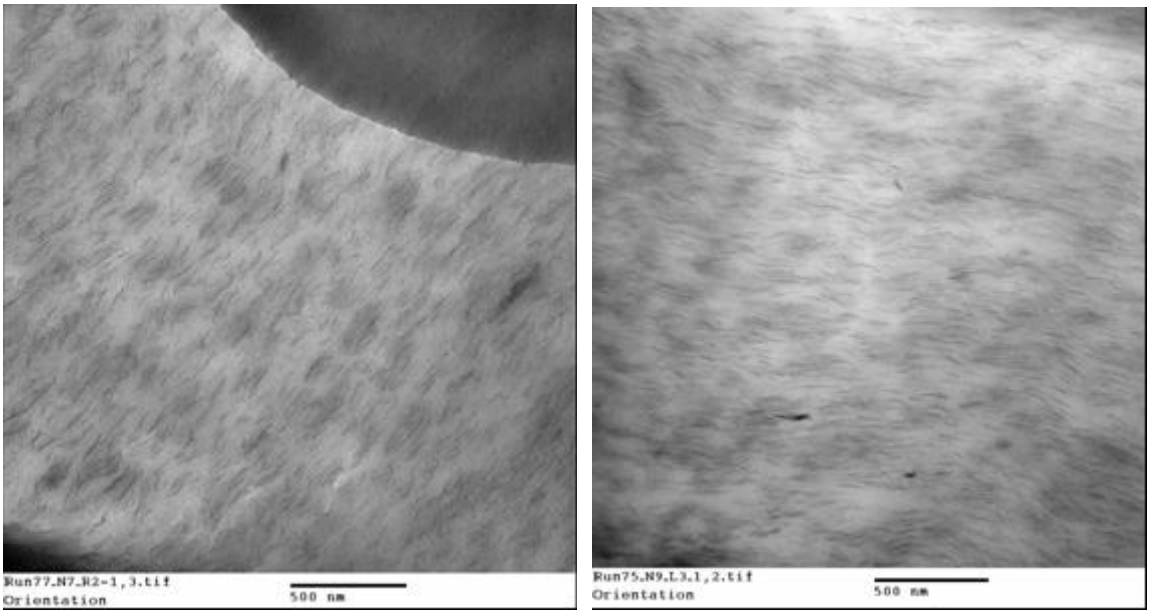


(b) (c)

**Fig. 4.15: A high degree of orientation of clay irrespective of N in all 5.6% films, (a) N=20 (b) N=7 and (c) N=9**

Apart from the high degree of orientation of platelets, structural investigation by TEM also showed dark specks in the microtomed sections of the nanocomposite films (Fig. 4.15). Some of these were due to the presence of agglomerated clay platelets and are marked as such in Fig 4.15 and Fig. 4.16. Some spherical contaminations (encircled in the micrographs) apart from the agglomerates were also noticed. These were believed to be residues that were not purged following the prior film production runs done in other research projects. Such residues may have been released by the highly viscous melt of the 8% MB.

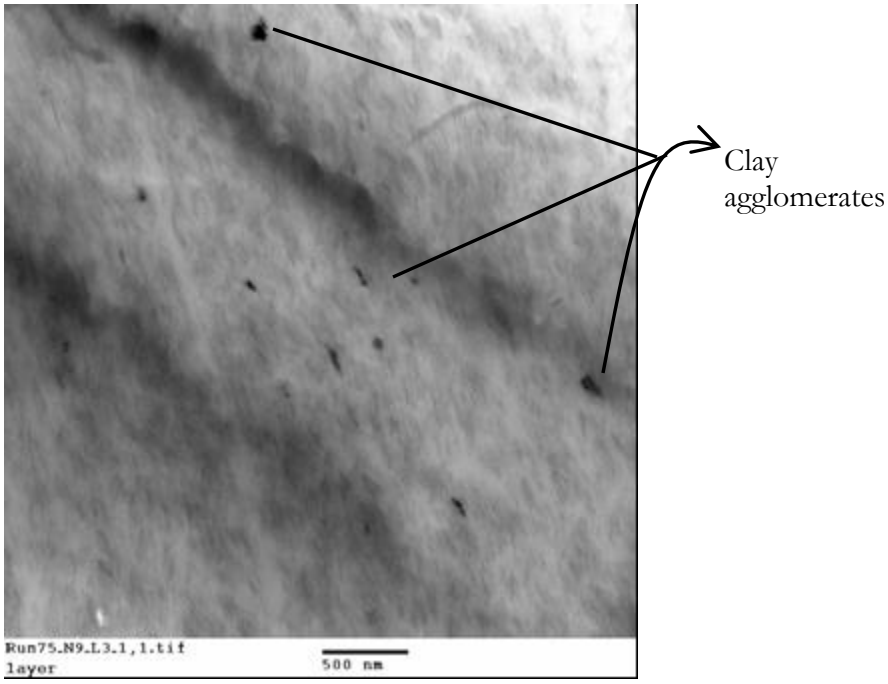


**Fig. 4.16: Image showing the presence of clay agglomerates and other contaminations in 5.6% films.**

### *4.1.2* X-ray diffraction

Fig 4.17 illustrates the x-ray diffraction data for pure PA6 pellets used for film production. The curve plotted as a dotted line and labeled 'overall pattern' is the raw data obtained from the run. Intensity is plotted against inverse of the distance Q ($Q=2\pi/d$ where d is the spacing between the atomic layers of crystal structure). As is typical for PA6, two dominant diffraction peaks at about $2\theta=20°$ and 23.7° (d=4.39Å and 3.75Å) corresponding to the stable α-crystalline form were observed along with a minute peak around 4.16Å ($2\theta=21.4°$) corresponding to the metastable γ-form (Kojima et al., 1994 & 1995). The figure also shows the method utilized to deconvolute the raw data into corresponding individual peaks (Fornes and Paul, 2003). The area under each curve gave the volume of each phase.

#### 4.1.2.1 As-processed films

The diffraction patterns produced for virgin PA6 films with and without chaotic advection (N=25 and N=0 respectively) are shown in Fig.4.18 and indicate the presence of a higher fraction of γ-form. This change from α-form to γ-form during the film formation is due to quench cooling of the considerably thin film exiting from the die onto the chill roll (Kyotani and Mitsuashi, 1972). Analysis of the curves by deconvolution method (illustrated in the inset) showed that both the films exhibited similar degree of crystallinity (~17%). The γ fraction was high for both films compared to α-form. Hence, it revealed that chaotic advection by itself did not affect the crystalline morphology of PA6 significantly. This provided a benchmark to compare the effect of nanoclay platelets and their structural arrangement within the nanocomposite on the matrix crystalline morphology.

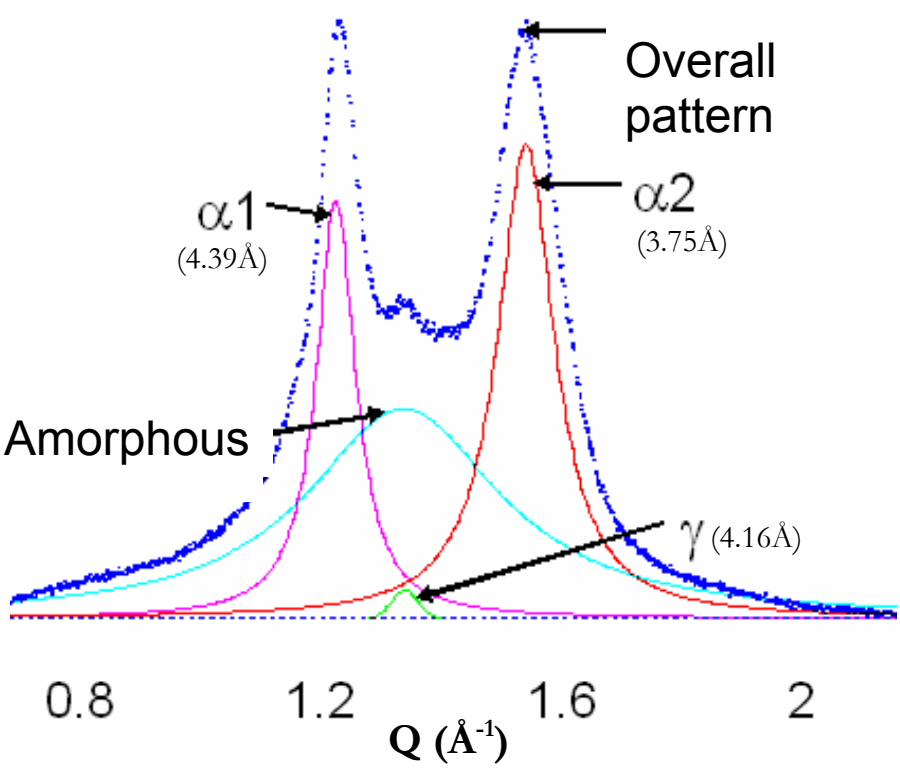


**Fig. 4.17: Powder x-ray diffraction pattern of PA6 pellets exhibiting its various phases. Also shown is the peak deconvolution method utilized to calculate fractions of the different phases present**

Fig. 4.19 compares the diffraction patterns obtained for 2% clay transient films with different values of N. It was observed that as N increased the intensity of the peak around 4.16Å increased and its width decreased. According to Fornes and Paul (2003), such changes in diffraction pattern indicate in general increased homogeneity of the ordered domains or increased γ-crystallinity. The change was quantified and amount of each phase is presented in Table 4.1. The fraction of γ-phase with respect to α-form increased monotonically though slightly with N. The total crystallinity reached a maximum around N=14.

These results were consistent with the in situ structural evolution found by TEM and presented in Section 4.1.1. It is well-known from literature that presence of clay platelets restricts the mobility of PA6 chains inducing the formation of γ crystalline form (Miltner, et al., 2005). At earlier stages of chaotic advection represented by films of low N values, only the fraction of PA6 chains present in the platelet-rich layers of the multi-layered nanocomposite were restricted by the platelets. The PA6 in the neighboring virgin layers were still mobile to form α crystal structure. Hence, these films exhibited a lower fraction of γ-form. With increased N and subsequent increased stretching and folding of the melt layers, virgin layers became thinner and were encroached by platelets from platelet-rich layers. As seen from the curve, the decline in α/γ ratio was more pronounced at the earlier stages of chaotic advection with multi-layered structure (upto~14) than later when the platelets were more homogenously dispersed. With decreased virgin layer thickness, the lateral spacing between the platelets increased monotonically and the crystallinity reached a maximum in tandem. The significance of the controlled arrangement of clay platelets on the morphology of the matrix was revealed.

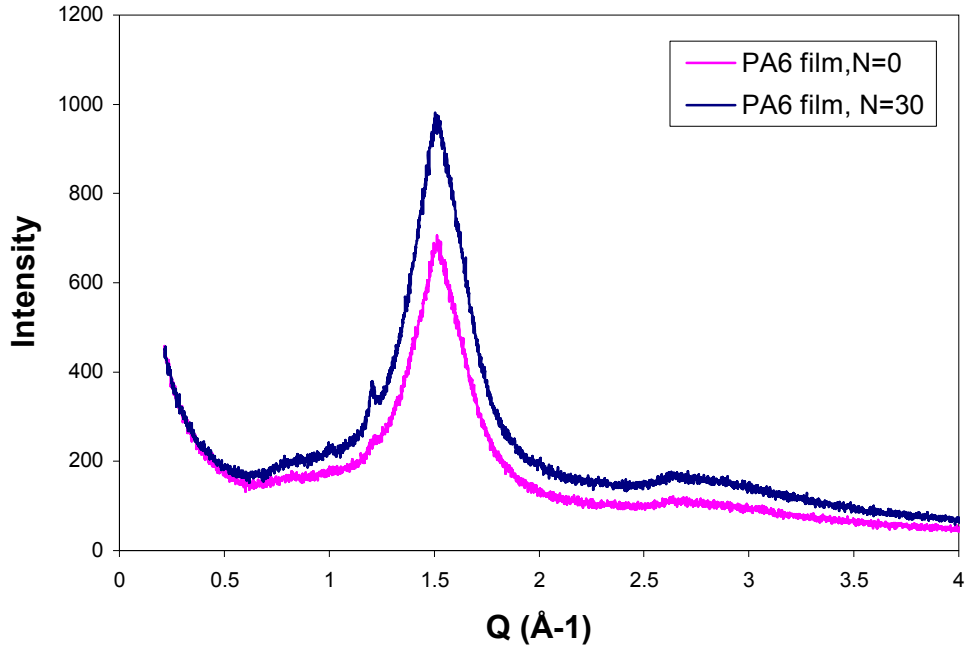


**Fig. 4.18: Diffraction patterns of the PA6 films showing dominance of γ-crystalline form**

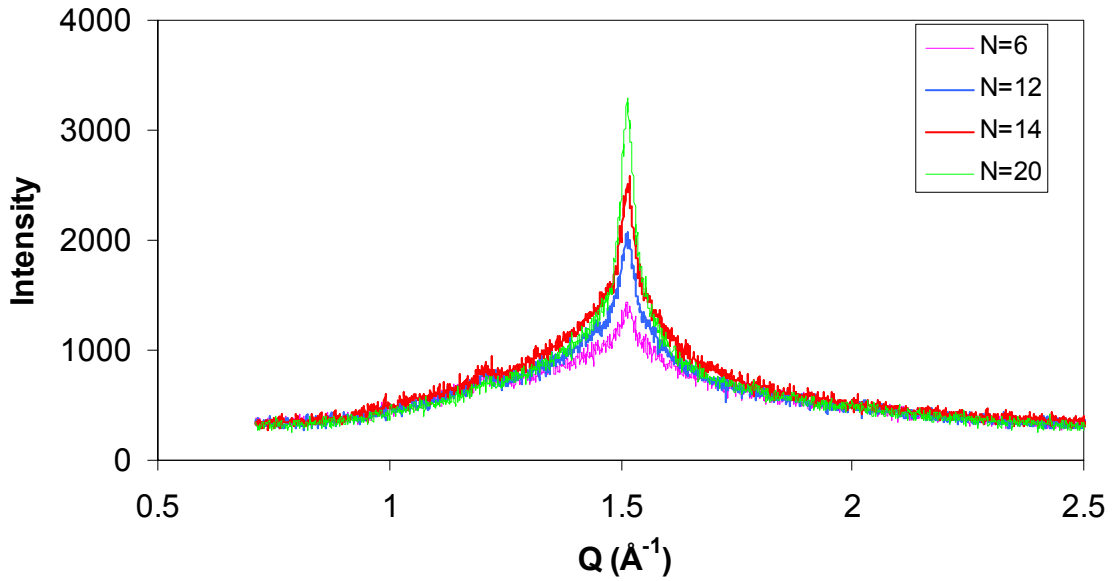


**Fig. 4.19: Diffraction patterns for 2% transient films demonstrating dependence of intensity and peak width on the extent of chaotic advection**

**Table 4.1: Crystallinity data obtained from theoretical fitting of powder x-ray patterns obtained for nanocomposite films produced by chaotic advection blender**

| Clay (wt%) | N value | % α | % γ | % total | % γ of total |
|---|---|---|---|---|---|
| 2 (transient) | **12** | 6 | 18 | 23 | 75 |
| | **14** | 6 | 21 | 27 | 76 |
| | **20** | 6 | 20 | 26 | 78 |
| | **25** | 4 | 18 | 23 | 82 |
| 2.8 | **8** | 12 | 8 | 20 | 42 |
| | **10** | 9 | 10 | 19 | 50 |
| | **12** | 8 | 11 | 19 | 57 |
| | **20** | 7 | 15 | 22 | 66 |
| | **25** | 5 | 9 | 14 | 66 |
| 3.5 | **7** | 5 | 27 | 32 | 84 |
| | **9** | 4 | 22 | 26 | 84 |
| | **11** | 4 | 20 | 24 | 83 |
| | **13** | 4 | 28 | 32 | 86 |
| | **20** | 5 | 27 | 31 | 85 |
| | **0** | 5 | 19 | 24 | 79 |
| 5.6 | **7** | 7 | 31 | 38 | 82 |
| | **9** | 6 | 19 | 25 | 77 |
| | **20** | 6 | 22 | 28 | 80 |
| | **0** | 6 | 32 | 37 | 85 |

Effect of clay content on degree of crystallinity of PA6 matrix of the nanocomposite was investigated. The average data obtained by testing 5 specimens for each film sample is presented in Table 4.1. An example of the diffraction patterns of films with similar structural arrangement of clay platelets (N=20) but with different clay content is shown in Fig. 4.20a. The corresponding crystallinity data obtained from the integration of the curves is shown in Fig. 4.20b. The comparison of degree of crystallinity or % γ among films of different clay content did not show a clear trend.

This result is consistent with that reported by Fornes and Paul (2003) who also did not observe any clear dependence of crystallinity on clay content for nanocomposites processed by injection molding using a similar type of PA6 (Fornes, et al., 2001). Though the processing techniques and the processing parameters (shear rate, rate of cooling) involved are different for the two samples, the film structure is known to correspond well to the skin region of the injection molded samples with some mixed features of the inner regions (Kojima et al, 1994 & 1995). The shear rate and rate of cooling encountered during cast extrusion of films is typically slightly less than that of the skin region but more than the core region of the injection molded samples.

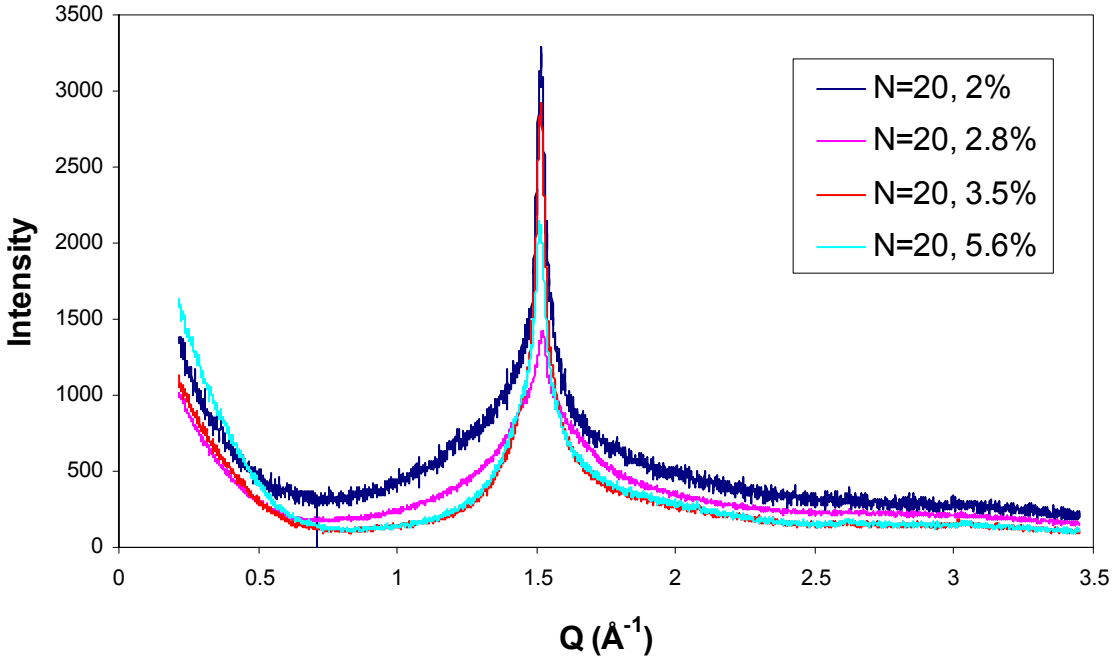


(a)

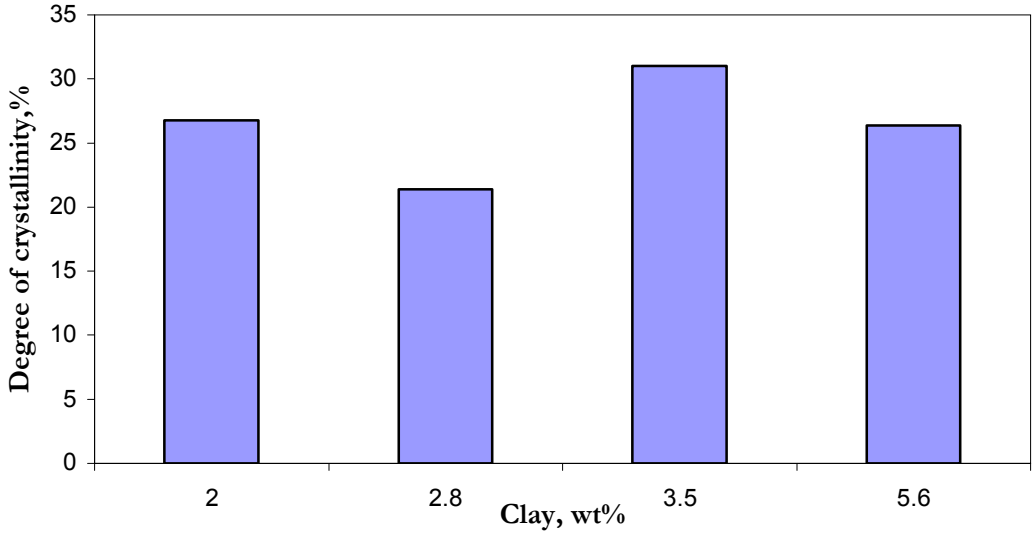


(b)

**Fig. 4.20: Effect of clay content on the crystallinity of PA6 matrix evaluated by x-ray diffraction technique**

The effect of structural arrangement of clay platelets on the matrix crystallinity of the steady state films was also inspected (Table 4.1). No clear trend was discernible for total crystallinity or for the γ-fraction of steady state films with N. A correlation between the structure of TEM and x-ray patterns observed for transient films was absent in steady state films. For example, the crystallinity for 2.8% films and 3.5% films is plotted as a function of N in Fig. 4.21. As described in Section 4.1.2, 2.8% films exhibited homogenous dispersion of platelets at all values of N. Considering chaotic advection by itself did not affect the crystallinity of virgin polymer films, the crystallinity of 2.8% films should not depend on N. But it is shown to vary with N. The 3.5% films with some level of multi-layering show a minimum in crystallinity instead of the maximum as shown by 2% transient film. These deviations may be due to the artifacts introduced by the variation in thickness among the samples (Table 2.5) and the limitations in the peak deconvolution method utilized for quantitative estimation of crystallinity. As noted by Fornes and Paul (2003) a number of complications are involved in estimating the crystallinity of semi-crystalline polymers and distinguishing the different crystalline forms due to superposition of the peaks.

X-ray images of PA6 and its nanocomposites were acquired in order to determine the orientation of the clay and PA6 crystallites. Fig. 4.22 shows diffraction patterns for a nanocomposite film when x-ray beam was incident on the specimen in three directions. The x-ray pattern for normal incidence exhibited only Debye-Scherrer ring (golden yellow) indicating no preferred orientation of the PA6 crystallites.

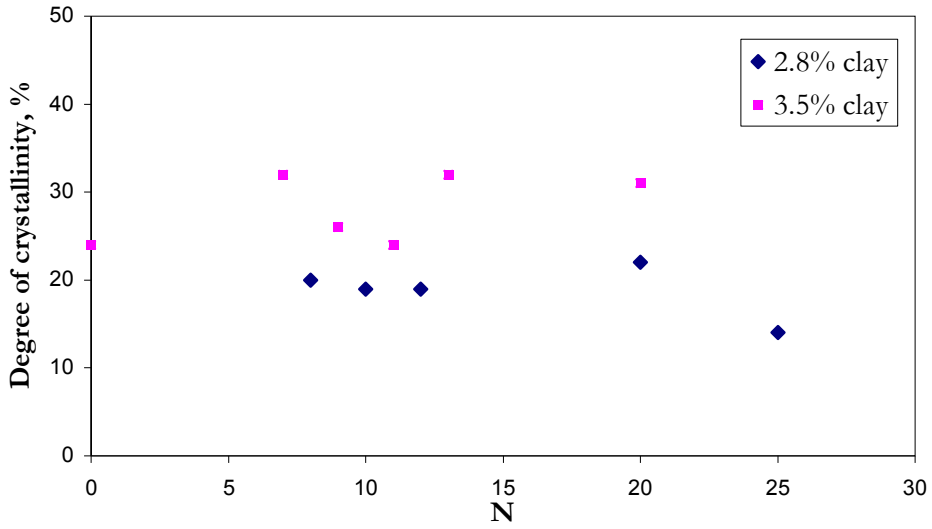


**Fig. 4.21: Plot showing the absence of a trend in crystallinity with respect to the structural arrangement of platelets in steady state films**

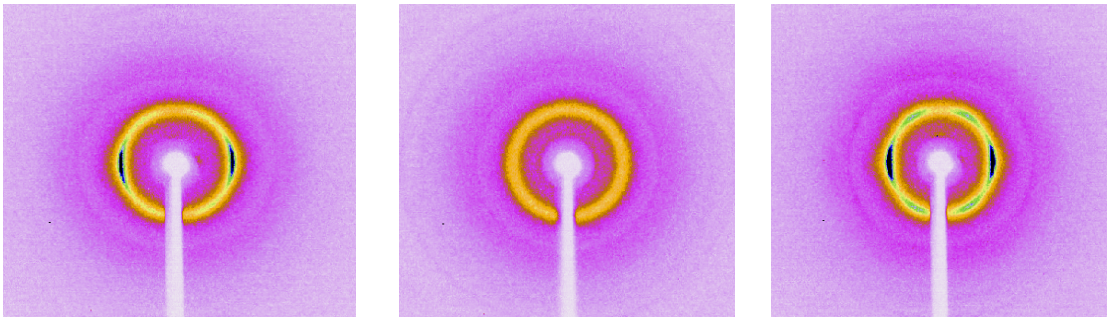

**End-view** **Through-view** **Edge-view**

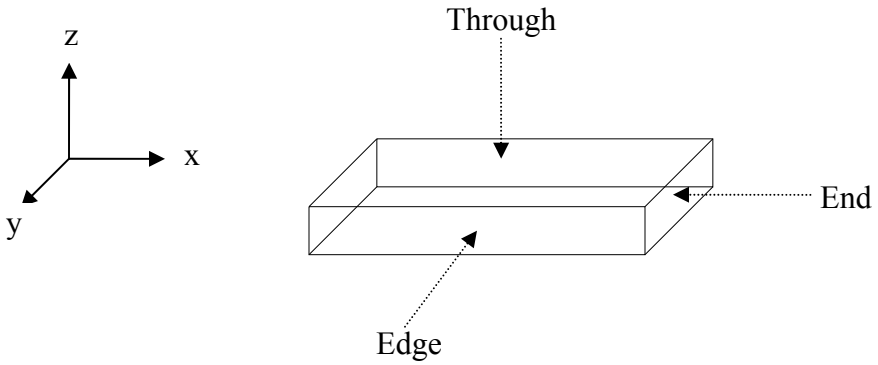


**Fig. 4.22: X-ray diffraction images for 5.6% clay films. Background is colored purple and the beam stopper is seen in white**

The edge and end view patterns for the nanocomposite film exhibited arcs (green) typical of the nanoclay-PA6 composite (Kojima et al., 1994) as shown in Fig. 4.22. These arcs are due to the overlapped reflection of 020 and 110 at $2\theta \approx 25°$ corresponding to γ crystal structure (Kojima et al., 1994). The six-fold arrangement of arcs was more pronounced in the edge-view than the end-view pattern. These diffraction patterns compare well with the diffraction patterns of nylon nanocomposite films with comparable clay content reported by Kojima et al., (1994) except for the absence of diffraction patterns at lower diffraction angles corresponding to orientation of clay platelets ($2\theta \sim 4°$) and 002 reflection of γ-form ($2\theta \sim 12.5°$). The absence was due to limitation of the instrument which had a large beam stopper (seen as the black region in the patterns).

The arcs in the edge and end view suggest that the {110} (planar zigzag planes of PA6 backbone) or {020} (hydrogen-bonded sheet planes) planes are oriented parallel to the film surface (Kojima et al, 1994; Li and Shimizu, 2006; Maiti and Okamoto, 2003). Also, since the clay platelets were found to be parallel to the film surface by TEM, the above planes were also oriented parallel to the clay platelets. The change in orientation of the crystalline lamellae can be realized through x-ray studies only by observation of the position of the 002 reflection corresponding to the c-axis or the molecular chain axis of the γ-crystal structure (Li and Shimizu, 2006). Therefore the effect of clay content and chaotic advection on the orientation of the crystalline lamellae could not be determined.

Fig. 4.23a shows the edge-view diffraction patterns obtained for transient 2% film with different values of N along with that of pure PA6 film for comparison. Only Debye-Scherrer rings typical for PA6 with no preferred orientation were observed for pure PA6 films (Kojima et al., 1994 & 1995; Li and Shimizu, 2006). The intensities of the arcs were

integrated along x-direction as shown in Fig 4.23b. It clearly revealed that the amount of orientation of the {110} and {020} planes along the film surface increased with increase in N. This was an indication of improvement in orientation of the clay platelets and polymer crystallites with increase in extent of chaotic advection.

The diffraction patterns along the three directions were qualitatively similar for the steady state films with 2.8% clay, 3.5% clay and 5.6% clay. The intensity of the arcs varied with N and also with clay content. But a comparative quantitative analysis of the orientation of the polymer chains was not possible due to variation in sample thickness and crystallinity.

#### 4.1.2.2 Biaxially stretched films

Stretching of the film slightly below its melting temperature causes the entangled polymer chains to align in the direction of stretching, thus increasing the ordering and promoting crystallization growth (Osswald et al., 2006; Sperling, 2006). This method is very commonly used in the film and fiber industry to increase orientation and crystallinity and impart improved properties. Hence effect of biaxial stretching on 2.8% films was also studied using X-ray techniques. Since all the 2.8% films had similar structure of volumetrically dispersed platelets, only three sets of films N=8, N=15 and N=20 were investigated. An example of the diffraction pattern obtained as a function of stretch ratio is shown in Fig. 4.24. The profile shows the re-emergence $\alpha_1$ and $\alpha_2$ peak seen in the figure. Similar $\gamma \rightarrow \alpha$ transition was observed upon drawing of PA6-MMT nanocomposite (Yoon et al., 2004; Ibanes et al., 2006). The intensity of the $\alpha_2$ peak increased with increase in stretch ratio.

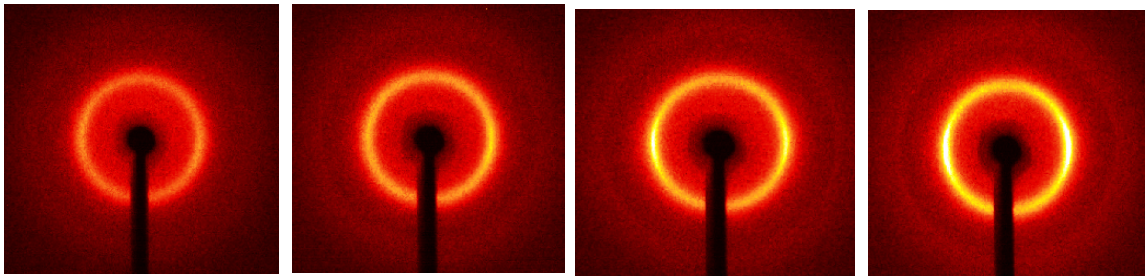

| Pure PA6 | N = 0 | N = 7 | N =15 |
|---|---|---|---|
| Clay = 0 | Clay = 2% | Clay = 2% | Clay = 2% |

(a)

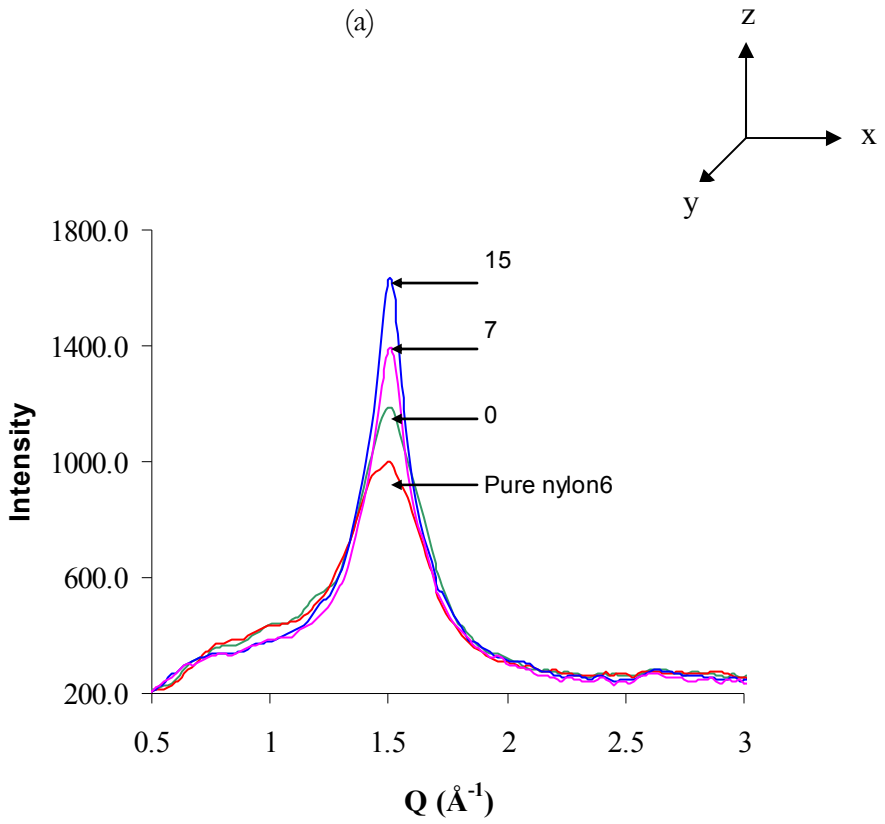


(b)

**Fig. 4.23: Edge-view diffraction images of 2% transient films. The intensities along the x-direction were integrated and is plotted here to show the effect of N on the orientation of crystallites**

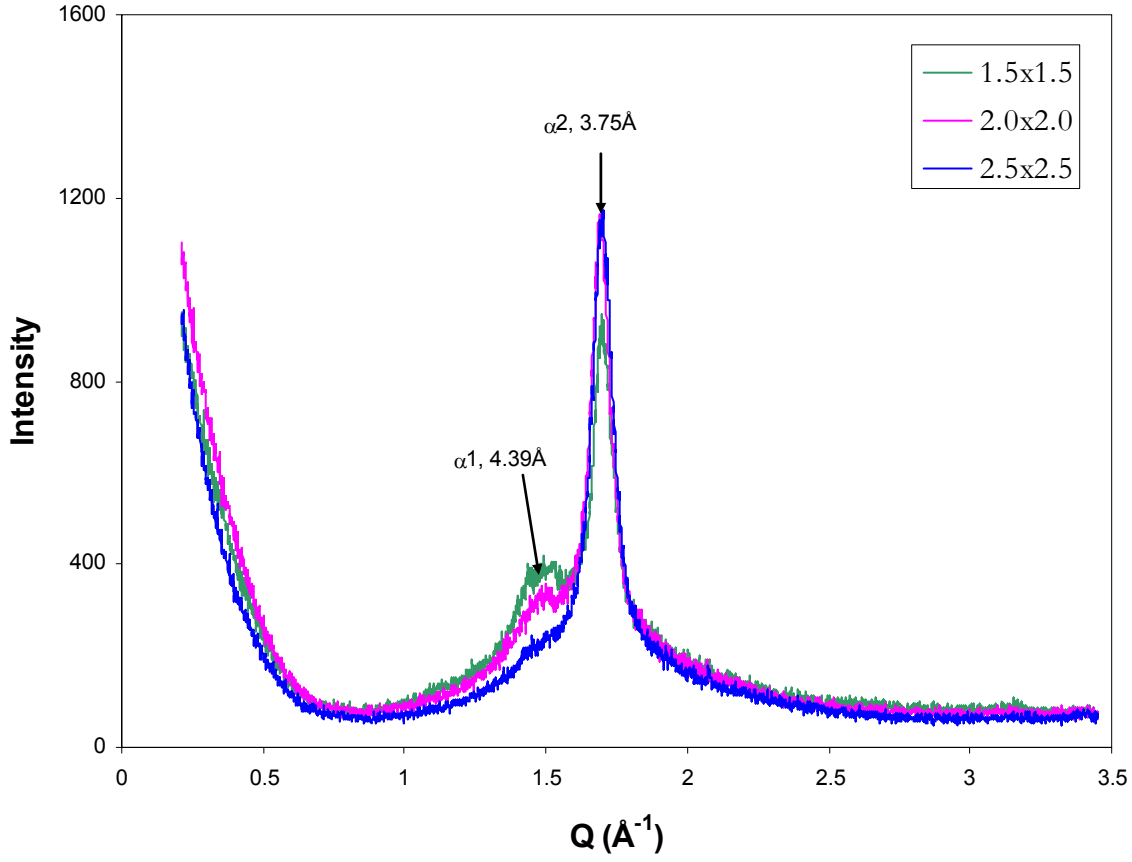


**Fig. 4.24: Powder x-ray diffraction profile of stretched 2.8% films with N=8 showing a predominant α-crystalline form**

Table 4.2 gives the relevant crystalline information obtained through peak fitting. Clearly, the degree of crystallinity (expressed as crystalline to amorphous ratio) and α/γ ratio increased with increase in stretch ratio for all the 3 sets of films.

Biaxial stretching of films with multi-layer structure was intended but was not carried out. The stretching of multi-layer structured films was expected to reduce the spacing between the platelets further and hence affect the crystalline orientation of the nanocomposite films and the barrier properties.

**Table 4.2: X-ray data of stretched 2.8% nanocomposite films obtained by peak fitting**

| | **Stretch ratio 1.5 x 1.5** | | **Stretch ratio 2.0 x 2.0** | | **Stretch ratio 2.5 x 2.5** | |
|---|---|---|---|---|---|---|
| **N value** | **α/γ** | **crystalline/ amorphous** | **α/γ** | **crystalline/ amorphous** | **α/γ** | **crystalline/ Amorphous** |
| **8** | 6.53 | 0.40 | 15.69 | 0.51 | 65.09 | 0.70 |
| **15** | 6.72 | 0.37 | 15.81 | 0.68 | 29.72 | 0.83 |
| **20** | 9.23 | 0.35 | 16.25 | 0.50 | 17.41 | 0.81 |

### *4.1.3* Differential scanning calorimetry

The effect of chaotic advection on the morphology of the matrix was investigated by DSC. A heating scan was employed to calculate the degree of crystallinity. Examples of the heating scans obtained for a nanocomposite is shown along with that of pure PA6 film in Fig. 4.25. A single endothermic peak around 220°C which corresponds to the melting of crystalline PA6 regions was observed for all film samples. Also, a shift in baseline around 50°C denoting the glass transition temperature ($T_g$) of PA6 was observed along with a broad

endothermic peak around 100°C due to moisture in the films. The moisture was accounted for by re-weighing the samples after the DSC runs and using the weight of the film sans moisture for calculations. The linear integration of the melting peak at 220°C provided the heat of fusion per gram of the sample ($\Delta H_f$). The limits for integration were chosen as the points where the slope of the curve changed as shown in Fig. 4.25. For a fair comparison, the heat of fusion per gram of PA6 in the nanocomposite ($\Delta H_{f,\ PA6}$) was calculated accounting for the volume fraction of clay ($\varphi_c$) as shown by Equation 4-1. The degree of crystallinity was then calculated using Equation 4-2.

$$\Delta H_{f,PA6} = \frac{\Delta H_f}{1-\varphi_c} \qquad \textbf{4-1}$$

$$\%\chi = \frac{\Delta H_{f,PA6}}{\Delta H_{f,ref}} \qquad \textbf{4-2}$$

$\Delta H_{f,ref}$ which is the heat of fusion of a 100% crystalline PA6 sample was chosen to be 240 J/g (Fornes and Paul, 2003).

#### 4.1.3.1 As-processed films

The degrees of crystallinity for the films produced by chaotic advection blender are plotted as a function of N for different clay contents in Fig. 4.26. The graph showed variability in the crystallinity levels within the samples. No dependence of N could be seen. The variation may be a sign of heterogeneity in the crystal structure across the width of the film as each specimen was extracted from different regions across the sample width as explained in Section 2.4.3.

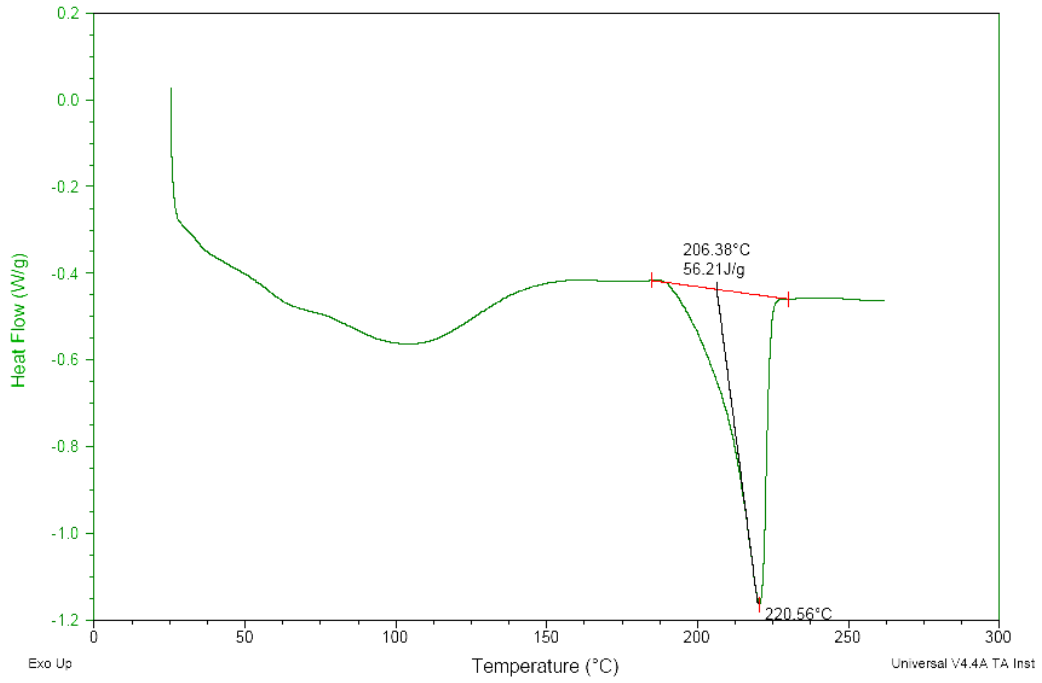


(a)

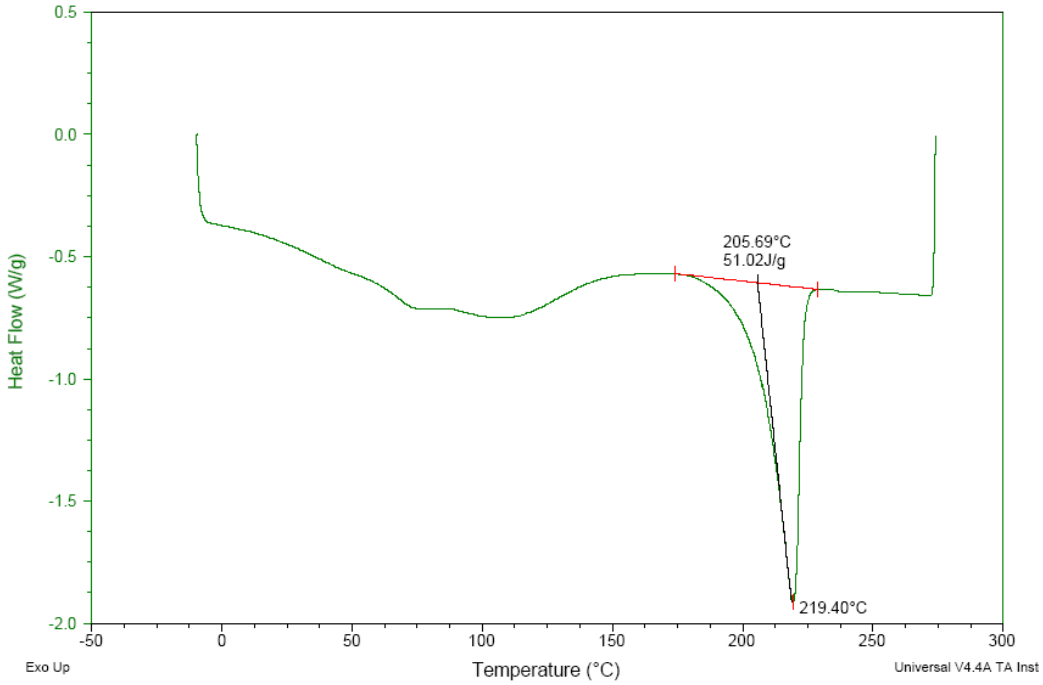


(b)

**Fig. 4.25: DSC plots obtained during heating scans for (a) 3.5% clay, N=9 film and (b) PA6 film at N=0**

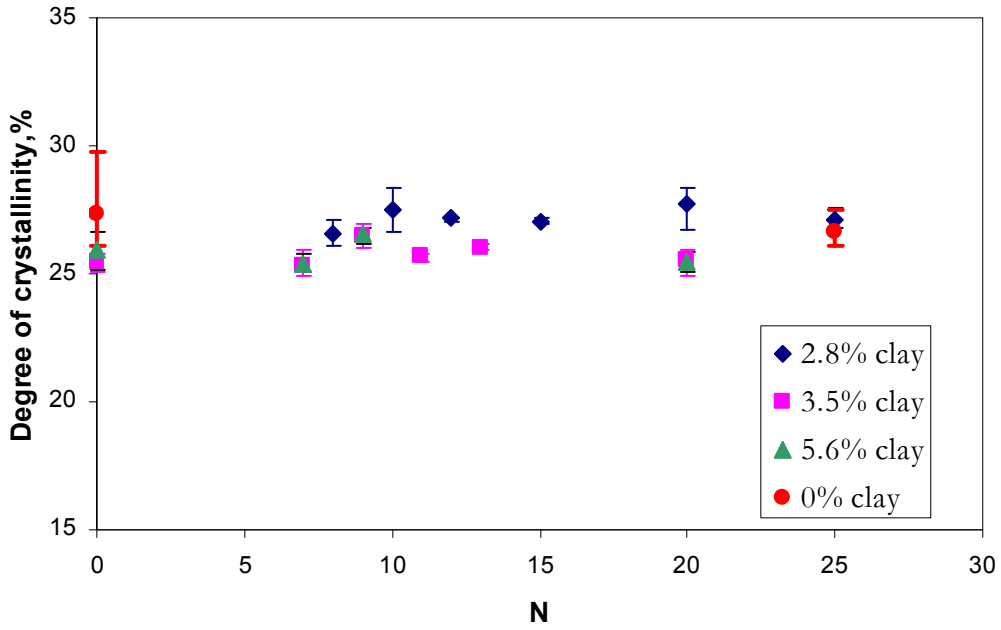


**Fig. 4.26: Degree of crystallinity of films measured by DSC as function of chaotic advection**

Variation in crystallinity among films with different clay content was also analyzed. Only minor changes were observed in the films as a function of clay content. At 2.8% Cloisite 30B, the films had a degree of crystallinity equal to or slightly greater than that of virgin PA6 films. Further addition of clay caused a very slight decrease in crystallinity. The changes in degree of crystallinity with clay content attained here compared well with degree of crystallinity trends of PA6-MMT composites available in literature obtained via DSC (Liu et al, 1999; Fornes and Paul, 2003). Although there were some differences in the shape and nature of the endotherms obtained. This difference may be attributed to a certain extent to the processing technique (injection molding) used to prepare the nanocomposite samples of reference. Liu et al. (1999) reported a dual peak with one peak temperature around 210°C and another peak at 220°C corresponding to γ-crystalline form and α-form respectively.

They did not specify the region from which the specimen was extracted for DSC although it is known that the crystalline morphology varies with distance from the surface of the injection molded nanocomposite sample (Kojima et al., 1995). On the other hand, Fornes and Paul (2003) reported the presence of a shoulder on the peak for nanocomposite specimens extracted from the core region of the injection molded sample while no such shoulder was present for the specimens extracted from the skin region of the injection molded sample. Instead a broad peak with a lower peak temperature was reported for the skin specimens. The DSC scans of the films produced by chaotic advection did not show any noticeable variation in the peak shape (Fig. 4.25). This may be a reflection of the sensitivity of the instrument used.

#### 4.1.3.2 Biaxially stretched films

The effect of biaxial stretching was also investigated on 2.8% steady state films using DSC. Since TEM examinations of films for all values of N and the 2.8% composition produced with the steady operating mode indicated homogenously dispersed platelets in the PA6 matrix (Fig. 4.7), only two sets of biaxially stretched film samples N=8 and N=15 were examined by DSC. Each set of films were stretched to three different ratios. The DSC plots of stretched film had a broader peak as shown by Fig. 4.27 compared to the unstretched films. The pre-heating and stretching at 200°C caused the growth of existing crystallites into coarser or thicker lamellae and formation of new crystallites. The combination of thicker crystallites and a size distribution among the crystallites causes the broadening of the peak (Fornes and Paul, 2003; Sperling, 2006).

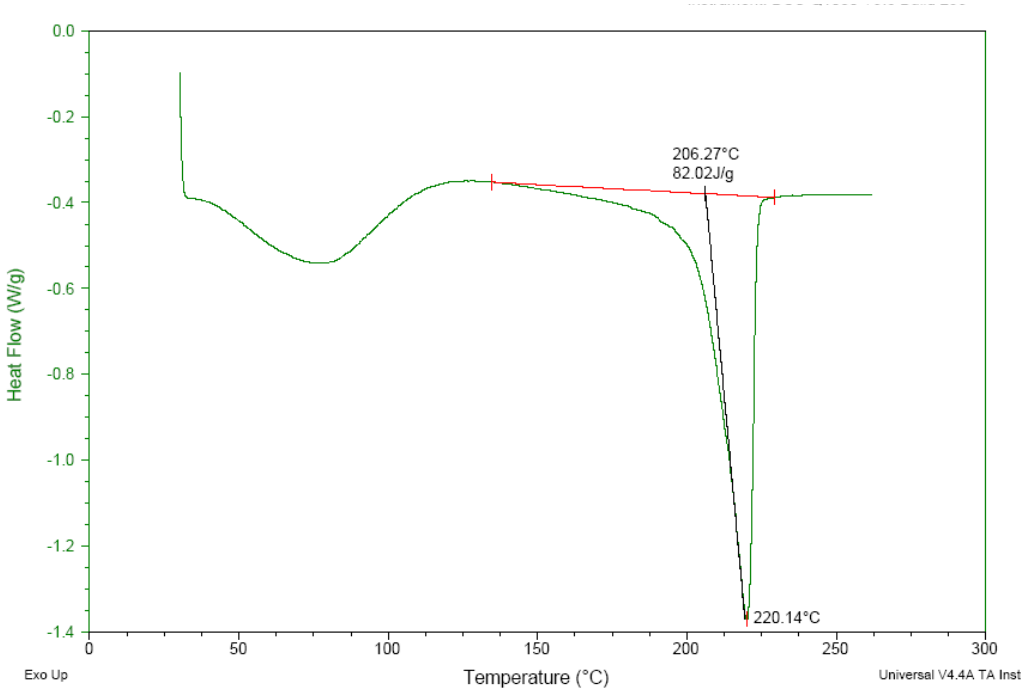


**Fig. 4.27: Heating DSC scan showing the broadening of the melting peak due to biaxial stretching of nanocomposite film (N=8, stretch ratio of 2.0x2.0)**

Degree of crystallinity was calculated from heat of fusion as before using Equations 4-1 and 4-2. The crystallinity was increased by biaxial stretching for all the samples to almost the same level (Table 4.3). No significant difference in crystallinity was observed with stretch ratio. Since the structure as shown by TEM images was similar for the 2.8% films at all values of N (Fig. 4.7), no effect of N on crystallinity of stretched films was observed. In comparison to unstretched films, the increase in crystallinity was about 25%.

As mentioned in Section 4.1.2.2, the 2% transient films and the 3.5% steady state films which exhibited a variation in structure with N were not biaxially stretched. But it is expected that such films would show an effect of N on crystallinity of the biaxially stretched films. The multi-layered structure would show a higher increase in crystallinity due to presence of unrestricted polymer chains in the virgin layers.

**Table 4.3: Crystallinity measured by DSC of stretched 2.8% nanocomposite films exhibiting a similar structure of homogenous dispersion of oriented platelets**

| | Degree of crystallinity, % | | |
|---|---|---|---|
| **N** | **Stretch ratio 1.5 x 1.5** | **Stretch ratio 2.0 x 2.0** | **Stretch ratio 2.5 x 2.5** |
| **8** | 33 | 33 | 33 |
| **15** | 33 | 32 | 32 |

## 4.2 Film Properties

The various film properties that are considered important for packaging applications are described in this section. The observed properties and trends are related to internal structure that was explained in the previous sections.

### *4.2.1* Optical microscopy

The surface quality of a film is a significant factor that contributes to the physical properties like oxygen transmission rate, impact strength and haze. Hence, the surface finish of the steady state films with different clay contents observed under an optical microscope is discussed before presenting the measured properties. Optical micrographs exemplifying the surface finish of 2.8% clay, 3.5% clay and 5.6% clay films produced by chaotic advection are shown in Fig. 4.28. For comparison, the surface finish of a PA6 nanocomposite film with 3% clay produced by an industrial blown-film process is also shown (Fig. 4.29). It is evident from the micrographs that the surface finish of the film produced by the industrial scale equipment with a customized nylon twin-screw extruder attached to a blow film die is much better than those produced by the laboratory scale chaotic blender utilizing small screw extruders and the in-house built die. Visual inspection of 2.8% film through naked eye

showed very minute particulate-kind of material present uniformly through out the film which did not affect the surface smoothness as they were within the film. These particulates gave the pitted surface appearance to the optical micrograph in the transmission mode. Infrared (IR) spectroscopy to identify the nature of these particulates was attempted. The particulates were embedded in the nylon matrix and could not be extracted out. Hence, the IR spectra of the film showed peaks related to only PA6 and nanoclay. Thus the nature of the particulates could not be identified.

The surface finishes of the films produced using the laboratory scale equipment was found to depend on the clay content in the film. The appearance of the die lines can be attributed to the inner surface finish of the die while the dependency on clay content can be explained by the direct dependence of surface finish of a cast film on the viscosity of the melt passing through the die (Giles et al, 2005). The apparent viscosity of the clay nanocomposites is known to increase with clay content (Krishnamoorti et al., 1996; Aalaie et al., 2007). The small screw extruders (feeding the melt to chaotic advection blender) of Fig. 2.2 with the screw elements designed for polyolefins rather than nylon or nylon nanocomposites were unable to adequately shear the masterbatches leading to increased viscous melts with increased clay contents. This was further confirmed by the better surface finish of the 5.6% films produced with a pre-mixed pellet feed (Fig. 4.28d). Due to the pre-mixing, the effective clay content in the extruders was reduced to 5.6% from 8%, thereby reducing the viscosity of the melt and leading to a better surface finish.

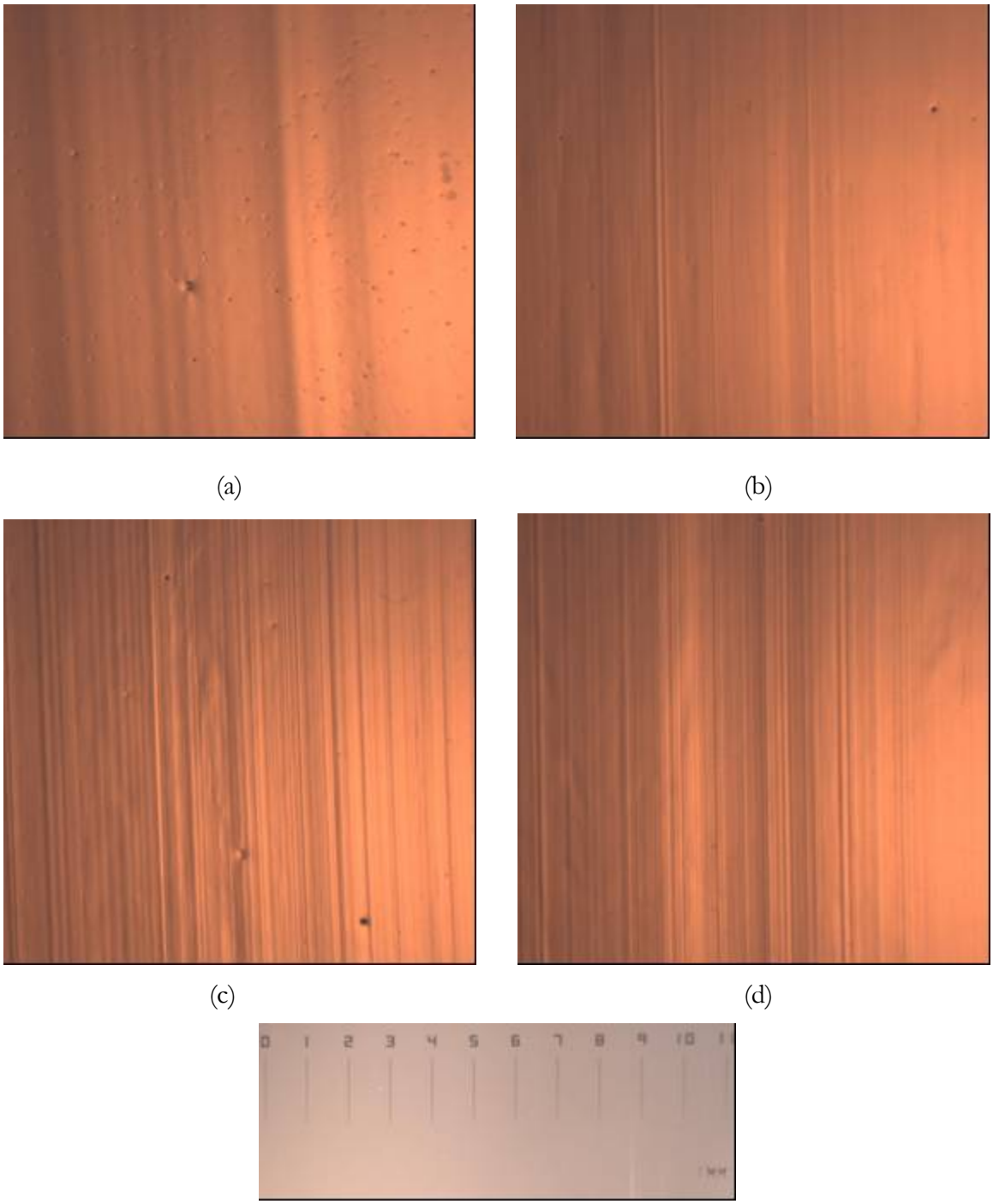


**Fig. 4.28: Optical micrographs showing the overall quality of the nanocomposite films produced by chaotic advection with (a) 2.8% clay, (b) 3.5% clay, (c) 5.6% clay, and (d) 5.6% clay film produced by pre-mixed pellet feed at N=0.**

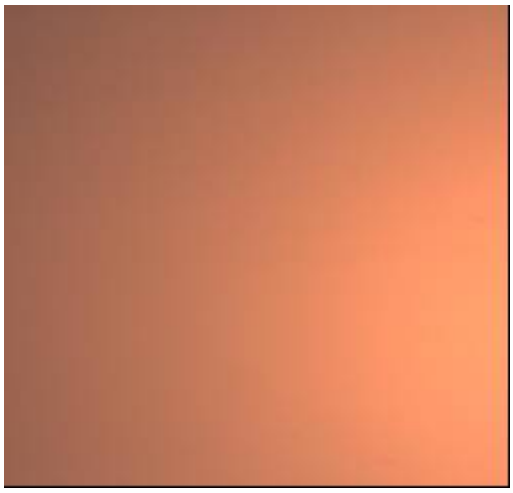

**Fig. 4.29: Optical micrograph showing the excellent quality of an industrial-scale blown nanocomposite film with 3% clay**

### *4.2.2* Oxygen transmission rate

The oxygen transmission rate of the film specimens were multiplied by their corresponding average thickness and reported in terms of permeability. The oxygen permeability values for various films are presented in Table 4.4. Pure PA6 film processed without chaotic advection had a permeability of 35.78 cc-mil/$m^2$-day. The permeability of PA6 film at N=25 was same as that of the film at N=0 within the error of measurement. The permeability of a polymer mainly depends on the degree of crystallinity for a given permeant gas at a given temperature and relative humidity (Oswald, et al., 2006; Sperling, 2006). The ordered structure of the polymer crystalline phase has lesser free volume than the amorphous phase making it more difficult for the gases to pass through. Hence the fact that both PA6 films (N=0 and N=25) had the same degree of crystallinity (refer to Section 4.1.2.1 and 4.1.3.1) is consistent with the invariance in permeability of pure PA6 films with chaotic advection.

**Table 4.4: Permeability of films produced using the continuous chaotic advection blender**

| Clay (wt%) | N | Permeability (cc-mil/$m^2$-day) |
|---|---|---|
| **0** | **0** | 35.78 |
| | **25** | 35.48 |
| **2.8** | **8** | 21.05 |
| | **10** | 22.31 |
| | **12** | 20.99 |
| | **15** | 23.53 |
| | **20** | 23.39 |
| | **25** | 21.79 |
| **3.5** | **7** | 17.55 |
| | **9** | 16.73 |
| | **11** | 18.60 |
| | **13** | 19.62 |
| | **20** | 16.78 |
| | **0** | 23.92 |
| **5.6** | **7** | 17.67 |
| | **9** | 15.85 |
| | **20** | 20.03 |
| | **0** | 12.68 |

Incorporating nanoclay into the PA6 matrix reduced the oxygen permeability of the films. Nanoclay, due to its inorganic nature, is impermeable to gases. Due to the large aspect ratio and nanoscale dimensions in an exfoliated state, even a low concentration of clay presents a high surface area and reduces the area of cross-section available to the diffusion. It also increases the path length of diffusing molecules by increasing tortuosity. The effect is more significant, as predicted by theoretical models, when these large-aspect ratio platelets are oriented in a direction perpendicular to the direction of diffusion (Fredrickson and Bicerno, 1999; Bharadwaj, 2001; Gusev and Lusti, 2001). The presence of nanoclay can also affect the crystallinity of the matrix (Fornes and Paul, 2003; Weon et al., 2005). Hence the effect of nanoclay platelet orientation and crystallinity changes caused by chaotic advection on oxygen permeability was analyzed and is explained in the succeeding paragraphs.

The reduction in oxygen permeability of the 2.8% nanocomposite films with respect to pure PA6 film (N=0) is plotted in Fig. 4.30 for as a function of N . The permeability shows very little variation with N. The TEM images of 2.8% film (Fig. 4.7, Section 4.1.1.2) revealed an internal structure with homogenous dispersion of oriented platelets. Also, the degree of crystallinity was similar for films produced with different extent of chaotic advection. Hence, the slight variation could have arisen by the heterogeneity introduced in the films by the presence of minute particulates as shown by the optical micrographs (Fig. 4.28a).

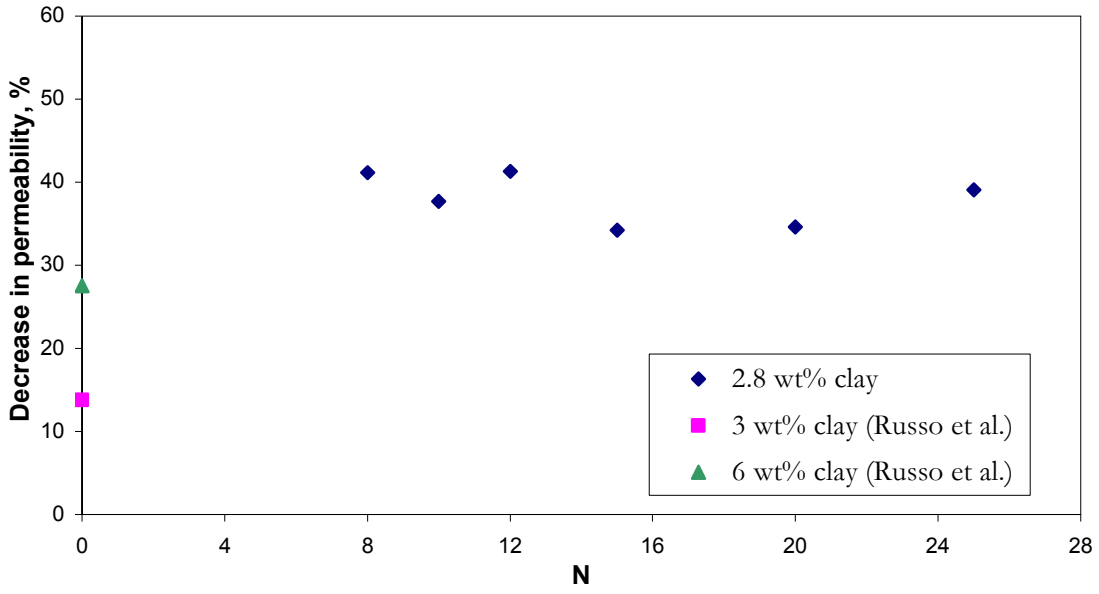


(a)

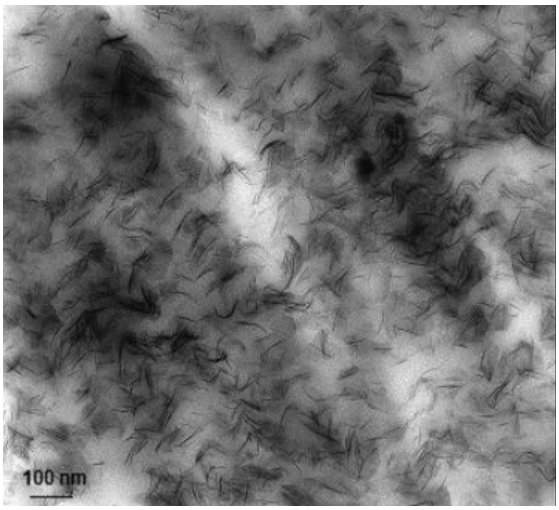


(b)

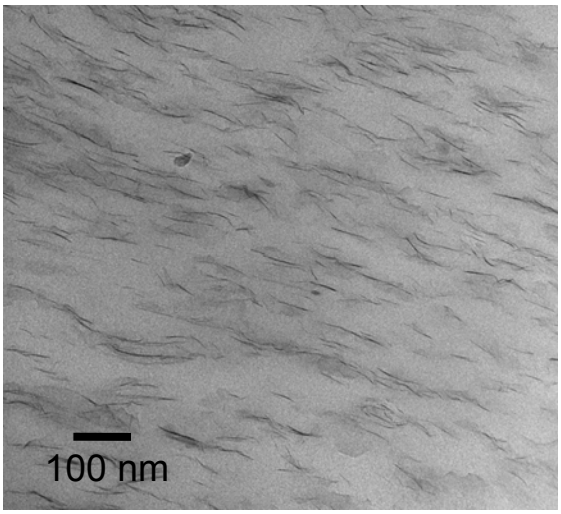


(C)

**Fig. 4.30: Effect of structure on the permeability of nanoclay composites. (a) Reduction in oxygen permeability with respect to virgin polymer film of 2.8% nanocomposite films in comparison to data reported in literature (Russo et al., 2006) shown along with micrographs representing the orientation of (b) 6 wt% film of Russo et al. (2006) and (c) 2.8% film of the current study**

As seen by the Fig. 4.30, a maximum reduction of 41% was observed for 2.8% films. The barrier property improvement was considerably higher than those reported in literature for 3 wt% and 6 wt% Cloisite 30B PA6 nanocomposite films (Russo et al., 2006). For reference, the values from literature are shown in Fig. 4.30. The lower permeabilities of the chaotic advection films were explained by contrast in the degree of orientation of the clay platelets. For clarity, a micrograph of 6 wt% clay film is reproduced from Russo et al. (2006) in Fig. 4.30 along with a micrograph of a 2.8% film of the current study. The films were reportedly extruded through a cast film die connected to a single screw extruder by Russo et al. (2006). This shows the effectiveness of the chaotic advection blender in imparting high degree of orientation to the nano-platelets that is associated with lower permeabilities.

Increasing the clay content to 3.5 wt% reduced the permeability further as shown by Fig. 4.31. A maximum reduction of 53% in permeability was observed. Although transmission electron microscopy showed the presence of a multi-layered structure with very thin virgin layers, permeability did not vary significantly with N. It is considered that at this low level of multi-layering, the structure is not effective in reducing the permeability. This was confirmed by the results from the three-dimensional permeability model detailed in the Chapter 3. The least reduction of 33% was shown by the films produced without chaotic advection using the pre-mixed pellet feed. The result is attributed to the low degree of orientation of the platelets as documented by transmission electron microscopic images (Fig. 4.13).

Poor surface finish, presence of contaminants, and agglomerates in the films led to poor barrier properties of the 5.6% films produced with chaotic advection. The permeabilities were the same as that for 3.5% clay films with the chaotic advection blender

(Fig. 4.31). The effect of surface finish was corroborated by the better barrier property shown by the 5.6% films produced from the pre-mixed pellet feed and without chaotic advection. It has a high degree of platelets alignment along the direction of flow and a surface finish comparable to 3.5% clay films. It provided a reduction of 64% in permeability.

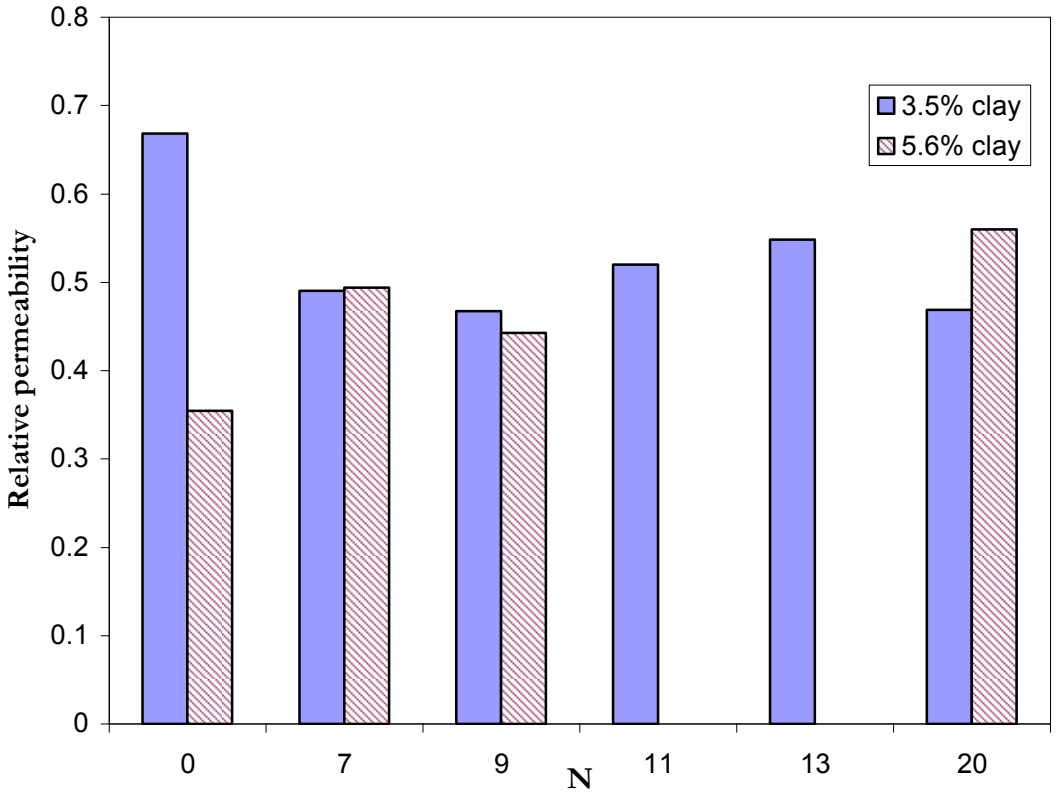


**Fig. 4.31: Permeability of 3.5% and 5.6% clay films with respect to the permeability of PA6 film. The variation in permeability of the films seen here can be attributed to their poor surface quality**

The unit cell permeability model in Chapter 4 showed that layered nanocomposites exhibited significant lowering of permeability when the layer thickness fraction of platelet-rich layers λ (refer Chapter 3) was 0.5 or less. Hence, to verify the model predictions permeability measurement of 2% transient films at N=8, N=16 and N=25 was carried out. According to the model, film at N=8 was expected show lower permeability than the films with higher N. The results are plotted as relative permeability in comparison to virgin polymer film at N=0 (Fig. 4.32). The nanocomposite with multi-layering reduced the permeability of the matrix by more than half of this original value. The permeability was shown to increase with increased dispersion of oriented platelets as shown by the films of higher N.

The predictions of the model for overall platelet volume fraction of 1% which is roughly equivalent to 2% by weight is shown in Fig. 4.32b. The aspect ratio of platelets was estimated to be approximately 100 from TEM images of the 2% nanocomposite. The reduction observed experimentally for multi-layered structure was much larger than that predicted by the model.

The deviation of the predicted values from the experimental measurements suggests the effects of various factors not taken into account in the model. The model assumed an isotropic matrix with a single permeability. In reality, the matrix in a nanocomposite consists of three different phase namely amorphous, α- crystalline form and γ-crystalline form. In addition, the crystalline defects introduced due to nanoclay in PA6 (Fornes and Paul, 2003) are reduced as they are restricted to platelet-rich layer. Finally, the model assumes that the permeability is independent of the number of layers which might not be true for the actual nanocomposite.

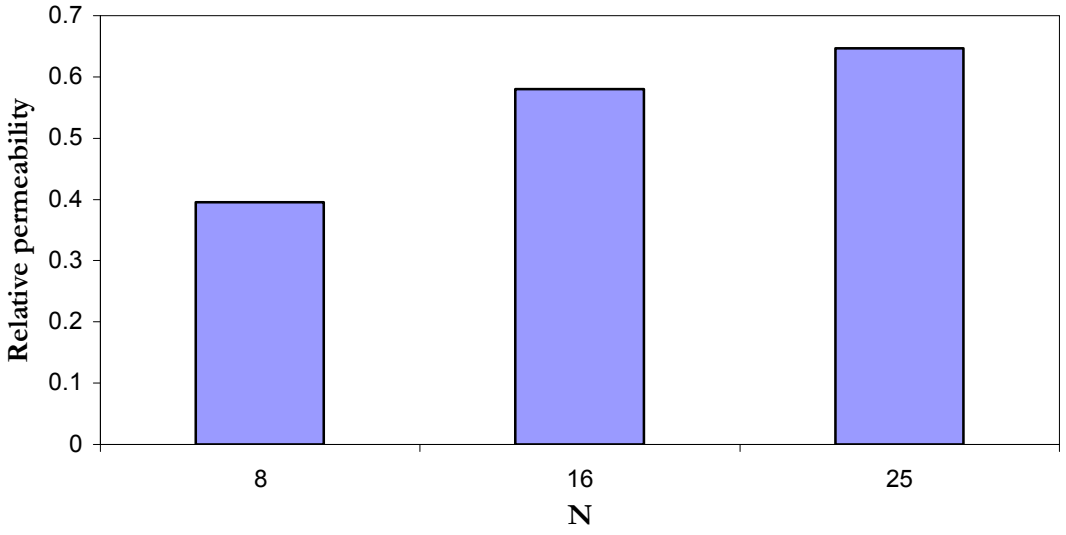


(a)

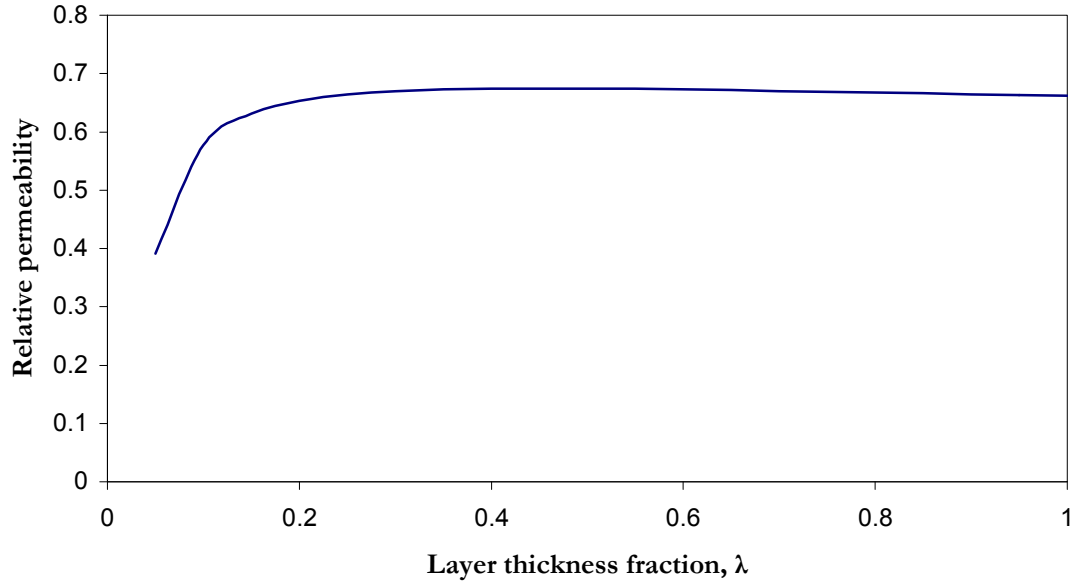


(b)

**Fig. 4.32: Effect of structural arrangement of platelets within the matrix on the permeability of the nanocomposite. (a) Experimental values for 2% transient films, (b) relative permeabilities predicted by the unit cell permeability model of Chapter 3 for an aspect ratio of 100 and volume fraction of 0.01**

The effect of clay content on the chaotically advected films is summarized in Fig. 4.32. The maximum reduction in oxygen permeability for each set of films is presented. Also plotted are the theoretical values calculated by the unit cell permeability model with homogenous dispersion for aligned platelets (refer Chapter 3 for methods). An approximate aspect ratio of 76 was measured by analyzing the TEM images of 2.8% and 3.5% clay films using ImageJ software (Public domain, National Institutes of Health). The experimental data was fitted with a curve and extrapolated as shown in Fig. 4.32. The relative permeabilities of nanocomposite films showed an exponential relationship with clay similar to the model. But the actual nanocomposites showed a greater reduction in permeability than predicted at each volume fraction of clay. Also, the reduction in permeability with increase in clay fraction was more that that predicted by the model as seen by greater deviation of the curve fitted for the experimental data from the curve due to the model. The greater enhancement for the actual films may be due to effects of other factors like the anisotropy of the polymer matrix as explained in the previous paragraph discussing the effect of multi-layering.

The results of chaotic advection study also compared well with the oxygen permeability values reported for PA6-nanoclay composites produced by in situ polymerization (Liang et al., 2001). For comparison, the reduction in permeability (approximate values) as reported by Liang et al. (2001) is shown in Fig. 4.33. While comparing the results, two factors must be borne in mind. First, the aspect ratio of clay platelets in melt-intercalated nanocomposites is typically lower than the platelets in situ polymerized nanocomposites. Second, different grades of organically modified clay have different amount of organic content. Cloisite 30B has an organic content of approximately

30% while Nanomer 1.24TL used by Liang et al. (2001) has a lower percentage (<10%). Despite the inherent disadvantage of the films of current study, the reduction in permeability compared well with that reported. The absence of details about the processing method, crystallinity and degree of orientation of the platelets within the nanocomposite impeded a more detailed comparative analysis. But the detailed comparison with the cast extruded nanocomposite films produced by Russo et al. (2006) clearly demonstrated the superiority of the nanocomposite films in terms of degree of alignment imparted by chaotic advection blender.

Biaxial stretching of the films proved effective in increasing the oxygen barrier properties as demonstrated by the data in Fig. 4.34 for 2.8% clay films. The permeability did not depend on the extent of stretching as noticed by almost similar reductions for the range of stretch ratios. For comparison, unstretched films denoted 1.0 x 1.0 is also shown in the plot. Stretching due to the accompanying increased crystallization (~25%) increased the oxygen barrier from ~40% for unstretched films to ~70%. The permeability results co-relate well with the crystallinity measurements done with DSC which also showed invariance of crystallinity with stretch ratio (Table 4.3).

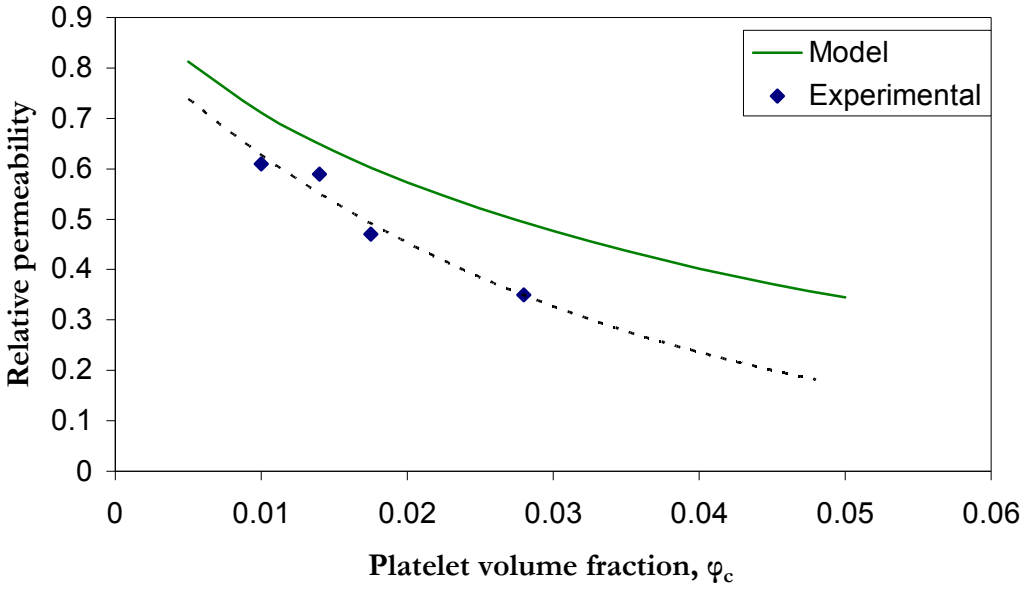


(a)

**Fig. 4.33: Effect of clay content on the relative permeability of nanocomposites with homogenous dispersed oriented platelets (a) Experimental measurements (b) theoretical values predicted by the unit cell permeability model (Chapter 3).**

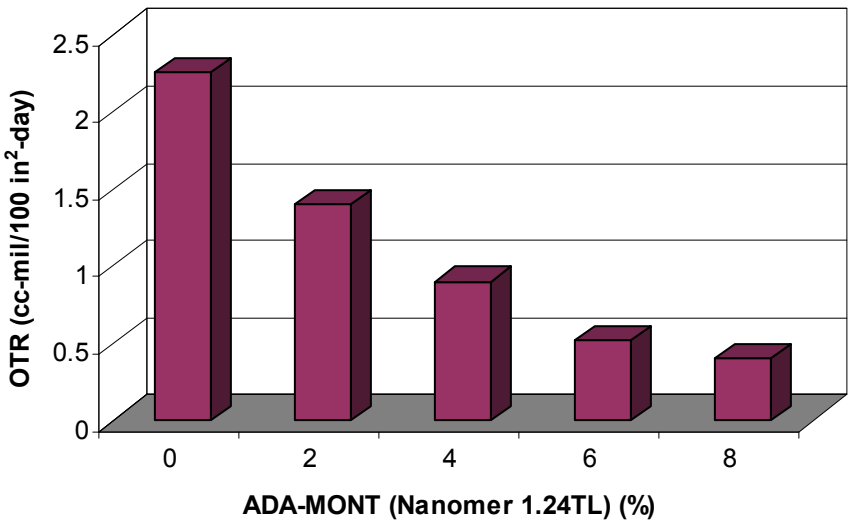


(b)

**Fig. 4.34: The variation in oxygen permeability with clay content reported by Liang et al. (2001) presented here for comparison**

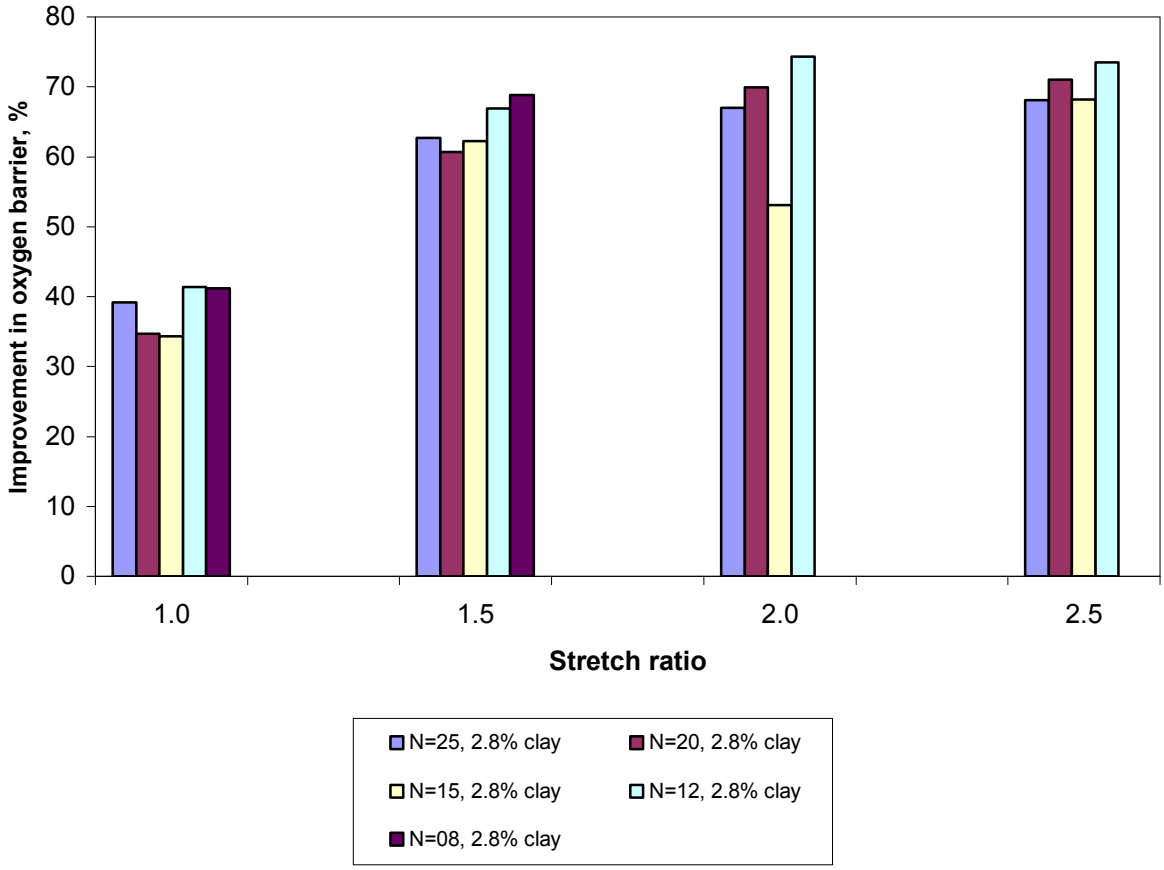


**Fig. 4.35: The improvement in oxygen barrier due to biaxial stretching of 2.8% films with a structure of homogenous dispersion of oriented platelets at every N. For comparison the permeability to the unstretched film (stretch ratio 1.0) is shown.**

### *4.2.3* Tensile properties

Tensile strength at maximum load was measured for films in machine direction and transverse direction. The values are reported for nanocomposite films as a plot in Fig. 4.36. For comparison, values of pure PA6 films are also shown. No specific trend with chaotic advection was observed for any set of films. The variation with N was masked by the large variations within the samples. The error bars representing the variation within samples is shown for 5.6% clay films. The other films showed a similar scatter in data.

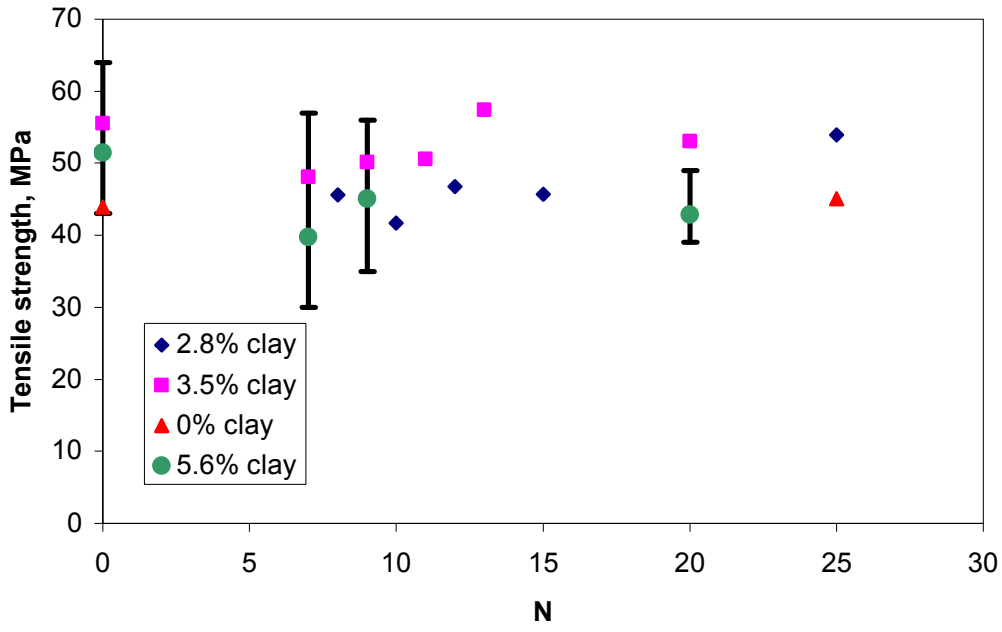


(a)

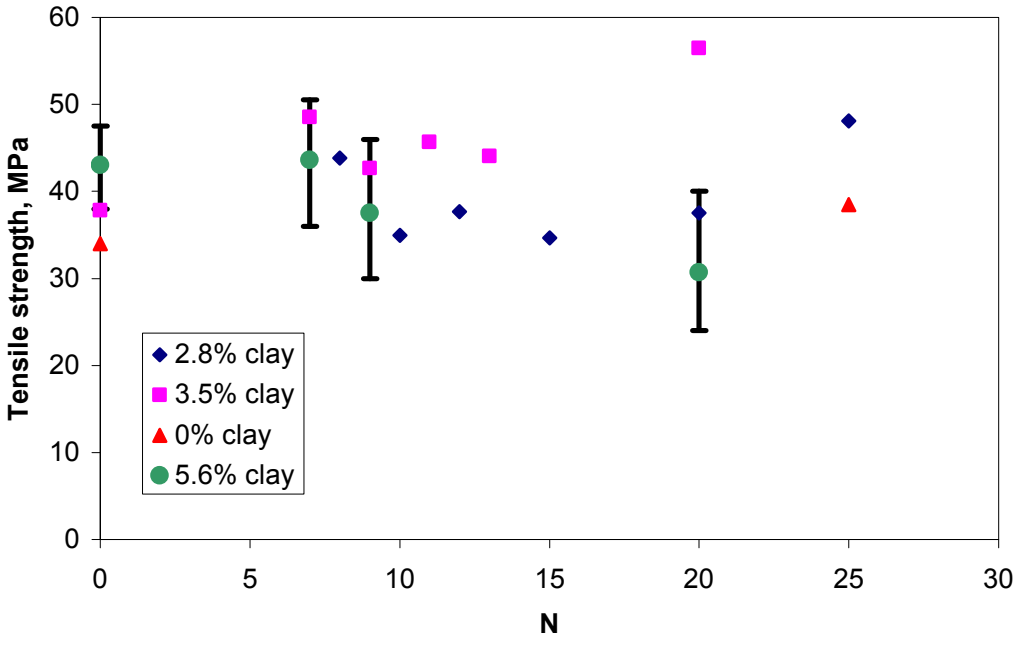


(b)

**Fig. 4.36: Tensile strength at maximum load of the films in (a) machine direction and (b) transverse direction**

Along the machine direction (4.36a), the tensile strength of 2.8% films was about the same as PA6 films while on an average the tensile strength of 3.5% films in machine direction was better than 2.8% and PA6 films. The films with more homogenous dispersion of platelets like N=13, 20 and films with no stir rod motion had better tensile strength than those exhibiting certain degree of multi-layering. But it was not possible to conclude with certainty the effect of structure with the available data. On an average, 3.5% films exhibited about an 18% increase in tensile strength along the machine direction. Keeping with its trend (Fig. 4.31), 5.6% clay films due to poor film quality revealed reduction in tensile properties.

A contradiction on the effect of nanoclay on the tensile strength of PA6-Cloisite 30B films exists in literature (Ranade et al., 2003; Russo et al., 2006). Ranade et al. (2003) using a similar grade of PA6 reported a slight increase in tensile strength (about 25% at 3% clay) while Russo et al., reported a decrease in tensile strength (about 20% at 3% clay). Despite the less than good quality of the chaotic advection films as evidenced by optical microscopy, the films compared well with the tensile strength values reported for PA6-Cloisite 30B films by Ranade et al. (2003).

The data points were more dispersed in the plot area as shown in Fig 4.36b for the transverse direction film samples and no trend could be recognized. On an average, the tensile strength along transverse direction was only slightly lower than tensile strength along machine direction indicating very little anisotropy in the films. This can be explained by the fact that the clay platelets have a disc-like structure. When they are aligned along the film surface as in this current case, they exhibit the same aspect ratio and impart similar improvements in both directions. The slight anisotropy present may be a result of unidirectional orientation of matrix crystal lamellae along the flow direction.

### *4.2.4* Tear strength

The resistance to tear propagation was measured for the nanocomposite films. The tear strength values depend on the thickness of the film but no known direct relationship exists between the two (ASTM D1922-03a). Hence, films of thickness deviating from its average by more than 10% cannot be compared. Bearing this in mind, tear strength values of pure virgin films and 2.8% films were plotted together as a function of N (Fig. 4.37a). Chaotic advection of virgin PA6 films increased the tear strength in the machine direction and decreased it by the same amount in the transverse direction. This is due to the dependence of resistance to tear propagation on the orientation of the crystalline region (Bobovitch et al., 2005). Bobovitch et al. (2005) reported that an increased orientation of the molecular chain axis led to reduced tear resistance of biaxially oriented polyethylene films. On this basis, it can be said that the chaotic advection increased the orientation of molecular chain axis of the polymer chains parallel to the film surface and along the transverse direction.

The data points from the 2.8% films mostly lay in between the two extremes demonstrated by the chaotically advected virgin PA6 films. Also, not much difference in tear resistance along the two principal directions was evident for nanocomposite films. The tear resistance was increased by an order of magnitude for the higher clay content films as shown in Fig. 4.34b. Since the thickness also increased by about 30%, the contributing factor could not be readily determined. Once again, there was no evident trend in either direction of testing.

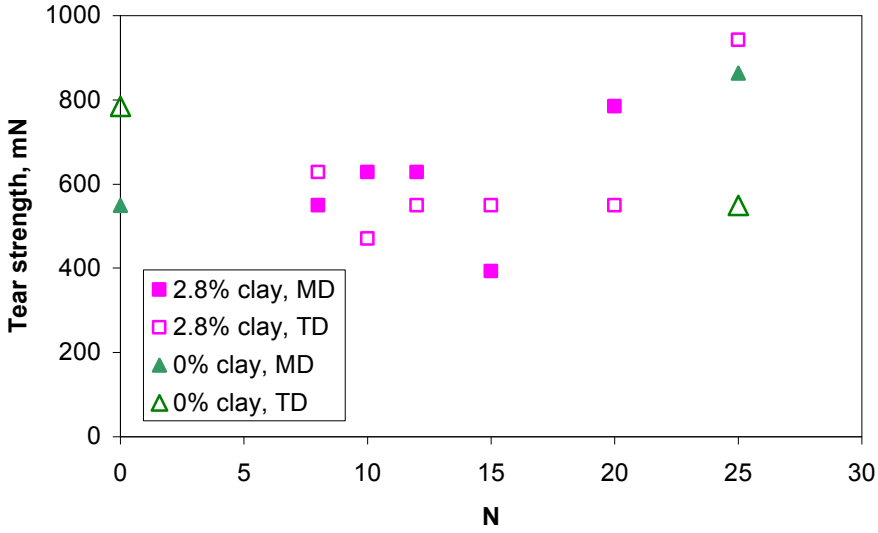


(a)

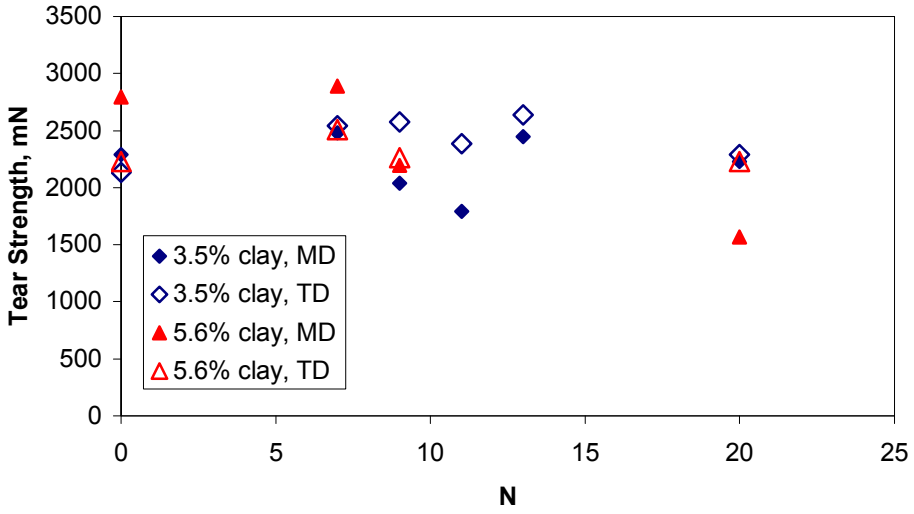


(b)

**Fig. 4.37: Resistance to tear propagation along both direction for (a) PA6 and 2.8% films with similar thickness and (b) higher clay content films**

### *4.2.5* Impact strength

Similar to tear strength, impact strength of 0% clay films revealed a dependence on chaotic advection. The impact strength of pure PA6 film dropped when it was subjected to chaotic advection. The impact properties of all the films are shown in Fig. 4.38a. The impact resistance of a film is also dependent partly on thickness, but no simple correlation exists. Hence, the impact data of 2.8% films could be compared to the PA6 films as both sets of films were of similar thickness. To facilitate comparison, the average thickness of films is plotted in Fig. 4.38b. The 2.8% films evidently had a lower resistance to impact than the pure PA6 films but it was not conclusive whether the reduction in impact resistance was due to the clay or the presence of the minute particles in the films (Fig. 4.28a). The minute particles may have acted as stress concentrators and caused the films to fail at a lower energy. The variation with N, though following the same trend as thickness, was within the range of variation amongst the specimens of each sample.

Due to thickness differences, the 3.5% clay films of different N's could not be compared amongst themselves. In general, thicker films showed better impact properties. Also, from the measured haze values discussed next, the quality of 3.5% films was found to be the best which may have led to better impact properties. 5.6% films also showed better impact properties than 2.8% films. This proves that internal defects were more critical than the surface quality of the film for impact strength.

Comparing the impact energy values of films with similar thickness, N=13 of 3.5% clay films, N=9 and 20 of 5.6% films with 0% clay films, it was judged that impact strength was not adversely affected by the presence of nanoclay particles.

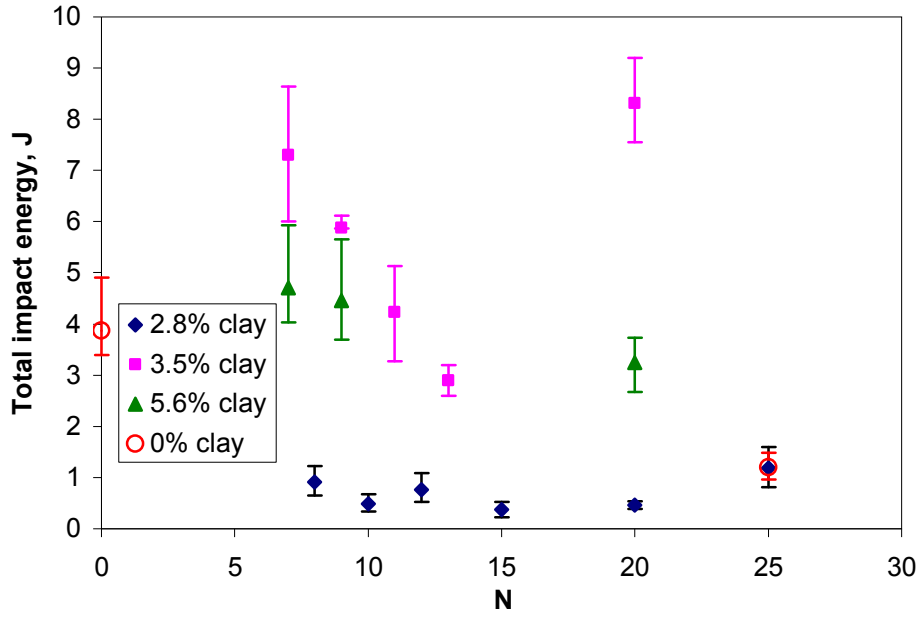


(a)

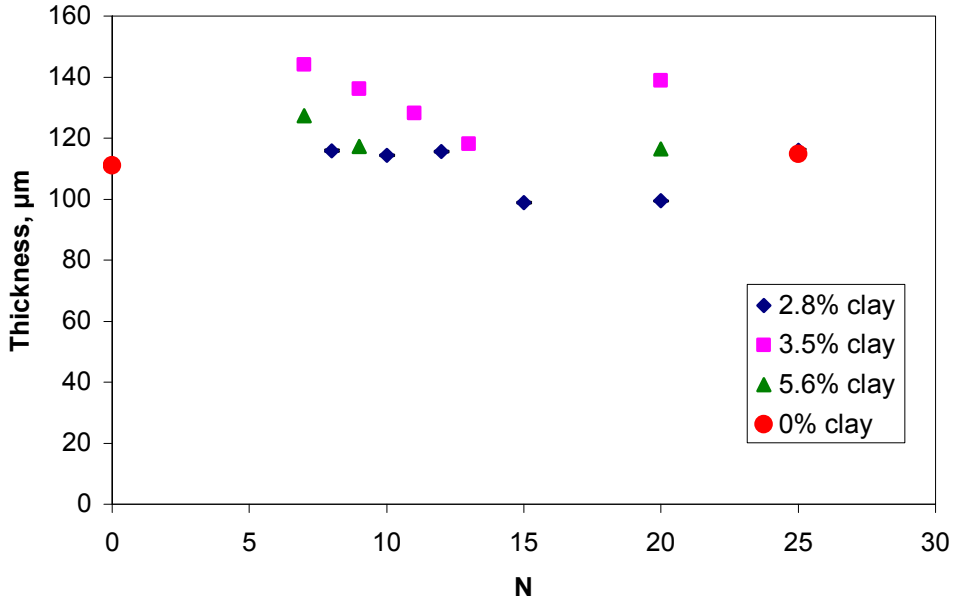


(b)

**Fig. 4.38: (a) Dart drop impact strength of the films, (b) corresponding thickness of the films (The thickness of films is not dependent on chaotic advection but is plotted here with respect to N to facilitate comparison of impact strength.)**

### *4.2.6* Haze

Haze data representative of the material can be obtained only when heterogeneous surface and internal defects are avoided. The films produced by the lab-scale equipment and die had inherent heterogeneity like die lines and particulates. Hence, the assessment of difference in optical clarity exclusively due to clay content was not possible. The effect of structure could not be evaluated either since no multi-layers with thick masterbatch layers were present in any of the composites.

Virgin PA6 film exhibited a haze in the range 7.6-8.7%. The values for the nanocomposites are presented as a graph in Fig. 4.39. From the data, it is evident that 3.5% films had the best film quality with its low haze values. The presence of minute particulates in 2.8% films may have led to increased light scattering and haze values. Similarly, the rough surface due to die lines would have contributed to the higher values of 5.6%. Despite the inherent artifacts, it can be rightly concluded that presence of nanoclay does not deteriorate the optical clarity of a film.

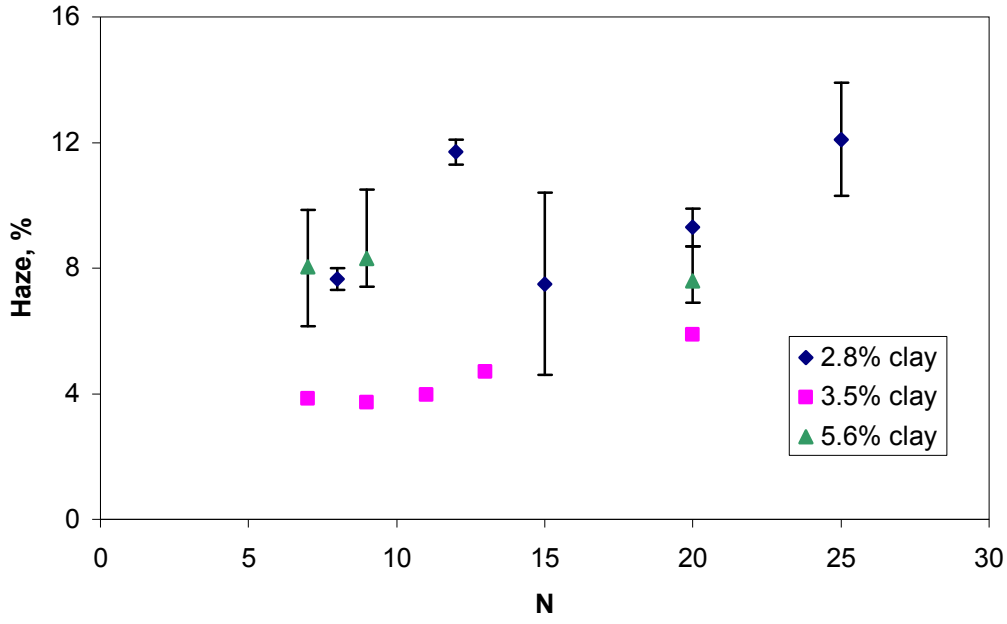


**Fig. 4.39: Percentage haze of the nanocomposite films of different clay content**

# CHAPTER 5

# 5 CONCLUSIONS AND RECOMMENDATIONS

## 5.1 Conclusions

A continuous chaotic advection blender was employed to produce structured nanocomposites. A hierarchical nanocomposite with a novel multi-layered structure with platelets oriented and localized within layers was produced and reported in a technical forum for the first time (Mahesha et al., 2005). An example of such a structure is shown in Fig. 5.1. The in-situ multi-layering was a consequence of the recursive stretching and folding of the melt domains of the masterbatch containing exfoliated nanoclay and major component polymer by chaotic advection. The platelets were localized within numerous layers and a composite with hierarchical structure and multiple nano-scales was formed. It comprised of platelets, thin regions of polymer between the individual platelets within the layers containing platelets, and pure polymer layers that could be produced with nanoscale thicknesses. Stretching of the masterbatch domain caused the nano-platelets to align and folding shuffled melt domains to promote compositional uniformity on larger scales (Fig. 5.2). This mechanism imparted a high degree of orientation to the nanoclay platelets throughout the volume of the composite upstream of the die in contrast to nanocomposites produced by conventional melt processing techniques in which platelet alignment occurs only in the near-wall regions within dies or molds.

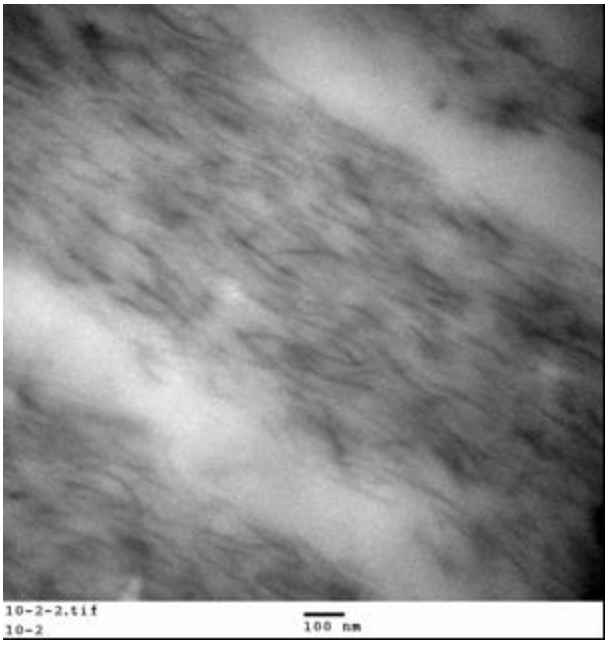


**Fig. 5.1: Micrograph showing the novel in-situ layered structure of a nanocomposite with multiple nano-scales produced by continuous chaotic advection blender**

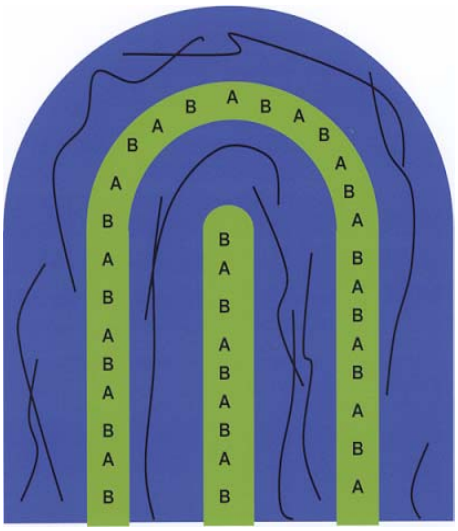

**Fig. 5.2: Schematic showing the multi-layering and orientation mechanism operative on polymer components, solid additives and molecular structure in a chaotic advection blender [Zumbrunnen et al., 2002]**

Although the multilayer nanocomposites were a primary focus, chaotic advection blenders can also give very well dispersed mixtures of platelets in a polymer matrix. Imparting sufficient chaotic advection to the melt domains such that layer thicknesses of the masterbatch and virgin polymer reduce and become comparable to the inter-platelet distance within masterbatch layer proved to be an effective method to disperse the clay platelets within the matrix even at the low shear rates involved. An example of such a dispersion of oriented platelets through out the matrix is shown in Fig. 5.3. Methods can be effective for preserving the high platelet aspect ratio in contrast to conventional mixing.

A high degree of orientation proved effective in enhancing the gas barrier properties of the nanocomposite. For example, the cast nanocomposite film produced by the continuous chaotic advection blender with only 3.5% organically modified clay (Cloisite 30B) exhibited a gas barrier property equivalent to a cast film produced by screw extrusion with 6% Cloisite 30B reported in literature by Russo et al. (2006). Both the films had homogenous dispersion of platelets within the matrix. The only observed difference between the films produced by chaotic advection and by screw extrusion was the degree of orientation. Further, localizing the clay platelets within numerous discrete regions to form a 2% clay film in the transient mode (Section 2.2.2) with discrete alternating virgin polyamide and masterbatch layers decreased the permeability by 39% with respect to a 2% clay film with homogenously dispersed oriented platelets. Unfortunately, thick discrete alternating layers similar to transient films could not be discerned by TEM in the range of N employed to produce the steady state films. This indicated that further process-structure optimization and improvements to the chaotic advection blender are needed. It should be noted that industry-scale chaotic advection blenders (smart blenders) that are considerably more

advanced than the laboratory blender used in this study became available commercially during the course of this study (Zumbrunnen, 2007).

Theoretical modeling on the effect of oriented platelets either localized in layers or homogenously dispersed on barrier properties showed a trend similar to the experimental results of the nanocomposites. Although, the permeability obtained by experimental measurements were lower than the model-predicted values. An example of the relative permeabilities is shown in Fig.5.4 for composites with homogenously dispersed aligned clay platelets as a function of clay content. Also, the curve fitted to the experimental data showed a slightly higher reduction in permeability with clay content than predicted by the model. This deviation may be attributed to the changes in the crystallinity and crystalline orientation of polymer matrix especially at the interface due to the presence of nanoclay platelets which were not taken into account in the model. The model also showed that in order to achieve high barrier materials with relative permeabilities 0.1 or lower at a reasonably low volume fraction of the platelets, a multi-layered structure with a high aspect ratio greater than 350 is required.

The presence of oriented nanoclay platelets even at a high clay content of 5.6% did not adversely the optical clarity of the film. Impact toughness, tear strength and percentage haze were similar to that of the virgin polymer film. In general, the mechanical properties of the nanocomposite films produced in this study were similar to those reported in literature (Ranade et al., 2003; Russo et al., 2006). Effect of chaotic advection on these properties could not be deduced, as the steady state films utilized for these measurements did not show significant differences in structure. A lack of structural difference suggests that layers

reduced rapidly in thickness in terms of the process parameter N. Obtaining a well-defined multi-layer structure in steady state may be achievable by further process development.

The crystalline nature of the polymer matrix also corresponded well with those reported in literature (Kojima et al., 1994; Fornes and Paul, 2001; Russo et al., 2006). But the effect of reduced spacing between the clay platelets due to their localization in layers on the orientation of the crystallite orientation could not be observed due to a limitation of x-ray diffraction instrument employed. The beam stopper of the instrument employed was large and masked the low and masked the patterns at low diffraction angles corresponding to the orientation of clay platelets and 002 reflection of γ-form.

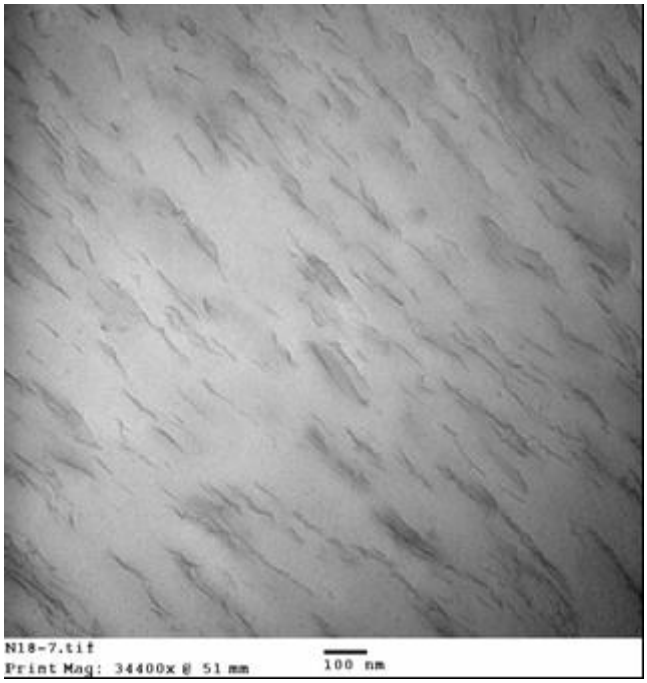


**Fig. 5.3: TEM image showing a nanocomposite with oriented and homogenously dispersed platelets produced by subjecting the melt domains to a high extent of chaotic advection**

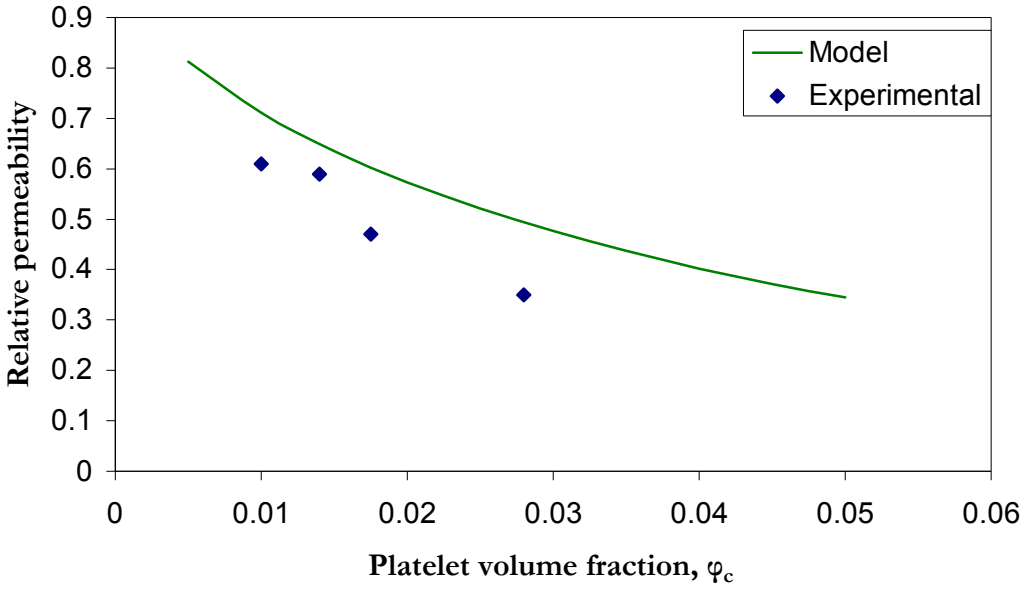


**Fig. 5.4: Permeability of nanocomposites with perfectly aligned homogenously dispersed impermeable platelets with an aspect ratio as measured by image analysis of TEM images of the produced nanocomposite films, S=1, α=76**

In summary, continuous chaotic advection blender operated in transient mode proved to be an effective tool to manipulate the placement and orientation of clay platelets to produce novel multi-layered structure with oriented clay platelets. Such novel structured composites proved to be effective in enhancing the gas barrier properties. Though the steady state films did not show discrete layering, the platelets had a high degree of orientation. Flows in dies attached to the blender provided added orientation but orientation occurred primarily in the chaotic advection blender itself. This high degree of orientation imparted higher barrier properties to films compared to those produced by conventional mixing. Since the structuring occurs upstream of the die, nanocomposites of any required profile can be extruded. Also, the low shear rates employed in chaotic blender makes it a useful process

high aspect ratio platelets without breaking them down to produce ultra-high barrier composites.

## 5.2 Recommendations

The theoretical model showed that localizing and orienting platelets of a much higher aspect ratio than employed in this study in multi-layers may lead to dramatic enhancements is barrier properties. An in-situ polymerized clay masterbatch typically has a higher clay aspect ratio because of the absence of mechanical shearing than the melt-intercalated masterbatches used in the current study. With such in-situ polymerized clay masterbatches in a chaotic advection blender, low shear rates that are possible with these novel machines can prevent or reduce breaking of platelets so that a high aspect ratio of platelets is retained. The stretching and folding mechanism of chaotic advection can give good alignment of the platelets and multi-layering through the bulk of the extruded nanocomposite.

A very recent effort (Dolgovskij et al., 2007) to produce a similar multi-layer nanocomposite using a layer multiplication device (Baer et al., 2000) proved less successful in simultaneously orienting the platelets within the layers. A lack of orientation is detrimental to barrier properties especially as the aspect ratio of the platelets increases as shown by the current model and one formulated by Osman et al. (2005). Such multi-layered structure even without a high degree of orientation can prove beneficial to properties albeit to a lesser extent. The localization of platelets restricts their negative effect such as formation of crystalline defects (Fornes and Paul, 2003). This would lead to a more ordered, homogenous crystalline matrix with reduced number of crystalline defects in matrix of the virgin layers and hence may provide improvement in properties.

Another factor which affects the physical properties of a film apart from the internal structure is the overall quality of the film in terms thickness variation, die lines, presence of point defects like gels or other particulates comprised of unmelted resin or degraded polymer. In the current study, only screw extruders that were designed for easily processable polymers such as polyethylene were available. These were nevertheless used to melt and feed the polyamide and its clay masterbatch to the chaotic advection blender. Consequently, processing was restricted. Melt flow rates were reduced in order to allow melting of the masterbatch and PA6 but some unmelted resin persisted in the form of small particles. The chaotic advection blender and its melt supply system were also used in parallel studies with other polymer types. Some were thermally sensitive and compatible with PA6 so additional particles resulting from degradation of these polymers were found in the nanocomposite films. A comparison of the film surface qualities between films of the current study and one nanocomposite film produced by a film manufacturer is shown in optical micrographs in Fig. 5.5. The film surface of the current study was rough due to die lines and had embedded particulates while the films produced by a film manufacturer had a smooth surface without visible point defects. Hence, in order to achieve a high quality nanocomposite film in future studies, an extruder suitable to the processing of the particular resin is recommended.

To produce steady state films with discrete alternating layers as seen in the transient films, a range of N lower than used in this study may be investigated. The effect of different chaotic advection processing parameters other than just extent of chaotic advection on the structure could also be explored.

Finally, the theoretical model can be modified to include the effect of crystallinity and crystalline morphology of the matrix in the composite. From the current study and

studies from the past, it is known that presence of nanoclay changes the crystalline nature of the polyamide-6 matrix (Kojima et al., 1994; Maiti and Okamoto, 2003; Fornes and Paul, 2003; Li and Shimizu, 2006). Li and Shimizu (2006) also showed that clay spacing also affected the orientation of the crystalline lamellae as shown in Fig. 5.6. The effect of crystallinity can be incorporated into the model by assuming a matrix consisting of two different phase corresponding to amorphous and crystalline regions. Then the effect of different levels of crystallinity and crystalline orientation can be assessed by constructing a finite element model and assigning different permeability values for each phase.

Employing an x-ray diffraction instrument with a smaller beam stopper (Section 4.1.2) is recommended in order to establish the effect of chaotic advection and the resulting multi-layer structure on the orientation of the polymer crystalline lamellae. It would be interesting and useful to comprehend the effect of the orientation of the crystals so as to design a nanocomposite with desired barrier properties.

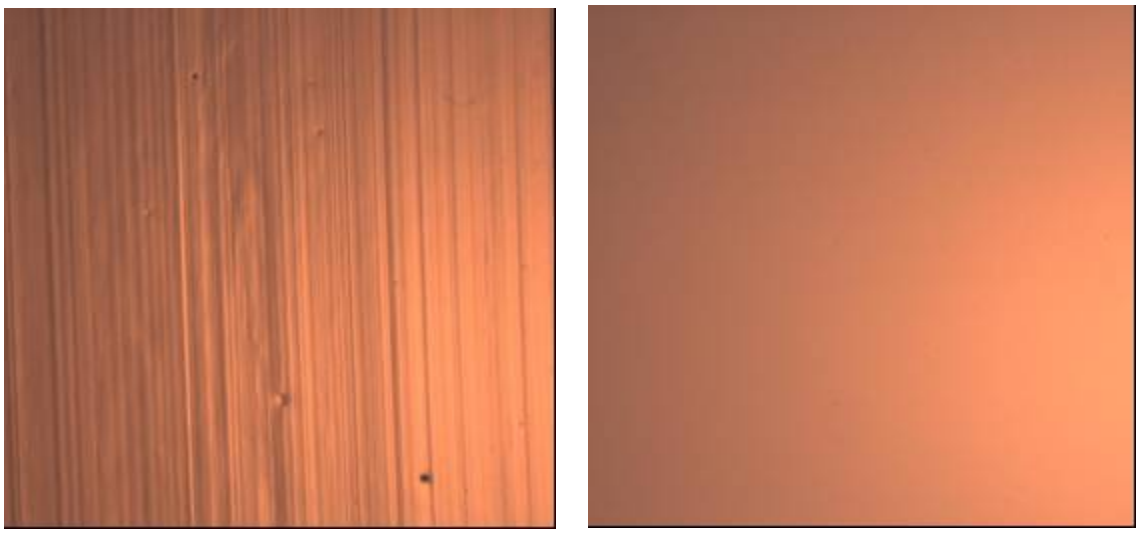

**(a)** **(b)**

**Fig. 5.5: Comparison of the surface qualities of nanocomposite films produced in (a) the laboratory and by (b) industry**

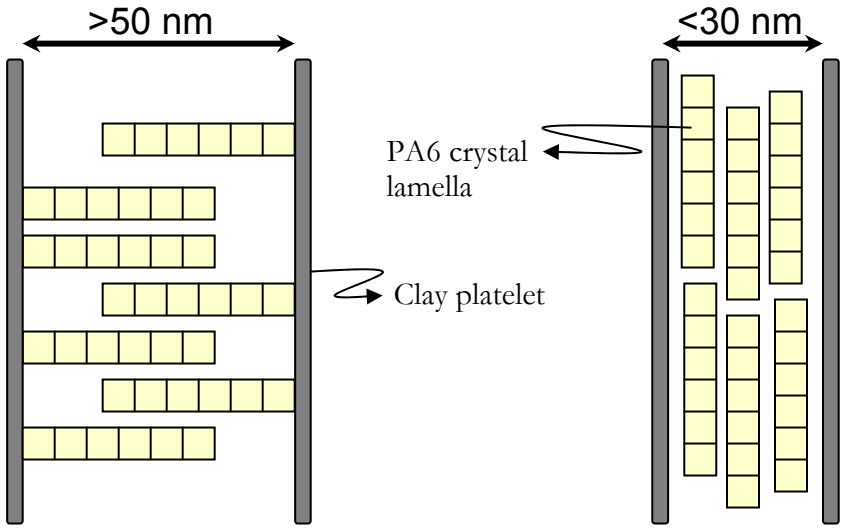


**Fig. 5.6: Effect of clay platelet spacing on the orientation of the crystalline lamellae of polyamide-6 matrix**

# REFERENCES


Aalaie, J., Khanbabaie, G., Khoshniyat, A.R., Rahmatpour, A., 2007, "Study on Steady Shear, Morphology and Mechanical Behavior of Nanocomposites Based on Nylon 6," *Journal of Macromolecular Science, Part B: Physics*, Vol. 46, pp. 305-316

Aranda, P., Ruiz-Hitzky, E., 1992, "Poly(ethylene oxide)-Silicate Intercalation Materials," *Chemistry of Materials*, Vol. 4, pp.1395-1403

Aref, H., 1984, "Stirring by Chaotic Advection," *Journal of Fluid Mechanics*, Vol. 143, pp.1-21

Aref, H., 2002, "The Development of Chaotic Advection," *Physics of Fluids*, Vol. 14, pp.1315-1325

Arimoto, H., Ishibashi, M., Hirai, M., Chatani, Y., 1965, "Crystal Structure of the γ-form of Nylon 6," *Journal of Polymer Science, Part A*, Vol. 3, pp. 317-326

Aris, R., 1986, "On a Problem of Hindered Diffusion," *Archive of Rational Mechanics and Analysis*, Vol. 95, pp. 83-91

Baer, E., Kerns, J., Hiltner, A., 2000, "Processing and Properties of Polymer Microlayered systems," *Structure Development During Polymer Processing, Eds. A.M Cunha and S. Farikov*, *Kluwer Academic Publishers*, Netherlands, pp. 327-344

Bharadwaj, R.K., 2001, "Modeling the Barrier Properties of Polymer-Layered Silicate Nanocomposites," *Macromolecules*, Vol. 34, pp. 9189-9192

Bobovitch, A.L., Tkach, R., Ajji, A., Elkoun, S., Nir, Y., Unigovski, Y., Gutman, E.M., 2006, "Mechanical Properties, Stress Relaxation and Orientation of Double-Bubble Biaxially Oriented Polyethylene Films," *Journal of Applied Polymer Science*, Vol. 100, pp. 3545-3553

Brydson, J.A., 1982, "Plastic Materials- 4$^{th}$ Edition," *Butterworth Scientific*, London

Cho, J.W., Paul, D.R., 2001, "Nylon 6 Nanocomposites by Melt Compounding," *Polymer*, Vol. 42, pp.1083-1094

Chougule, V.A., Kimmel, R.M., Zumbrunnen, D.A., 2005, "Development of Novel Barrier films using Chaotic Advection 'Smart Blending' Device," *Proceedings of 63rd Annual technical Conference, Society of Plastics Engineers*, Boston, MA, pp. 2976-2981

Chougule, V.A., Zumbrunnen, D.A., 2005, "In Situ Assembly using a Continuous Chaotic Advection Blending Process of Electrically Conducting Networks in Carbon Black-Thermoplastic Extrusions," *Chemical Engineering Science*, Vol. 60, pp. 2459-2467

Crownover, R.M., 1995, "Introduction to Fractals and Chaos," *Jones and Barlett*, Boston

Cussler, E.L., Hughes, S.E., Ward, III W.J., Aris, R., 1988, "Barrier membranes," *Journal of Membrane Science*, Vol. 38, pp.161-174

Danescu, R.I., Zumbrunnen, D.A., 1998, "Creation of Conducting Networks among Particles in Polymer Melts by Chaotic Mixing," *Journal of Thermoplastic Composite Materials*, Vol. 11, pp. 299-318

Danescu, R.I., Zumbrunnen, D.A., 2000, "Production of Electrically Conducting Plastic Composites by Three-Dimensional Chaotic Mixing of Melts and Powder Additives," *Journal of Vinyl & Additive Technology*, Vol. 6, pp. 26-33

Dennis, H.R., Hunter, D.L., Chang, D., Kim, S., White, J.L., Cho, J.W., Paul, D.R., 2001 (January), "Nanocomposites: The Importance of Processing," *Plastics Engineering*, pp. 56-60

Dennis, H.R., Hunter, D.L., Chang, D., Kim, S., White, J.L., Cho, J.W., Paul, D.R., 2001, "Effect of Melt Processing Conditions on the Extent of Exfoliation in Organoclay-Based Nanocomposites," *Polymer*, Vol. 42, pp. 9513-9522

Dhoble, A., Kushreshta, B., Ramaswami, S., Zumbrunnen, D.A., 2005, "Mechanical Properties of PP-LDPE Blends with Novel Morphologies Produced with a Continuous Chaotic Advection Blender," *Polymer*, Vol. 46, pp. 2244-2256

Fornes, T.D., Paul, D.R., 2003, "Crystallization Behavior of Nylon 6 Nanocomposites," *Polymer*, Vol. 44, pp. 3945-3961

Fornes, T.D., Yoon, P.J., Keskkula, H., Paul, D.R., 2001, "Nylon 6 Nanocomposites: The Effect of Matrix Molecular Weight," *Polymer*, Vol. 42, pp. 9929-9940

Fredrickson, G.H., Bicerano, J., 1999, "Barrier Properties of Oriented Disk Composites," *Journal of Chemical Physics*, Vol 1.10, pp. 2181-2188

Giles, H.F., Wagner, J.R. Jr., Mount, E.M. III, 2005, "Extrusion- The Definitive Processing Guide and Handbook," *William Andrew Publishing*

Gomillion, B.L., 2000, "Fiber Production with In-Situ Formation of Fibrillar Microstructures by Chaotic Mixing," *Thesis (Ph.D)*, Clemson University

Gupta, B., Lacrampe, M-F., Krawczak, P., 2006, "Polyamide-6/Clay Nanocomposites: A Critical Review," *Polymer and Polymer Composites*, Vol. 14, pp.13-38

Gusev, A.A., Lusti, H.R., 2001, "Rational Design of Nanocomposites for Barrier Applications," *Advanced Materials*, Vol. 13, pp. 1641-1643

Holmes, R., Bunn, D.W., Smith, D.L., 1955, "The Crystal Structure of Polycaproamide: Nylon 6," *Journal of Polymer Science*, Vol. 17, pp.159-177

Ibanes, C., Boissieu, M. D., David, L., Seguela, R., 2006, "High Temperature Behaviour of the Crystalline Phases in Unfilled and Clay-Filled Nylon 6 Fibers," *Polymer*, Vol. 47, pp. 5071-5079

Kojima, Y., Usuki, A., Kawasumi, M., Okada, A., Kurauchi, T., Kamigaito, O., Kaji, K., 1994, "Fine Structure of Nylon 6-Clay Hybrid," *Journal of Polymer Science Part B: Polymer Physics*, Vol. 32, pp. 625-630

Kojima, Y., Usuki, A., Kawasumi, M., Okada, A., Kurauchi, T., Kamigaito, O., Kaji, K., 1995, "Novel Preferred Orientation in Injection-Molded Nylon 6-Clay Hybrid," *Journal of Polymer Science Part B: Polymer Physics*, Vol. 33, pp.1039-1045

Kojima, Y., Usuki, A., Kawasumi, M., Okada, A., Kurauchi, T., Kamigaito, 1993, "Sorption of water in Nylon 6-Clay Hybrid," *Journal of Applied Polymer Science*, Vol. 49, pp. 1259-1264

Kwon, O., Zumbrunnen, D.A., 2001, "Progressive Morphology Development to Produce Multilayer Films and Interpenetrating Blends by Chaotic Mixing," *Journal of Applied Polymer Science*, Vol. 82, pp.1569-1579

Kwon, O., Zumbrunnen, D.A., 2003, "Production of Barrier Films by Chaotic Mixing of Plastics," *Polymer Engineering and Science*, Vol. 43, pp. 1443-1459

Kyotani, M., Mitsuashi, S., 1972, "Studies on Crystalline Forms of Nylon 6 II. Crystallization from the Melt," *Journal of Polymer Science Part A2*, Vol. 10, pp. 1497-1508

Lan, T., Kaviratna, P.D., Pinnavaia, T.J., 1994, "On the Nature of Polyimdie-Clay Hybrid Composites," *Chemistry of Materials*, Vol. 6, pp. 573-575

Leaversuch, R., 2001 (October), "Nanocomposites Broaden Roles in Automotive, Barrier Packaging," *Plastics Technology*, Vol. 47, pp.64-69

Li, Y., Shimizu, H., 2006, "Effect of Spacing between the Exfoliated Clay Platelets on the Crystallization Behavior of Polyamide-6 in Polyamide-6/Clay Nanocomposites," *Journal of Polymer Science Part B: Polymer Physics*, Vol. 44, pp.284-290

Liang, Y., Omachinski, S., Logsdon, J., Cho, W., Lan, T., 2001, "Nano Effect in Nylon-6 Nanocomposites," *Proceedings of 59th Annual technical Conference, Society of Plastics Engineers*, Dallas, TX, pp. 434-436

Lincoln, D.M., Vaia, R., Wang, Z.-G., Hsiao, B.S., 2001, "Secondary Structure and Elevated Temperature Crystallite Morphology of Nylon-6/Layered Silicate Nanocomposites," *Polymer*, Vol 42, pp.1621-1631

Liu, L., Qi, Z., Zhu, X., 1999, "Studies on Nylon6/Clay Nanocomposites by Melt-Intercalation Process," *Journal of Applied Polymer Science*, Vol.71, pp. 1133-1138

Liu, Y.H., Zumbrunnen, D.A., 1996, "Emergence of Fibrillar Composites Due to Chaotic Mixing of Molten Polymers," *Polymer Composites*, Vol. 17, pp. 187-197

Liu, Y.H., Zumbrunnen, D.A., 1999, "Toughness Enhancement in Polymer Blends due to the In-Situ Formation by Chaotic Mixing of Fine- Scale extended Structures," *Journal of Materials Science*, Vol. 34, pp. 1921-1931

Mahesha, C., Parulekar, Y., Zumbrunnen, D.A., 2005, "Novel Clay Nanocomposites with Platelets Oriented by Chaotic Advection", *Proceedings of 63rd Annual Technical Conference, Society of Plastics Engineers*, Boston, MA, pp. 1920-1923

Maiti, P., Okamoto, M., 2003, "Crystallization Controlled by Silicate Surfaces in Nylon 6-Clay Nanocomposites," *Macromolecular Materials and Engineering*, Vol. 288, pp. 440-445

Medellin-Rodriguez, F.J., Burger, C., Hsiao, B.S., Chu, B., Vaia, R., Phillips, S., 2001, "Time-Resolved Shear Behavior of End-Tethered Nylon 6-Clay nanocomposites Followed by Non-Isothermal Crystallization," *Polymer*, Vol. 42, pp. 9015-9023

Messersmith, P.B., Giannelis, E.P., 1995, "Synthesis and Barrier Properties of Poly(ε-Caprolactone)-Layered Silicate Nanocomposites," *Journal of Polymer Science Part A: Polymer Chemistry*, Vol. 33, pp. 1047-1057

Miles, K.C., Nagarajan, B., Zumbrunnen, D.A., 1995, "Three-Dimensional Chaotic Mixing of Fluids in a Cylindrical Cavity," *Transactions of the ASME*, Vol. 117, pp. 582-588

Nielsen, L. E., 1967, "Models for the Permeability of Filled Polymer Systems," *Journal of Macromolecular Science, Part A: Chemistry*, Vol. 1, pp. 929-942

Okada, A., Kawasumi, M., Usuki, A., Kojima, Y., Kurauchi, T., Kamigaito, O., 1990, "Synthesis and Properties of Nylon 6/Clay Hybrids," *MRS Symposium Proceedings*, Pittsburg, Vol. 171, pp.45-50

Osman, M.A., Mittal, V., Lusti, H.R., 2004a, "The Aspect Ratio and Gas Permeation in Polymer-Layered Silicate Nanocomposites," *Macromolecular Rapid Communications*, Vol. 25, pp. 1145-1149

Osman, M.A., Mittal, V., Morbidelli, M., Suter, U. W., 2004b, "Epoxy- Layered Silicate Nanocomposites and Their Gas Permeation Properties," *Macromolecules*, Vol. 37, pp.7250-7257

Osman, M.A., Rupp, J.E.P., Suter, U.W., 2005, "Gas Permeation Properties of Polyethylene-Layered Silicate Nanocomposites," *Journal of Materials Chemistry*, Vol. 15, pp.1298-1304

Osswald, T.A., Baur, E., Brinkmann, S., Oberbach, K., Schmactenberg, E., 2006, "International Plastics Handbook: The Resource for Plastic Engineers," *Hanser Gardner Publications, Munich*, 4th Edition

Ottino, J.M., 1989, "The Kinematics of Mixing: Stretching, Chaos, and Transport," Cambridge University Press, Cambridge, Great Britain

Parulekar, Y., 2003, "Barrier Properties of Films Containing Clay Nano-Composites Oriented by Chaotic Mixing," Masters Thesis, Clemson University

*Plastics Technology*, 2000(March), Vol. 46, pp. 31

Ranade, A., S'souza, N.A., Gnade, B., Dharia, A., 2003, "Nylon-6 and Montmorillonite-Layered Silicate (MLS) Nanocomposites," Journal of Plastic Film & Sheeting, Vol. 19, pp. 271-285

Ray, S.S., Okamoto, M., 2003, "Polymer/Layered Silicate Nanocomposites: A Review from Preparation to Processing," *Progress in Polymer Science*, Vol. 28, pp.1539-1641

Ray, S.S., Yamada, K., Okamoto, M., Ueda, K., 2002, "Polylactide-Layered Silicate Nanocomposite: A Novel Biodegradable Material," *Nano Letters*, Vol. 2, pp.1093-1096

Russo, G.M., Simon, G.P., Incarnato, L., 2006, "Correlation between Rheological, Mechanical, and Barrier properties in New Copolyamide-Based Nanocomposite Films," *Macromolecules*, Vol. 39, pp. 3855-3864

Samon, J.M., Schultz, J.M., Wu, J., Hsiao, B., Yeh, F., Kolb, R., 1999, "Study of Structure Development during the Melt Spinning of Nylon-6 Fiber by Online Wide-Angle Synchrotron X-ray Scattering Techniques," *Journal of Polymer Science Part B: Polymer Physics*, Vol. 37, pp.1277-1287

Shah, A. P., Gupta, R.K., 2002, "Moisture Diffusion through Vinyl Ester Nanocomposites Made with Montmorillonite Clay," Polymer Engineering and Science, Vol. 42, pp. 1852-1863

Sherman L.M., 2007 (May), "Nanocomposites: Less Hype More Hardwork on Commercial Viability," *Plastics Technology*, Vol. 53, pp. 76

Usuki, A., Hasegawa, N., Kato, M., 2005, "Polymer-Clay Nanocomposites," *Advances in Polymer Science*, Vol. 179, pp. 135-195

Usuki, A., Kawasumi, M., Kojima, Y., Fukushima, Y., Okada, A., Kurauchi, T., Kamigaito, O., 1993, "Swelling Behavior of Montmorillonite Cation Exchanged for ω-Amine Acid by ε-Caprolactam," *Journal of Materials Research*, Vol. 8, 1179-1183

Usuki, A., Koiwai, A., Kojima, Y., Kawasumi, M., Okada, A., Kurauchi, T., Kamigaito, O., 1995, "Nylon 6/Clay Nanocomposites," *Journal of Applied Polymer Science*, Vol. 55, pp. 119-123

Usuki, A., Kojima, Y., Kawasumi, M., Okada, A., Kurauchi, T., Kamigaito, O., 1993, "Synthesis of Nylon 6-Clay Hybrid," *Journal of Materials Research*, Vol. 8, 1179-1183

Vaia, R.A., Giannelis, E.P., 1997, "Polymer Melt Intercalation in Organically- Modified Layered Silicates: Model Predictions and Experiment," *Macromolecules*, Vol. 30, pp. 8000-8009

Vaia, R.A., Ishii, H., Giannelis, E.P., 1993, "Synthesis and Properties of Two-Dimensional Nanostructures by Direct Intercalation of Polymer Melts in Layered Silicates," *Chemistry of Materials*, Vol. 5, pp. 1694-1696

Vieth, W.R., 1991, "Diffusion In and Through Polymers: Principles and Applications," *Hanser Publications, Munich*

Weon, J.-I., Xia, Z.-Y., Sue, H.-J., 2005, "Morphological Characterization of Nylon-6 Nanocomposites Following a Large-Scale Simple Shear Process," *Journal of Polymer Science Part B: Polymer Physics*, Vol. 43, pp. 3555-3566

Xu, R., Manias, E., Snyder, A.J., Runt, J., 2001, "New Biomedical Poly(urethane urea)-Layered Silicate Nanocomposites," *Macromolecules*, Vol. 34, pp. 337-339

Yano, K., Usuki, A., Okada, A., 1997, "Synthesis and Properties of Polyimide-Clay Hybrid Films," *Journal of Polymer Science Part A: Polymer Chemistry*, Vol.35, pp. 2289-2294

Yano, K., Usuki, A., Okada, A., Kurauchi, T., Kamigaito, O., 1993, "Synthesis and Properties of Polyimide-Clay Hybrid," *Journal of Polymer Science Part A: Polymer Chemistry*, Vol. 31, pp. 2493-2498

Yoon, K., Polk, M.B., Min, B.G., Schiraldi, D.A., 2004, "Structure and Property Study of Nylon-6/Clay Nanocomposite Fiber," *Polymer International*, Vol. 53, pp. 2072-2078

Zeng, Q.H., Yu, A.B., Lu, G.Q., Paul, D.R., 2005, "Clay-Based Polymer Nanocomposites: Research and Commercial Development," *Journal of Nanoscience and Nanotechnology*, Vol. 5, pp.1574-1592

Zhang, D.F., Zumbrunnen, D.A., 1996, "Chaotic Mixing of Two Similar Fluids in the Presence of a Third Dissimilar Fluid," *AIChE Journal*, Vol. 42, pp. 3301-3309

Zhang, D.F., Zumbrunnen, D.A., 1996, "Influences of Fluidic Interfaces on the Formation of Fine Scale Structures by Chaotic Mixing," *Journal of Fluids Engineering*, Vol. 118, pp. 40-47

Zhang, D.F., Zumbrunnen, D.A., Liu, Y.H., 1998, "Morphology Development in Shear Flows of Straight and Folded Molten Fibers," *AIChE Journal*, Vol. 44, pp. 442-451

Zheng, J., Siegel, R.W., Toney, C.G., 2003, "Polymer Crystalline Structure and Morphology Changes in Nylon-6/ZnO Nanocomposites," *Journal of Polymer Science Part B: Polymer Physics*, Vol. 41, pp. 1033-1050

Zumbrunnen, D. A., 1994, "Auto-Synthesis of Fine-Scale Composite Materials by Chaotic Mixing," Proceedings of the First International Conference on Composites Engineering, International Community for Composites Engineering, New Orleans, Louisiana, pp. 601 – 602

Zumbrunnen, D. A., Kwon O., 2004, "Chaotic Mixing Methods and Structured Materials Formed Therefrom," *United States Patent No. 6,770, 340 B2*

Zumbrunnen, D.A., 2000, "Smart Blending: A Means to Obtain Fibers and Plastic Products with Tailored Properties," Journal of Textile Institute, Vol. 91, pp. 92-104

Zumbrunnen, D.A., Chibber, C., 2002, "Morphology Development in Polymer Blends Produced by Chaotic Mixing at Various Compositions," *Polymer*, Vol. 43, pp. 3267-3277

Zumbrunnen, D.A., Inamdar, S., 2001, "Novel Sub-Micron Highly Multi-Layered Polymer Films Formed by Continuous Flow Chaotic Mixing," Chemical Engineering Science, Vol. 56, pp. 3893-3897

Zumbrunnen, D.A., Inamdar, S., Kwon, O., Verma, P., 2002, "Chaotic Advection as a Means to Develop Nanoscale Structured in Viscous Melts," *Nano Letters*, Vol. 2, pp. 1143-1148

Zumbrunnen, D.A., Miles, K.C., Liu, Y.H., 1996, "Auto-Processing of Very Fine-Scale composite Materials by Chaotic Mixing of Melts," Composites Part A, Vol. 27A, pp. 37-47

Zumbrunnen, D.A., Subrahmanian, R., Kulshreshta, B., Mahesha, C., 2006, "Smart Blending Technology Enabled by Chaotic Advection," *Advances in Polymer Technology*, Vol. 25, pp.152-169